National University of Lesotho

A Chemical Process Design for Green Hydrogen Production Through Water Electrolysis in Lesotho

Tsepiso Angelina Ramaisa (202200038)

A dissertation submitted in partial fulfilment
of the requirements for the degree of

Master of Science in Sustainable Energy

Offered by the

Energy Research Centre
Faculty of Science & Technology

July 2024

ABSTRACT

This research addresses the pressing need for process design models that are specifically adapted to Lesotho's distinct resource profile, particularly its vast hydroelectric capacity. At present, there is a noticeable gap in process models designed for green hydrogen production that take into account the unique energy conditions of Lesotho. To address this shortcoming, the study presents a detailed chemical process design for hydrogen production through water electrolysis, utilizing Lesotho's renewable energy. The process model developed includes detailed mass balances to ensure precise quantification of material flows. Critical process parameters, including molar and mass fractions as well as stream molar flow rates, are defined to accurately describe the system, providing a solution that is specifically optimized for Lesotho's energy resources. The key unit operations, including separators, mixers and an electrolyser, are carefully modelled. Separators are used for phase separation and component purification, while mixers are designed to efficiently combine process streams. The electrolyser, central to the process, is modelled according to the electrochemical reactions which take place and mass transfer considerations. To ensure accurate phase equilibrium calculations, the Rachford-Rice equations are applied. Additional equations are formulated to characterise equipment performance and to address system constraints, such as product purity requirements. The developed model serves as a tool for enhancing hydrogen production and assessing overall process efficiency. It offers a framework for examining how different operating conditions and design parameters affect system performance. Future research should focus on incorporating renewable energy sources like wind and solar to diversify and enhance the sustainability of hydrogen production in Lesotho. Performing comprehensive energy balances will offer deeper insights into the system's efficiency and potential for optimization. Moreover, including economic and environmental assessments will provide a more thorough evaluation of the commercial feasibility of green hydrogen production in the country. These suggestions not only address current gaps but also lay the groundwork for developing a more integrated and scalable model for green hydrogen production, which could be applied to other regions with similar renewable energy resources, supporting both regional and global efforts towards sustainable energy transitions.

ACKNOWLEGEMENTS

I would such as to express my sincere gratitude to Professor Thimothy Thamae for his invaluable guidance, mentorship, and unwavering support throughout this research endeavour. His expertise and encouragement were instrumental in shaping this work. Special thanks to Mr. Moruti Kao for his contributions and assistance. I am eternally grateful to my friends and family for their constant support and belief in me. Furthermore, I would such as to acknowledge the Energy Research Centre for providing the necessary knowledge and resources for me to conduct this research study. The support of these individuals was crucial to the successful completion of this dissertation.

Table of Contents

Table of figures

List of Tables

1 INTRODUCTION

1.1 Background

The escalating global demand for primary energy, driven by economic expansion, population growth, and technological progress, is predominantly met by fossil fuels. However, this reliance on fossil fuels leads to substantial greenhouse gas emissions, exacerbating climate change. Therefore, it is crucial to focus on alternative sources to mitigate the consequences of climate change [1]. One of the most promising clean and sustainable energy sources is hydrogen, which does not emit any carbon but only produces water as a by-product [2].

Lesotho's energy sector has consistently been under the control and dependence of two government-owned entities: the Lesotho Electricity Company (LEC), serving as the exclusive transmitter, distributor, and supplier of electricity, and the Lesotho Highlands Development Authority (LHDA), acting as the primary power producer through the 'Muela hydropower (MHP) station [3]. Despite this, a new entity, the Lesotho Electricity Generation Company (LEGCO), has been established in 2022 to develop a 30MW solar facility in Ha Ramarothole [4]. The peak energy demand has been constantly increasing over the past years, reaching 204 MW in 2022, and has greatly surpassed the 72 MW hydropower domestic generation, which has been stagnant since 1998 [5], [6].

Given the anticipated energy crisis, it is imperative to investigate all technically exploitable energy resources. Consequently, Lesotho has a chance to diversify its energy sources and diminish reliance on imported fossil fuels by tapping into the potential for green hydrogen production from renewable sources. Lesotho has ample renewable energy resources, including hydro, solar, and wind. The daily solar radiation levels in Lesotho range from 4.5 to 6.5 kWh/m^2 on average, with certain regions in the South West experiencing even more substantial averages exceeding 7 $kWh/m^2/day$ [3].

According to Mpholo et al [7], Lesotho has more than 5 m/s at 10 m above ground level (a.g.l) wind speed at modelled potential sites. Such sites include Lets'eng-la-Terae, Sani and Masitise, and they have average wind speeds of 4.93 m/s, 5.5 m/s, and 5.97 m/s at 10 m a.g.l. Concerning hydroelectric power, Lesotho has numerous rivers and dams that represent promising locations for energy generation, as shown in Figure 1.

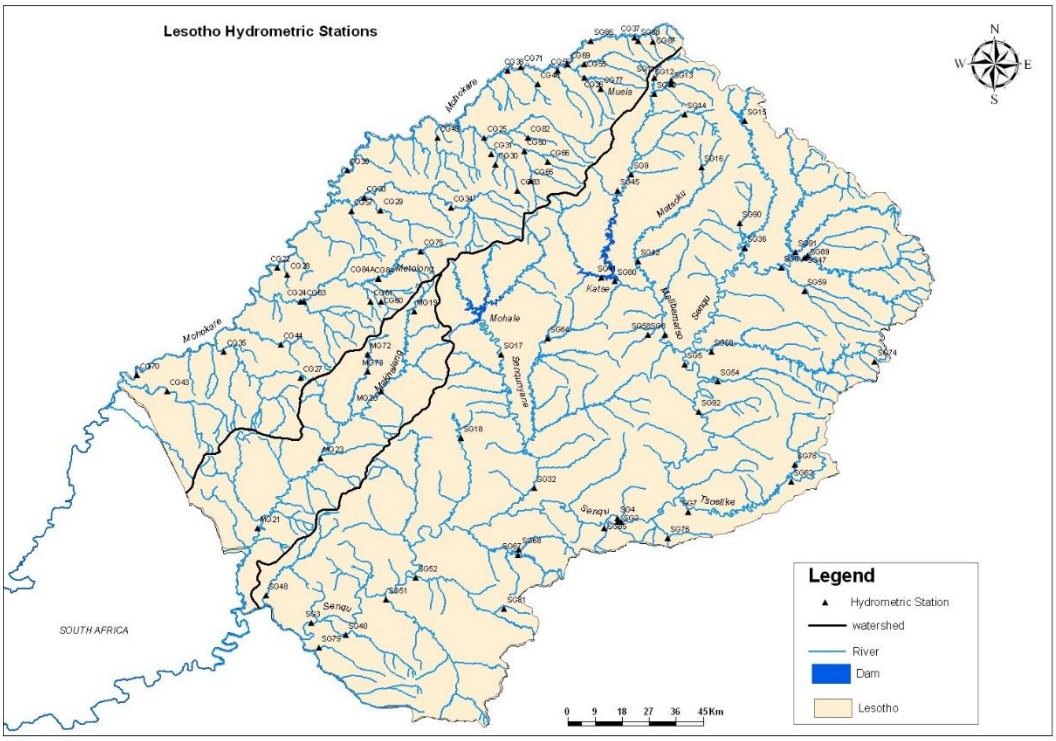

Figure 1: Water catchment areas and hydrometric stations [8].

A substantial portion of the global hydrogen supply is generated through steam methane reforming (SMR). However, the noteworthy drawback of SMR lies in its carbon dioxide emissions, releasing over five kilograms of CO_2 for every kilogram of hydrogen produced, thereby contributing to an increase of the greenhouse effect. As a result, water electrolysis presents a potential and environmentally friendly alternative for generating hydrogen without emitting carbon dioxide. It is essential to emphasize that the carbon-neutral benefit depends on obtaining the necessary energy from renewable sources, considering the substantial energy intensity associated with the electrolysis process [1], [9-13].

This emerging electrolysis technology harnesses renewable energy from the sources such as solar and wind, along with water, to generate hydrogen. The process prevents the emission of extra carbon dioxide or detrimental gases into the atmosphere. Green hydrogen shows the potential as a resolution to diverse environmental issues associated with traditional hydrogen production (SMR) , which predominantly depends on fossil fuels [14]. At present, the share of global green hydrogen production from water electrolysis is limited to 5%, primarily because fossil fuel-derived black/grey/blue hydrogen is more cost-effective [15]. Therefore, the primary obstacle in the production of green hydrogen is the cost economics or LCOH (Levelized Cost of H_2).

The most promising green hydrogen production technologies include alkaline electrolysis (ALE), polymer electrolyte membrane (PEM), and solid oxide electrolysis (SOE). Among these, ALE has achieved the highest level of commercial advancement, while PEM and SOE are still in the early stages of development and have a lower technology readiness level (TRL) [16]. Moreover, hydrogen is considered an energy carrier that can store or deliver a significant amount of energy. The energy density of hydrogen is nearly three times higher than that of gasoline or diesel with a Higher Heating Value (HHV) of ~141.9 kJ/g and a Lower Heating Value (LHV) of ~119.9 kJ/g [17]. The environmental impact of hydrogen compared to the other fuels can be quantified through the following equations [17]:

$$EIF = \frac{kgCO_2\ product\ of\ combustion\ reaction}{kg\ fuel} \quad (1)$$

$$GF = \frac{EIF_{max} - EIF}{EIF_{max}} \quad (2)$$

$$HCF = \frac{kgH_2\ in\ the\ fuel}{kg\ fuel} \quad (3)$$

where EIF, GF, HCF, and EIF_{max} represent the environmental impact factors (EIF), greenisation factors (GF), hydrogen content factors (HCF), and the maximum value of EIF (EIF_{max}), respectively. [17]. As illustrated in Figure 2, energy sources with a higher green factor (GF) exhibit an elevated hydrogen content (high HCF) and minimal environmental impact (low EIF) [17].

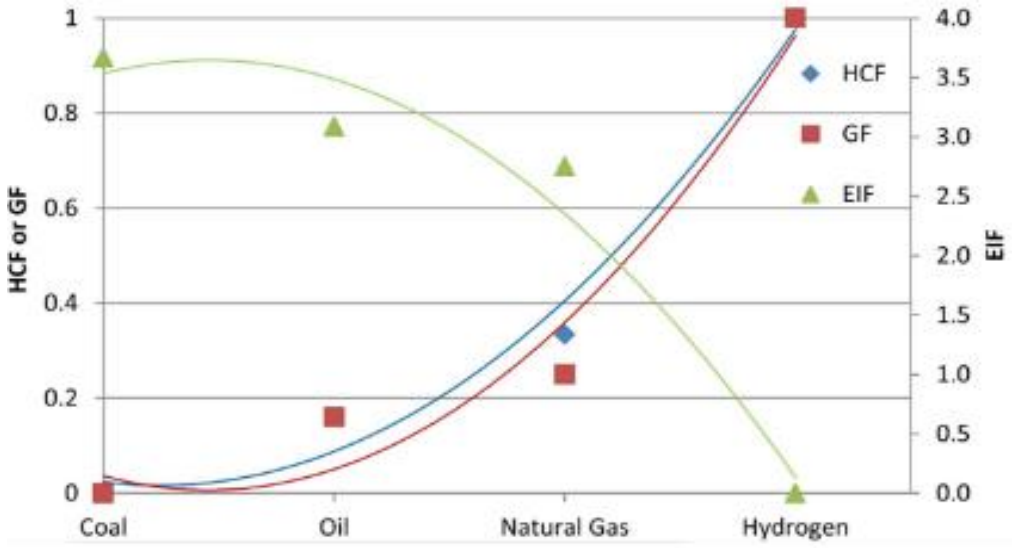

Figure 2: HCF, GF, and EIF of coal, oil, natural gas, and hydrogen [17].

Green hydrogen has versatile applications across various sectors. In electricity generation, it serves as a clean fuel source in power plants, where it undergoes conversion into electricity through fuel cells. The transportation sector can harness the benefits of green hydrogen as a suitable fuel for a range of vehicles, including automobiles, buses, trains, and trucks. Stored in fuel tanks, green hydrogen can be efficiently transformed into electricity within the vehicle using fuel cells [18].

Industries that rely on hydrogen as a fuel or raw material, such as fertilisers, chemical, and glass manufacturing, stand to gain advantages by incorporating green hydrogen into their processes. Furthermore, the aviation industry shows promise in using green hydrogen as a fuel for aircraft, particularly in hybrid models that employ both batteries and fuel cells to convert it into electricity. The versatile and clean attributes of green hydrogen make it a valuable competitor in advancing sustainability across these diverse sectors [18]. However, several challenges, such as high costs, efficiency of fuel cells, safety for storage and transportation as well as infrastructure development hinder the widespread use of green hydrogen [19]. It is expected that despite these barriers, technological breakthroughs and more funding for the industry will overcome them [18].

1.2 Problem Statement

A comprehensive assessment of the process design and possible benefits of establishing a green hydrogen production ecosystem in Lesotho for use in a variety of industries, such as home, agricultural, and transportation, still needs to be accomplished. In spite of the ample renewable resources in Lesotho, there is a significant lack of information concerning the most effective design methodology for the production of green hydrogen. This research seeks to bridge this gap in scientific and literary knowledge, addressing the void created by the absence of relevant studies.

1.3 Research Questions and Objectives

The primary objective of this chemical process design study for green hydrogen generation is to develop a detailed, optimised, and feasible process to produce hydrogen. Hence, the objectives of this study are:

- To identify the key processes and reactions involved in green hydrogen production.

- Establish mass balance and auxiliary equations for the entire system.
- Verify model accuracy through simulation results.

The following are some research questions that the study is intended to answer;

- What material balance equations are needed to track the flow of reactants and products throughout the hydrogen production process?
- How do the different components (electrolyser, separators, heater, coolers, mixers and purge) interact in the system?
- How does the efficiency of the electrolyser change with different operational parameters?

1.4 Justification

A comprehensive study examining the prospects of green hydrogen production in Lesotho holds significant promise in guiding the nation towards a sustainable and clean energy future. By delving into the country's abundant natural resources, encompassing vast expanses of land, ample water sources, and the potential for harnessing solar, hydro, and wind energy, the research study elucidates how these elements can be optimally used. Furthermore, advancements in technology offer a critical avenue for enhancing efficiency in green hydrogen production.

Beyond environmental considerations, the study has the potential to uncover substantial economic advantages associated with transitioning to a hydrogen-based economy. These benefits include job creation, reduced dependence on imports, enhanced energy self-reliance, and the creation of lucrative investment opportunities. Moreover, the study offers valuable insights for developing a sustainable solution tailored to meet Lesotho's unique energy needs. The study's robust analysis can help inform the development of targeted policies to assist the growth of the green hydrogen sector. It can also assist attract domestic and foreign investors who are interested in capitalising on the country's renewable energy opportunities. Finally, this research initiative has the potential to illuminate a path for Lesotho to leverage its inherent resources and technological advancements for a greener, economically robust, and energy-efficient future.

1.5 Report Structure

This research is organized in the following manner: Chapter 2 presents a review of the literature related to hydrogen, hydrogen production and generation of green hydrogen, storage methods as well as the design of plant processes. Chapter 3 outlines the theoretical approach/modelling development. The results and discussions are presented in Chapter 4, while Chapter 5 offers concluding remarks, recommendations, and final observations.

2 LITERATURE REVIEW

2.1 Hydrogen Element

The most prevalent element in the universe is hydrogen (H_2). It is primarily present on earth in water and organic compounds, in particular, hydrocarbons, which are crucial parts of a variety of our energy sources, such as methanol, natural gas, and petrol [20, 21, 22]. With only one electron and one proton, hydrogen is the lightest and simplest element [20]. It is a flammable and colourless gas, and has no odour [23]. Hydrogen has an atomic mass of 1.00794 atomic mass units, which can be rounded to 1.008 [24].

With a specific gravity of 0.0696, hydrogen is one of the lightest gases known as mentioned before. As a result, it is highly buoyant and can rise through the atmosphere with ease. Since it requires a considerable amount of energy to liquefy and has a startlingly low boiling point (-252.78°C), liquid hydrogen is a dangerous cryogenic fluid. Liquid hydrogen has a density of 67.806 kg/m^3. It maintains an astonishing lightness, even though a gallon of water contains a greater mass of hydrogen. It is rare for liquid hydrogen to reach the ground in its liquid condition because of its extraordinarily low boiling point, which causes any leak to vaporise quickly [25].

2.2 History of Hydrogen

2.2.1 Early Discoveries of Hydrogen

The discovery of hydrogen, a substance that has been known for more than 200 years, was made possible in the early 16th century by Paracelsus, a Swiss alchemist, who realised that a gas was produced when sulfuric acid reacted with iron [26]. English chemist and physicist Robert Boyle also made the discovery of hydrogen as a separate element in 1761. Iron filings and weak acids were used in his synthesis [23]. Moreover, Henry Cavendish identified hydrogen as a distinct element in the year 1776. As a result of his significant discoveries, which were recorded in a paper submitted to the Royal Society of London, he also received the title "discoverer of hydrogen" [23], [24], [26], [27]. In the year 1783, Antoine Lavoisier synthesised hydrogen as well [23], and in 1788, he named it "hydrogen" (alternatively "hydrogenium"), a term derived from the Greek word "hydro", signifying "water" [24].

Hydrogen production saw the emergence of new technology around 1800 when English scientists William Nicholson and Anthony Carlisle pioneered the production of hydrogen using electrolysis. In 1898 James Dewar created a regenerative cooling device that was used to liquefy it [24], [26]. Liquid hydrogen was used in 1839 when Sir William Robert Grove, a

British scientist and attorney, developed the first fuel cell that ran on hydrogen. His discovery set the path for the advancement of contemporary fuel cell technology, which is used in various applications, such as electric vehicles, power generation, and small devices [23].

In addition, hydrogen was used from 1900 to maintain the airframe of the first balloon constructed by German Count, Ferdinand von Zeppelin [26]. Historical advancements in the use of hydrogen have also been made by NASA, which was founded in 1958 with the intention of exploring space. By 1961, it was the biggest user of liquid hydrogen in the world, using it as a fuel for rockets and other spacecraft [24].

2.3 Hydrogen Production

Despite being the most abundant element in the universe, hydrogen is never found on its own because it readily reacts with other elements. Therefore, hydrogen production relies on the principle of removing other molecules from hydrogen compounds [28]. A wide variety of methods and energy sources can be used to generate hydrogen. Based on the process of production and the source of energy, hydrogen is categorised through a color-coded scheme [29]. Currently, there are three primary methods of hydrogen production: Grey hydrogen production using fossil fuels such as natural gas or coal, leading to significant CO_2 emissions; Blue hydrogen generation by integrating grey hydrogen production with carbon capture and storage (CCS) technologies to reduce CO_2 emissions as well as producing Green hydrogen by harnessing renewable energy sources such as solar or wind power to electrolyse water, resulting in a process entirely devoid of carbon emissions [30]. Additional types of hydrogen have been introduced to the spectrum, including turquoise hydrogen, which is generated through methane pyrolysis (leading to solid carbon formation rather than CO_2) and pink hydrogen, which is produced through water electrolysis powered by nuclear energy [31].

Around 87 million tonnes of raw materials, both renewable and non-renewable, are used to manufacture hydrogen annually [24]. Fossil fuels such as coal and natural gas are nearly exclusively used in the manufacture of hydrogen globally [30]. As of 2020, the vast majority of hydrogen (95%) was produced from non-renewable fossil fuels, primarily through steam reforming of natural gas. Given its prominence in China, coal comes in second place. It utilises 107 million tonnes of coal (or 2% of the world's total coal consumption) and contributes to an estimated 23% of the world's devoted hydrogen production. These processes emit 830 million tonnes of CO_2 per year. The remaining portion (5%) is produced from oil and electricity from

renewable resources through water electrolysis [32], [33]. In Figure 3, the hydrogen production pathways and their associated sources are depicted.

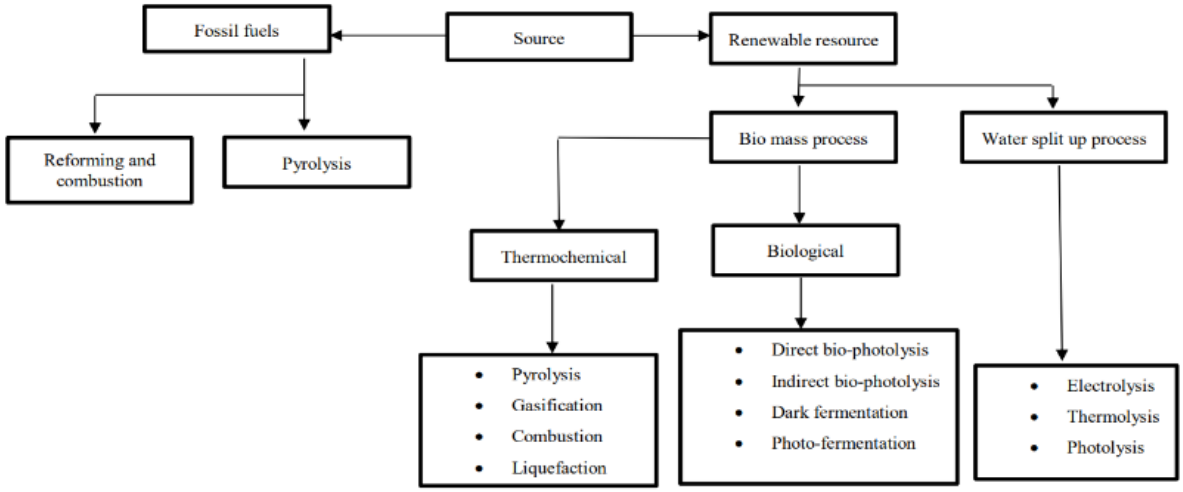

Figure 3: Classification of Hydrogen production routes and sources [34].

2.3.1 Hydrogen Production from Fossil Fuels

The processing of fossil fuels involves the utilization of hydrogen-rich fossil fuels such as gasoline, hydrocarbons, methanol, or ethanol to generate a hydrogen-enriched gas stream. Presently, the predominant industrial method for hydrogen production is the processing of methane (natural gas) [35]. Processes such as: Steam reforming (SR), Partial oxidation (POX), and Auto-thermal reforming (ATR), can be used to produce hydrogen gas from hydrocarbon fuels. Carbon monoxide (CO) is produced in large quantities as a result of these processes. Consequently, at a later phase, one or more chemical reactors are utilised to primarily convert CO into carbon dioxide (CO_2) by means of reactions such as methanation reactions or the water-gas shift (WGS) and preferential oxidation (PrOx) [35], [36].

2.3.1.1 Fossil Hydrocarbon Reforming Technologies

The most advanced method for producing hydrogen is hydrocarbon reforming. For this process, other reactants such as steam or oxygen are needed in addition to hydrocarbons [36].

2.3.1.1.1 Steam Reforming

When a mixture of steam and hydrocarbons react at high temperatures, carbon oxides and hydrogen are produced. This process is known as the steam reforming reaction. Through the process of steam reforming, hydrogen can be extracted from natural gas and, less commonly, from naphtha and liquefied petroleum gas [33]. The low operating and production expenses

and excellent operational efficiency are its main advantages. The steam reforming reaction can be represented as follows:

Hydrogen and carbon monoxide are produced, giving rise to synthesis gas

$$CH_4 + H_2O \rightarrow CO + 3H_2 \quad (4)$$

The carbon monoxide is subsequently transformed to carbon dioxide and extra hydrogen via the water-gas shift process [37].

$$CO + H_2O \rightarrow CO_2 + H_2 \quad (5)$$

The overall steam reforming reaction is depicted below:

$$CH_4 + 2H_2O \rightarrow CO_2 + 4H_2 \quad (6)$$

Due to the strong endothermic nature of the reforming reaction, a significant quantity of heat is needed. Because of this, these reactions are normally conducted between 800 and 1000 °C [38].

2.3.1.1.2 Partial Oxidation

An alternate strategy to steam reforming reactions is partial oxidation. Methane, coal, heavy fuel oil, and other feedstock can all be used in this process [33], [39]. A combination of hydrogen, carbon monoxide, and other partially oxidised species are produced from hydrocarbon fuels by the exothermic process of partial oxidation [40]. Reactions with oxygen are very exothermic in this method, which means that no external energy source is required. This is one of its advantages [41]. For partial oxidation processes at lower temperatures, heterogeneous catalysts are typically used since high reaction temperatures (>1000 °C) restrict the product dispersion of these reactions. Transition-metal-based catalysts may alter oxidation states and adsorb reactants and intermediates onto their surface, making them more affordable than noble metals for partial oxidation processes [42]. The following is the reaction of partial oxidation:

$$CH_4 + O_2 \rightarrow CO + 2H_2 \quad (7)$$

$$CH_4 + 2O_2 \rightarrow CO_2 + 2H_2O \quad (8)$$

$$CH_4 + H_2O \rightarrow CO + 3H_2 \quad (9)$$

The gaseous mixture that results from partial oxidation includes carbon oxy-sulphide (COS), hydrogen sulphide (H_2S), H_2, CH_4, CO, and CO_2. To provide the endothermic reactions with

enough heat, a portion of the gas is burned. This process results in a substantial production of greenhouse gases [35].

2.3.1.1.3 Auto-thermal Reforming

Auto-thermal reforming combines the exothermic partial oxidation with O_2, generating the necessary energy for the endothermic steam reforming reactions [43]. This means that there is a simultaneous oxidation and reforming process in the reformer, resulting in a thermodynamically neutral reaction, since the reformer is filled with both steam and oxygen [44]. This method demands less energy input compared to partial oxidation or steam reforming due to its high thermal efficiency [45]. The auto-thermal reforming reaction occurs as follows:

$$CH_4 + 1.5O_2 \rightarrow CO + 2H_2O \quad (10)$$

$$CO + H_2O \rightarrow CO_2 + H_2 \quad (11)$$

$$CH_4 + H_2O \rightarrow CO + 2H_2 \quad (12)$$

2.3.2 Overview of Green Hydrogen Production

As the world transitions to a decarbonized future, green hydrogen generation powered by renewable energy is gaining traction [46], [47]. Green hydrogen is widely regarded as a promising fuel for advancing sustainable development and energy transition in the future. This stems from the fact that green hydrogen can be generated using environmentally friendly feedstock, including biomass and water, in conjunction with renewable energy sources through processes such as water splitting and biomass conversion. Importantly, these processes are devoid of any greenhouse gas emissions. Consequently, green hydrogen is gaining traction as the key solution for addressing climate change concerns and fulfilling global net-zero targets [48].

Furthermore, there is a growing anticipation that the global demand for green hydrogen and its diverse applications will experience a remarkable surge in the coming decade. Encouragingly, numerous initiatives are currently in progress on a global scale to generate green hydrogen using renewable energy sources such as wind, hydro, biomass and solar power [47, 48, 49]. Numerous research studies have explored the viability of producing green hydrogen using various renewable energy sources.

In their research, Mazzeo et al. [50] explored the integration of diverse renewable sources, specifically wind and solar energy, to facilitate the widespread production of hydrogen on a

large scale. Researchers devised a methodology to evaluate renewable energy systems in various locations worldwide. Al-Sharafi et al. [51] examined the feasibility of harnessing solar and wind energy resources for power generation and hydrogen production at various sites within Saudi Arabia. Ishaq and Dincer [52] conducted a comparison of hydrogen generation methods based on renewable energy sources, with a focus on biomass, solar, and geothermal technologies. Their findings demonstrate the higher energetic efficiency of the biomass gasification process when compared to hydrogen generating systems utilising solar or geothermal energy [52].

Moreover, a techno-economic analysis of decentralised hydrogen production in Europe was conducted by Bhandari et al [53]. Six scenarios were analysed in that study, taking into account the support of the national grid, an auxiliary battery, and two distinct electrolyser technologies (alkaline and Proton Exchange Membrane), which will be discussed later in this study. They discovered that the best outcomes came from grid-connected solar photovoltaic (PV) systems that ran an alkaline electrolyser. Onshore hybrid energy systems that produce green hydrogen using solar and wind power have been examined [54, 55, 56, 57].

Kalinci and colleagues opted for an alternative approach as they examined the diverse methods of biomass-to-hydrogen conversion [58]. Initially, they categorized these methods into two primary groups: thermo-chemical processes and biological conversions [58]. Subsequently, they delved into a comprehensive discussion of these systems, scrutinizing their energetic facets, while also offering a concise summary of potential comparative methodologies.

However, there have been limited studies conducted on harnessing wind, hydro, solar and bio energy for hydrogen production in African countries [59, 60, 61, 62]. Ayodele and Munda conducted an evaluation of the viability and economic efficiency associated with producing green hydrogen from South Africa's wind energy reserves [62]. Their findings indicated a potential annual hydrogen output ranging from 6.51 to 226.82 metric tons, with associated production costs varying between $1.4 and $39.55 per kilogram and contingent upon the specific wind turbine model employed. Previous research has established a consensus that solar energy and onshore wind are the most favourable sources for producing green hydrogen. This preference stems from their well-established industries and extensive infrastructures, featuring large-capacity farms deployed globally [49].

Presently, no studies have been undertaken regarding green hydrogen production in Lesotho, despite the country's abundant resources such as land, water from rivers and valleys, wind

speeds of 6 m/s or higher and average daily solar irradiation of over 5 kWh/m^2 for generating substantial quantities of green hydrogen [63], [64]. Consequently, this study marks the inaugural study in a series of forthcoming investigations.

2.3.3 Hydrogen Generation from Renewable Sources

While the majority of hydrogen is currently derived from hydrocarbons, as previously stated, there is a growing focus on using renewable resources to generate green hydrogen [65]. In this context, green hydrogen can be generated using water or compounds derived from biomass.

2.3.3.1 Hydrogen Production from Water

Water is the most abundant resource on Earth, and it is a primary source for hydrogen production. When sufficient energy from wind, solar or biomass is supplied water can be separated into hydrogen and oxygen [28], [66]. This separation process, known as water splitting, involves the passage of an electrical current (electrolysis) through two electrodes to break down water into its constituent elements, hydrogen and oxygen [67]. Other forms of energy can also be used to split water, including thermal energy (thermolysis), photonic energy (photo-electrolysis), and bio-photolysis (microorganisms) [36].

Table *1* offers a concise overview of the essential technologies employed in hydrogen production from water. It encompasses details about the energy sources, operational parameters, and the technological advancement level of the processes under development.

Among the range of energy technologies, using renewable electricity for water electrolysis to produce hydrogen (H_2) is the best option for energy storage because H_2 is the ultimate energy carrier and can be converted into electricity through fuel cell technologies. Therefore, developing water electrolysis technologies is crucial and urgent in order to produce H_2 [68]. Solar and wind energy sources are well-suited and readily available for the production of hydrogen through water electrolysis, owing to their extensive power distribution [69].

Table 1: Hydrogen Production Technologies from Water

Technology	**Energy source**	**Operating conditions**	**Maturity**

Electrolysis	Electricity	Up to 30 bar commercial 50−900 °C (depending upon the method used)	Commercial
Thermolysis	Heat	Temperature of >2500 °C (<1000 °C for thermochemical cycles)	Research and development
Photoelectrolysis	Solar	Ambient conditions	Research and development
Biophotolysis	Microorganism metabolism	Ambient conditions	Research and development

2.3.3.1.1 Water Electrolysis

Water electrolysis represents an electrochemical method for splitting water as well as generating green hydrogen through electricity to make it an emission-free technology. The fundamental process of water electrolysis can be described using Equation 13 as follows:

$$H_2O + Electricity(237.2\ kJ\ mol-1) + Heat(48.6\ kJ\ mol-1) \rightarrow H_2 + {}^{1}/_{2}\, O_2 \qquad 13$$

The aforementioned chemical reaction, denoted as Equation 13, necessitates a theoretical thermodynamic cell voltage of 1.23 V at room temperature in order to facilitate the electrolysis of water into hydrogen and oxygen. Nevertheless, experimental observations reveal that an operational cell voltage of 1.48 V is essential for efficient water splitting. This increment in voltage is attributed to the necessity of surmounting kinetic and ohmic resistances within the electrolyte and cell constituents of the electrolyser [70, 71, 72]. Over the last two centuries, water electrolysis has emerged as a widely recognized technology for the environmentally sustainable generation of hydrogen. Nevertheless, on a global scale, 4% of the total hydrogen output, equivalent to 65 million tons, is attributed to water electrolysis, primarily stemming from economic constraints. A substantial proportion of this hydrogen production is derived as a by-product within the Chlor-alkali industry [73], [74], [75].

2.3.3.1.1.1 Classification of Water Electrolysis Technologies

Water electrolysis technologies can be classified into four distinct types, each characterized by specific electrolytes, operating conditions, and ionic agents (OH^-, H^+, O^{2-}). These types of electrolysis technologies include (i) Alkaline Water Electrolysis (AWE), (ii) Anion Exchange Membrane (AEM) water electrolysis, (iii) Proton Exchange Membrane (PEM) water

electrolysis, and (iv) Solid Oxide Water Electrolysis (SOWE). Despite the differences in electrolyte and ionic agents, the fundamental operating principles remain consistent across all these variants [2].

Illustrated in Figure 4 is the global installed electrolysis capacity based on technology and spanning the years 2015 to 2020. In the year 2020, alkaline electrolysers constituted the majority with 61% of the installed capacity, whereas PEMs comprised 31%. In addition, an installed capacity of 0.8 MW was associated with Solid Oxide Water Electrolysis Cells (SOWECs), and an unspecified electrolyser technology [48]. The installed capacity of electrolysers globally is expected to rise significantly in the next ten years, possibly reaching 54 GW by 2030 when taking into account both planned and ongoing projects. The overall capacity could exceed 91 GW if early planning projects are also included. Geographically, the leading regions are Australia and Europe, with 22 GW and 21 GW of projects under development, respectively. With 5 GW and the Middle East with 3 GW of projects in various phases of development, Latin America and the Middle East follow closely behind as shown in Figure 5 [48].

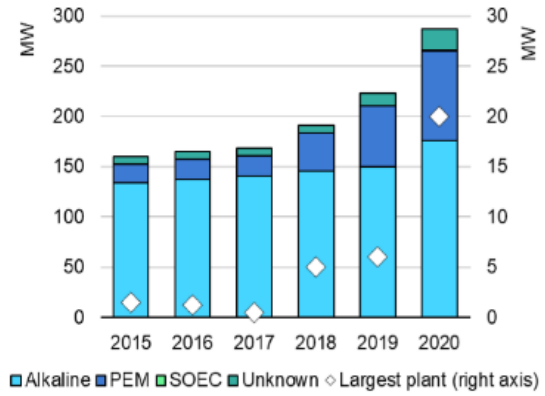

Figure 4: Global installed electrolysis capacity by technology (2015-2020) [48].

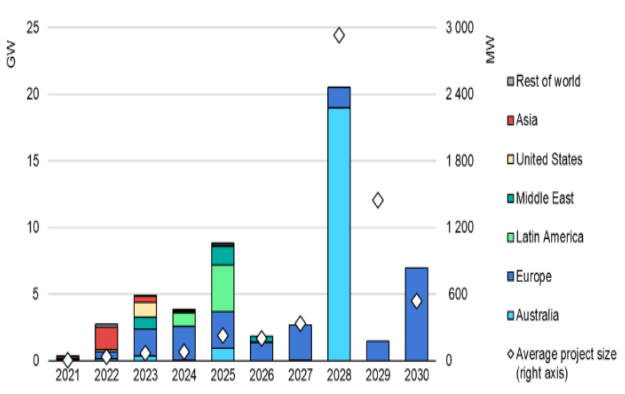

Figure 5: Projects under construction or planned, 2021-2030 for newly installed electrolyser capacity [48].

I. Alkaline (ALK) Water Electrolysis

Alkaline water electrolysis stands out as the most established and widely adopted technology for splitting water, commanding a significant market share [76]. This technology has an electrical efficiency of up to 70% and is characterised by the low cost and long operational life [77]. Hence, employing this technology in Lesotho, a country characterized by numerous rivers and streams with alkaline water, could be a viable and sustainable choice. In 1789, Troostwijk

and Diemann introduced the concept of alkaline water electrolysis. Further developments in 1939 resulted in the construction of the first industrial alkaline water electrolyser plant, which was able to produce 10 000 N m^3 H_2h^{-1} [69]. During the latter part of the early 19th century, over 400 industrial alkaline electrolyser units were effectively installed and used for industrial purposes [78].

Alkaline electrolysis functions at relatively lower temperatures, typically ranging from 30 to 80 ℃. It utilises an aqueous solution (KOH/NaOH) as the electrolyte, with an electrolyte concentration ranging from approximately 25% to 30% [69], [76]. Nickel electrodes and an asbestos diaphragm are used in the alkaline water electrolysis method [39]. Figure 6 illustrates a schematic depiction of alkaline water electrolysis along with its underlying mechanism. The reactions occurring at the anode and cathode can be described through Equations 14, 15 and 16.

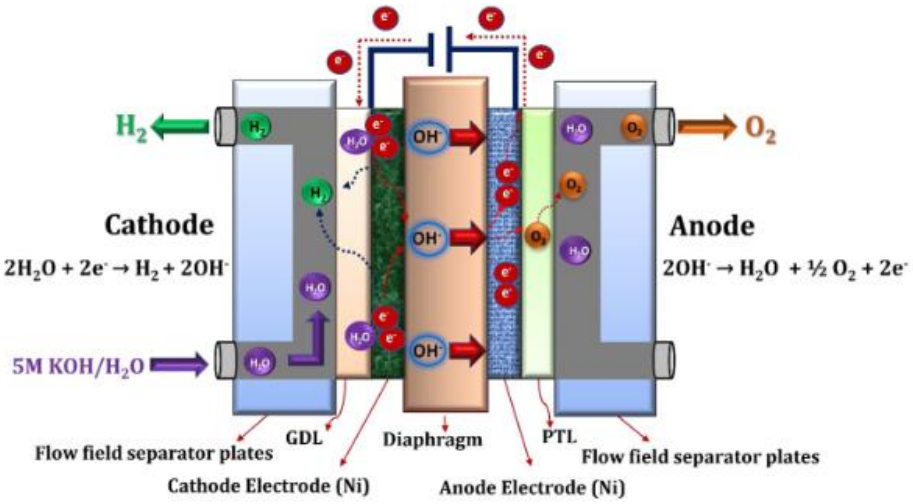

Figure 6: Schematic representation of alkaline water electrolysis working mechanism [69].

$$ANODE:\ 2OH_{(aq)}^{-} \rightarrow 0.5O_{2(g)} + H_2O_{(l)} + 2e^{-} \quad (14)$$

$$CATHODE:\ 2H_2O_{(l)} + 2e^{-} \rightarrow H_{2(g)} + 2OH^{-}{}_{(aq)} \quad (15)$$

$$\text{OVERALL REACTION: } H_2O_{(l)} \rightarrow 0.5O_{2(g)} + H_{2(g)} \quad (16)$$

Alkaline water electrolysis cells are primarily composed of end plates, separator plates (also known as bipolar plates), current collectors (also known as gas diffusion layers) and diaphragms/separators. Generally, diaphragms used in alkaline water electrolysis as separators

are made of materials such as asbestos, zirfon, or nickel-coated perforated stainless steel [79], [80]. While the bipolar and end plates use stainless steel or stainless steel covered with nickel as separator plates, the gas diffusion layers use nickel mesh or foam [69].

The alkaline water electrolysis process begins with the reduction of two molecules of alkaline solution (KOH/NaOH) to one molecule of hydrogen (H_2) and the generation of two hydroxyl ions (OH) at the cathode. The produced H_2 is released from the cathode surface, recombining in a gaseous form. Simultaneously, the hydroxyl ions (OH^-) migrate through a porous diaphragm, driven by the electrical circuit between the anode and cathode. Upon reaching the anode, the hydroxyl ions (OH^{-1}) undergo discharge, resulting in the formation of ½ molecule of oxygen (O_2) and one molecule of water (H_2O). The oxygen (O_2) recombines at the electrode surface and is released as a gas [2], [81]. The diaphragm, which is positioned in the middle of the cell, keeps the anode and cathode apart. This keeps the gases generated at each electrode from combining and guarantees that the process of electrolysis proceeds efficiently [2].

Nonetheless, a significant obstacle in alkaline water electrolysis stems from restricted current densities (0.1–0.5 A/cm^2) attributed to moderate OH^- mobility and the employment of corrosive (KOH) electrolytes [29]. Because the KOH electrolyte is highly sensitive to ambient CO_2, it leads to the formation of K_2CO_3 salt, causing a reduction in the number of hydroxyl ions and ionic conductivity. In addition, the K_2CO_3 salt closes the pores of the anode gas diffusion layer, resulting in a decreased transfer of ions through the diaphragm and a subsequent decline in hydrogen production. Furthermore, alkaline water electrolysis yields gases (Hydrogen and Oxygen) with low purity (99.9%) because the current diaphragm fails to effectively prohibit gases from crossing between half-cells [69].

Innovation is underway to create alternative diaphragm materials through the development of new materials [67]. In this regard, certain researchers such as Liu et al. [82], Lv et al. [83] and Qazi et al. [84] are persistently working to improve efficiency and reduce the costs associated with green hydrogen production through this technology. This represents a significant breakthrough for developing countries such as Lesotho, emphasizing the importance of cost-effectiveness in advancing sustainable practices.

II. Anion Exchange Membrane (AEM)

Miller et al. [85] describe how the AEM water electrolysis technology is similar to traditional alkaline water electrolysis. A crucial difference between AEM water electrolysis and alkaline water electrolysis is the use of quaternary ammonium ion exchange membranes in place of

conventional diaphragms or asbestos. One benefit of AEM water electrolysis is that transition metal catalysts can be used at a lower cost than noble metal catalysts. In addition, it eliminates the need for a high-concentration solution (5 KOH) that is present in conventional alkaline water electrolysis and permits the use of purified water or a low-concentration alkaline solution (1M KOH) as the electrolyte [86].

In spite of its notable benefits, this technology necessitates additional research and improvements focused on enhancing the stability of the Membrane Electrode Assembly (MEA) and improving cell efficiency. Researchers such as Thangavel et al. [87], Jang et al. [88], [89] and Guo et al. [90] have explored and documented strategies to address the challenges encountered by the technology. These aspects are particularly crucial for the successful deployment of the technology in large-scale or commercial applications. In the field of producing green hydrogen, AEM water electrolysis is a developing technology. Because AEMWE is more efficient and performs better than conventional electrolysis technologies, many research organisations and universities have been actively working to further its development in recent years [91], [92].

Figure 7 presents a schematic representation of AEM water electrolysis, showcasing its fundamental mechanism. The processes taking place at the anode and cathode can be elucidated using Equations 17, 18, and 19. In AEM water electrolysis cells, the typical components include a membrane (separator), electrode materials with gas diffusion layers (current collectors), separator plates (bipolar plates), and end plates. Anion exchange membranes commonly consist of quaternary ammonium ion exchange materials such as Fumatech, Sustanion, and Fumasep. Anode and cathode electrode materials often employ transition metal-based electro-catalysts, with nickel and nickel-copper alloy materials being common choices. The gas diffusion layers for the anode and cathode incorporate materials such as carbon cloth, nickel foam, and porous nickel mesh. Bipolar and end plates are typically constructed using stainless steel, often nickel-coated [93].

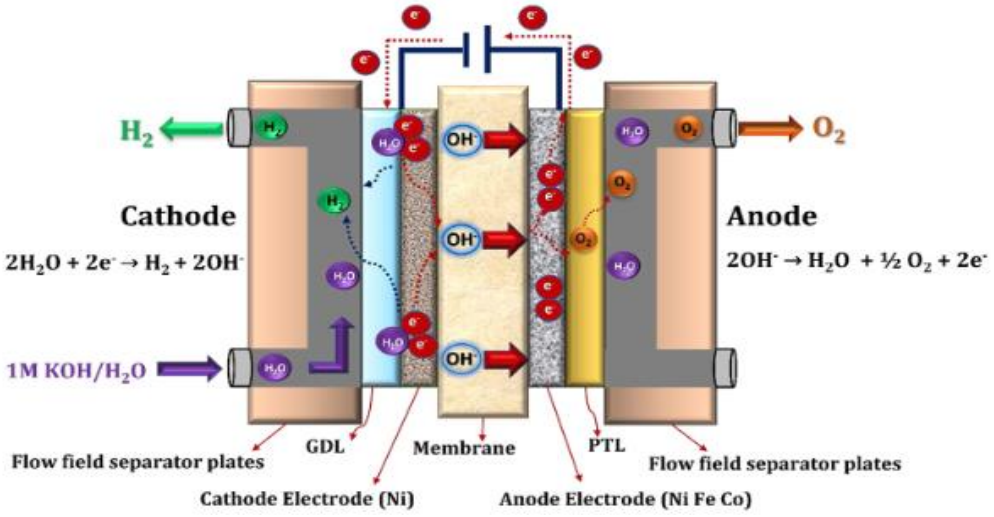

Figure 7: Diagram illustrating the basic principles of AEM water electrolysis [69].

$$ANODE:\ 2OH_{(aq)}{}^{-} \rightarrow 0.5O_{2(g)} + H_2O_{(l)} + 2e^{-} \quad 17$$

$$CATHODE:\ 2H_2O_{(l)} + 2e^{-} \rightarrow H_{2(g)} + 2OH^{-}{}_{(aq)} \quad 18$$

$$OVERALL\ REACTION: H_2O_{(l)} \rightarrow 0.5O_{2(g)} + H_{2(g)} \quad 19$$

The electrochemical process of this technology involves two key half-cell reactions: the hydrogen evolution reaction (HER) and the oxygen evolution reaction (OER). Initially, water molecules undergo a reduction at the cathode, yielding hydrogen (H_2) and hydroxyl ions (OH^-) through the addition of two electrons. The OH^- ions traverse the ion exchange membrane, propelled by the positive pull of the anode, while the generated hydrogen exits the cathode surface. Concurrently, electrons travel from the anode through the external circuit. On the anode side, the hydroxyl ions, having relinquished electrons, recombine to form oxygen and water molecules. Subsequently, the anode releases the produced oxygen [69].

III. Proton Exchange Membrane (PEM) Water Electrolysis

Solid polymer membranes have been studied for use in PEM fuel cell technology as a potential solution to the corrosion caused by the alkaline electrolysis process. The first PEM water electrolysis phenomenon was idealized by Grubbs and developed by General Electric Co. in 1966 [67]. PEM electrolysers stand out due to their numerous benefits compared to alternative electrolysis technologies. These advantages encompass a streamlined design, elevated current densities exceeding 2 A/cm^2, remarkable voltage efficiency, swift responsiveness to power input (on the scale of milliseconds), rapid start-up times, operational efficiency at lower

temperatures (50–80 ℃), exceptional gas purity at 99.99% and the ability to operate at high pressures, around 80 bar. This high operational pressure provides the added advantage of delivering hydrogen at elevated output pressures, thereby reducing the energy required for hydrogen compression and storage [94].

PEM water electrolysis is one of the more advantageous ways to convert renewable energy sources into highly pure hydrogen, both in terms of sustainability and environmental impact [2]. Furthermore, PEM electrolysis plant balancing is quite relatively simple, making it more appealing for industrial applications. The most advanced electro-catalysts for PEM electrolysis are noble metals with high activity, such as Pt and Pd, which operate as the cathode's HER. IrO_2/RuO_2 serves as the catalyst for the OER occurring at the anode. While PEM water electrolysis holds considerable promise, various challenges impede its widespread acceptance. A significant obstacle is the elevated expenses associated with essential components, including electrode materials, current collectors, and bipolar plates. [2]. In addition, there is a need for further improvements to minimize the cost of hydrogen production using PEM water electrolysis. As of 2020, the existing cost of hydrogen production stands at USD 700–1400 per kilowatt-hour (kW/H_2), with a projected cost reduction target of USD ≤ 200 per kilowatt-hour (kW/H_2) by the year 2050 [95].

Commonly employed proton exchange membranes include Nafion, Fumapem, Flemion, and Aciplex, with Nafion (specifically Nafion 115, 117, and 212) being the most prevalent. This preference is attributable to the manifold benefits offered by Nafion, encompassing elevated proton conductivity, substantial current density, robust mechanical strength, and chemical stability. In the realm of anode and cathode electrode materials, state-of-the-art choices revolve around noble metal-based electrocatalysts, notably IrO2 for the OER and carbon-supported Pt for the HER [96, 97, 98, 99].

Illustrated in Figure 8 is a schematic overview of PEM water electrolysis, providing an insight into its underlying mechanism. The reactions occurring at the anode and cathode can be explained by referencing Equations 20, 21 and 22. The primary components of the PEM water electrolysis cell encompass the membrane electrode assembly (comprising a membrane and materials for the anode and cathode electrodes), the gas diffusion layer, separator plates (also known as bipolar plates), and end plates, respectively [2], [100], [101], [102].

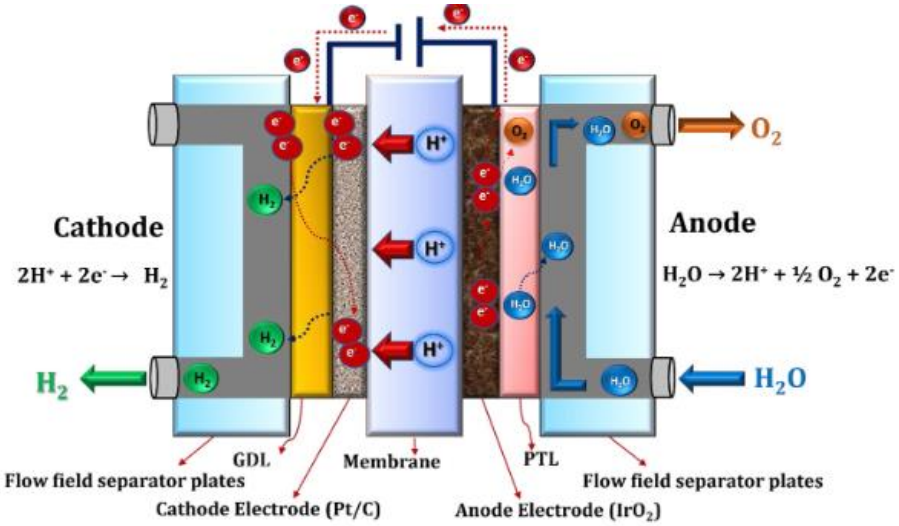

Figure 8: PEM working principle diagram [69].

$$ANODE: \quad H_2O_{(l)} \rightarrow 2H^+_{(aq)} + 0.5O_{2(g)} + 2e^- \qquad 20$$

$$CATHODE \ : \ 2H^+_{(aq)} + 2e^- \rightarrow H_{2(g)} \qquad 21$$

$$OVERALL\ REACTION: \ 2H_2O_{(l)} \rightarrow H_{2(g)} + 0.5O_{2(g)} \qquad 22$$

During PEM water electrolysis procedure, the electrochemical division of water into hydrogen and oxygen takes place. During this sequence, water molecules are initially decomposed at the anode to yield oxygen (O_2), protons (H^+), and electrons (e^-). The resulting oxygen is eliminated from the anodic surface, while the remaining protons traverse the proton-conducting membrane towards the cathode, and the electrons traverse the external circuit to reach the cathode. Upon reaching the cathode, the protons and electrons undergo recombination and thus producing hydrogen gas [69].

IV. Solid Oxide Water Electrolysis (SOWE)

The solid oxide water electrolysis cell (SOEC) belongs to the category of electrochemical conversion cells. It transforms electrical energy into chemical energy [103]. The solid oxide electrolysis (SOE) was initially presented by Donitz and Erdle during the 1980s [104], [105]. The significant focus on solid oxide electrolysis arises from its capacity to efficiently convert electrical energy into chemical energy, yielding high-purity hydrogen [105]. Generally, the solid oxide water electrolyser uses water in the form of steam at elevated temperatures (500–

850 ◦C). This can significantly lower the power consumption required for the water-splitting process, leading to an enhanced energy efficiency [69], [106], [107].

Since power consumption is the main factor affecting the total cost of producing hydrogen by electrolysis, improving energy efficiency has the potential to significantly lower the cost of hydrogen [108]. In addition, solid oxide water electrolysis presents two key benefits when contrasted with the current electrolysis methods. Firstly, its elevated operating temperature contributes to the advantageous thermodynamics and reaction kinetics, leading to unparalleled conversion efficiencies [68]. Secondly, solid oxide water electrolysis offers high conversion efficiency without the need for noble metal electro-catalysts. However, the commercialization of this technology has been hindered by limited long-term stability. Currently, the reported stability stands at 20,000 hours with a thin yttria-stabilized zirconia electrolyte [109].

Solid oxide water electrolysis technology is actively being developed and commercialised. Many organisations and research institutes throughout the world are currently working to continue developing this technology as well as addressing the existing challenges such as either substituting new perovskite materials or electrochemically modifying the present electrode materials to increase long-term stability [110]. Within this framework, Li et al. [111] synthesized a composite oxide material denoted as $Ni_{1-x}Cd_xO$-SDC and investigated its application as the hydrogen electrode in reversible solid oxide cells. In 2021, Kim and colleagues [112] presented novel cobalt-free perovskite materials denoted as $Ba_{1-x}Nd_xFeO_{3-\delta}$, which were introduced as an oxygen electrode in solid oxide cells.

Figure 9 presents a schematic representation of Proton Exchange Membrane (PEM) water electrolysis, offering a detailed depiction of its fundamental mechanism. The processes taking place at both the anode and cathode are elucidated through the utilization of Equations 23, 24 and 25. Three primary components make up a solid oxide water electrolysis cell include an anode and cathode, two permeable electrodes, and a thick ceramic electrolyte that can conduct oxide ions (O^{2-}). A typical electrolyte is yttria-stabilized zirconia (YSZ) which is a ceramic material based on dense zirconium oxide that has been doped with 8% yttria. Its cubic crystal structure is stabilised by the addition of yttria. The selection is based on the proven stability and outstanding performance of the yttria-stabilized zirconia electrolyte, especially at high temperatures (700–850 ◦C) [113], [114]. The latest advancement in hydrogen (cathode) electrode material is a ceramic metal called Ni-YSZ, which is a non-noble metal catalyst with

high electrical conductivity and is made of YSZ and nickel [113] and perovskite materials that stand out as the predominant choice for oxygen (anode) electrodes [115].

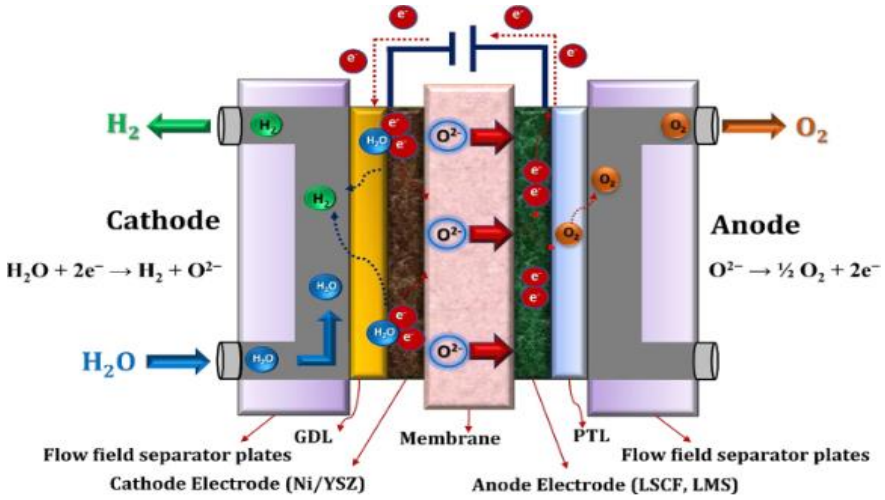

Figure 9: Diagram illustrating the basic principles of solid oxide water electrolysis [110].

$$ANODE \ : \ O^{2^-} \rightarrow 0.5O_{2(g)} + 2e^- \quad (23)$$

$$CATHODE :: \quad H_2O_{(l)} + 2e^- \rightarrow H_{2(g)} + {O^{2-}}_{(g)} \quad (24)$$

$$OVERALL\ REACTION: \quad H_2O_{(l)} \rightarrow H_{2(g)} + 0.5O_{2(g)} \quad (25)$$

Most solid oxide water electrolysis processes are carried out at high temperatures and need the use of steam as a source of water. Green oxygen and hydrogen are produced because of this process. Initially the reduction of water molecules at the cathode results in the addition of two electrons to generate oxide ions (O^{2-}) and hydrogen (H_2). Once released, the hydrogen moves away from the cathode surface and the remaining oxide ions (O^{2-}) travel across an ion exchange membrane to arrive at the anode. Electrons and oxygen are produced at the anode as the oxide ions (O^{2-}) are further reduced [116].

Table 2 outlines the advantages and disadvantages of the four water electrolysis technologies.

Table 2: Advantages and disadvantages of water electrolysis technologies [110].

Electrolysis technology	Advantages	Disadvantages
Alkaline water electrolysis	• Successfully applied in various industrial settings • Uses electro-catalysts without noble metals • Offers cost-effectiveness • Demonstrates prolonged stability over the long term.	• Restricted electrical current levels • Interference between gases • Elevated concentration (5M KOH) of liquid electrolyte.
AEM water electrolysis	• Electrodes devoid of noble metals • Liquid electrolyte with low concentration (1M KOH).	• In a phase of development • Limited stability
PEM water electrolysis	Technology available for commercial use • Functions at elevated current densities • Ensures high purity of gases. • Designed with compact system specifications. • Exhibits rapid response	• Expense associated with cell components • Electro-catalysts made from noble metals • Electrolyte with an acidic nature
Solid oxide water electrolysis	• Elevated operational temperature • Optimal efficiency	• In the process of development • Limited stability

2.3.3.2 Hydrogen Production from Solar Energy

A potentially viable and economically competitive source of renewable hydrogen in the near future involves the integration of photovoltaic panels with electrolysers as shown in Figure 10 [117]. The initial solar hydrogen production system (SHS) infrastructure was established in El Segundo, California, in 1995 [65]. This pioneering facility featured a sophisticated combination of advanced PV cells and electrolysers, capable of producing approximately 50–

70 cubic meters of hydrogen daily. Subsequent to this milestone, multiple SHS installations have been implemented to explore the practicality of solar-driven hydrogen production and to identify strategies for optimising the economic viability of this technology.

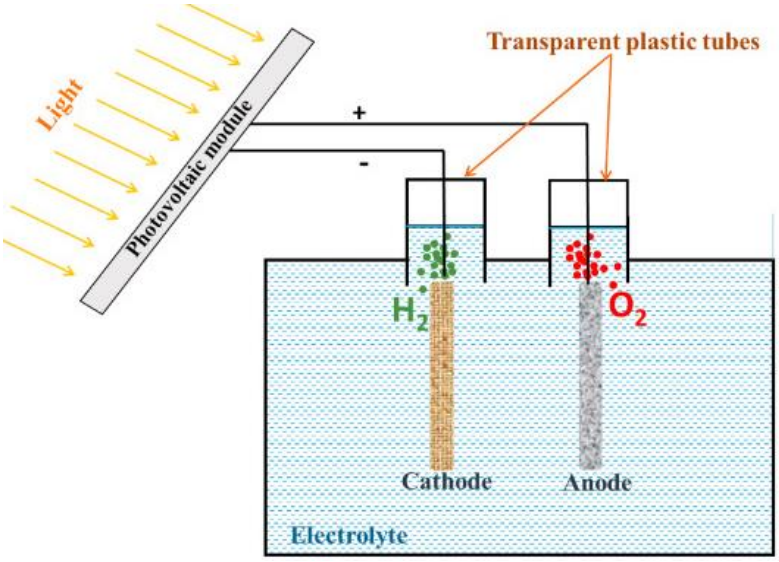

Figure 10: Schematic of photovoltaic panels coupled with an electrolyser [117].

These systems, often termed solar-hydrogen hybrid systems, use energy generated by photovoltaic panels to drive the electrolysis process. However, the current efficiency of such systems is insufficient to rival the economic competitiveness of hydrogen derived from fossil fuels. For instance, a recent demonstration highlighted a small-scale, high-cost photovoltaic to Proton Exchange Membrane electrolyser unit, achieving a peak solar-to-hydrogen efficiency of 31%. This was accomplished through the use of a high-efficiency triple-junction solar cell and two Proton Exchange Membrane electrolysers connected in series [118].

Nevertheless, the reported efficiency may be overly optimistic, as the demonstration employed a compact system with only a 2.5 cm × 2.5 cm active area on the electrolyser. In addition, the efficiency rating did not consider the energy consumption associated with heating, cooling, pumping and operational systems that are crucial for a commercial-scale setup. The demonstrated system relied on precious metals and high-cost materials, thus making it unsuitable for widespread commercial applications. The efficiency also declined over a 48-hour test period due to equipment degradation [118].

Producing hydrogen through the use of a PV system comes with certain constraints, including elevated installation costs and reduced efficiency in comparison to fossil fuels [65].

Nevertheless, the decreasing cost of manufacturing photovoltaic cells has resulted in a more economical per kilowatt-hour (kWh). By integrating the PV system with other energy sources or incorporating a battery storage system, overall efficiency can be enhanced, mitigating the challenges of exclusively generating hydrogen during daylight hours [117].

Jia et al. [118] emphasized the importance of using durable electrolysers to maintain system efficiency and utility, particularly in the context of commercial-scale operations. A photovoltaic system with enhanced efficiency generates more energy for a given module area, resulting in an increase in hydrogen production [117]. In this context, Kelly et al [119] introduced strategies aimed at aligning PV cells to optimise solar absorption in cloudy conditions.

This approach has the potential to enhance solar energy capture by more than 40%. In addition, given that elevated temperatures can compromise the efficiency of PV cells, a recommended solution involves redirecting the heat generated by PV systems to electrolysis. This transfer of heat to electrolysis serves to boost system efficiency, as higher temperatures are conducive to improved performance [119]. Therefore, the utilisation of solar energy for hydrogen generation in Lesotho is grounded in the opportunity to tap into the ample solar resources with optimal efficiency.

Floating photovoltaic (FPV) systems are also being explored as potential power sources for generating green hydrogen, particularly in coastal regions, due to their ability to enhance the feasibility of hydrogen production. Current projections suggest that by 2030, FPV is expected to contribute 10% of the total solar energy output. FPV exhibits a number of benefits over onshore PV, including low environmental impact, no fixed infrastructure, high power density, and easy dismantling. However, these benefits are offset by greater investment costs. [120].

In this scenario, Temiz and Dincer [121] introduced a comprehensive system designed to produce energy, ammonia, and hydrogen and to provide both heating and cooling effects. The system incorporates an FPV system, a district heating and cooling system, and a unit for generating hydrogen and ammonia, accompanied by pumped-hydro storage as illustrated in Figure 11. Their research indicates that, in usual circumstances, the hydrogen-based energy storage alternative exhibits a round-trip energy efficiency of 46.50% over the course of a typical meteorological year.

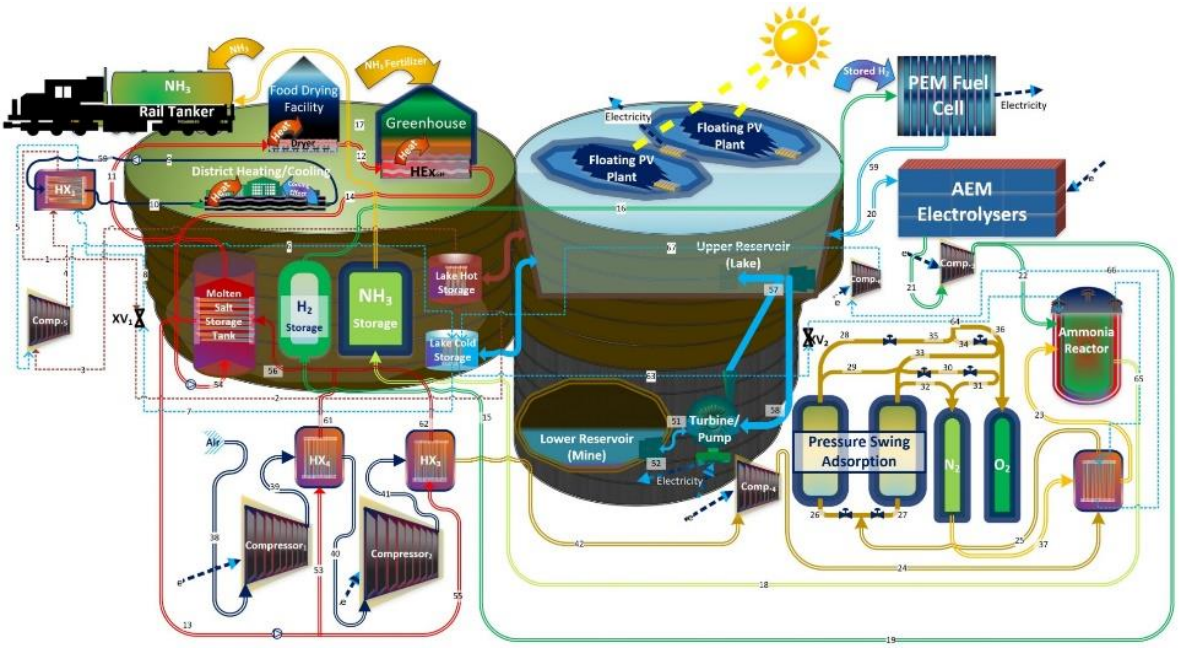

Figure 11: Design of the envisioned multi-generational system [121].

2.3.3.3 Hydrogen Production from Wind Energy

The process of water electrolysis powered by wind energy operates on the same underlying principle, as illustrated in Figure 12, which was previously explained in the context of solar energy. Using wind energy stands out as a straightforward and environmentally friendly method for hydrogen generation. The successful production of hydrogen through wind energy necessitates the presence of a well-established wind turbine infrastructure, an electrolysis unit, and a suitable system for storing the generated hydrogen [122].

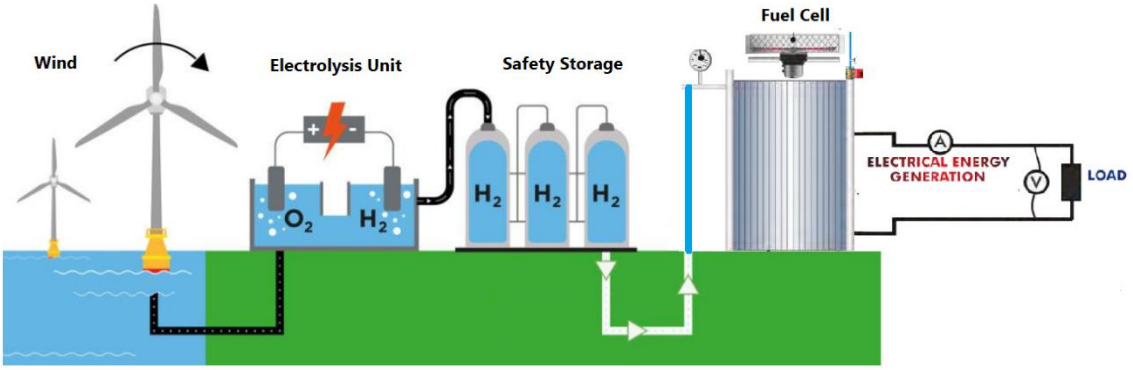

Figure 12: Illustration of hydrogen production from wind energy [123].

Numerous studies have explored the viability of generating hydrogen from wind energy. For example, Ayodele and Munda [62] conducted research in South Africa to assess the feasibility of implementing wind turbines. Their findings indicated that, depending on the turbine's capacity, the windiest location could yield anywhere from 6.51 to 226.82 metric tonnes of hydrogen. Similarly, Almutairi and colleagues [124] reported that the maximum wind energy potential at Iran's Bahabad and Halvan stations could generate 19.844 and 19.429 tons of hydrogen per year, respectively. A separate investigation conducted in Ukraine demonstrated a combined wind power capacity of 688 GW across its territory, capable of yielding an average annual production of 43 million tons of green hydrogen through electrolysis [125].

AbdelBasset et al. [126] underscored the significance of wind electrolysis and the need for precise energy assessments to ensure sustainable hydrogen production. Accurate estimates of wind speed were identified as crucial for enhancing system safety, streamlining dispatch processes, and minimizing revenue losses caused by the unpredictable nature of wind generation. AbdelBasset et al. highlighted how the previous oversight of the impact of virtual components on wind speed characteristics led to inaccurate predictions.

Generating hydrogen through wind power however faces certain challenges that must be addressed. They include the established structure of wind turbines, the need for an electrolyser capable of accommodating fluctuations in wind conditions, and the implementation of an effective hydrogen storage system [57].

2.3.4 Hydrogen Storage

Due to its low density when in a gaseous state, hydrogen necessitates a considerable volume to accommodate a small mass, impacting its suitability for energy storage purposes. For example, at standard pressure and temperature conditions, one cubic meter is needed to contain 1 kg of hydrogen [127]. Consequently, considerable research endeavours are focused on enhancing the density of hydrogen, which involves techniques such as using pressurized vessels and/or liquefaction. These approaches demand a substantial amount of energy in the form of work, heat, and, in some instances, materials that can bind hydrogen [117].

Hydrogen storage is typically categorized into two main types: physical storage and chemical storage. Figure 13 presents a diagram illustrating the different aspects of hydrogen storage. Detailed or concise explanations of these aspects can be found below.

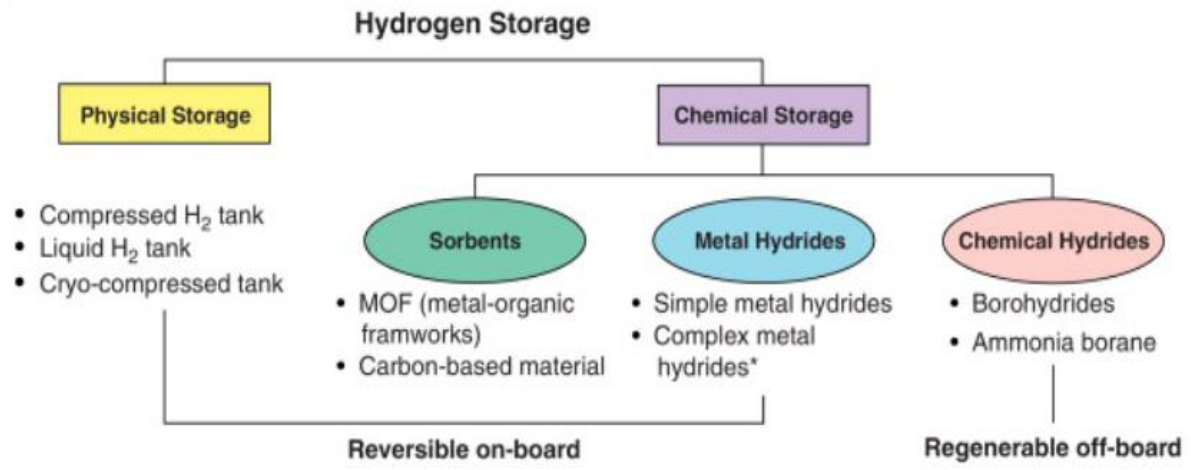

Figure 13: Illustration of Hydrogen storage [28].

2.3.4.1 Physical Storage

i. Compressed H_2 Storage

The method of storing hydrogen through pressurization has been employed for numerous years. This approach to hydrogen storage entails rapidly storing hydrogen gas under elevated pressure, typically ranging between 350 and 700 bar [128]. At present, the prevalent method for storing hydrogen involves the use of gaseous cylindrical pressure vessels with varying pressure levels, shapes and dimensions [129]. According to the aforementioned criteria, four distinct vessel types are illustrated in Figure 14 and are used to store compressed hydrogen gas [130]:

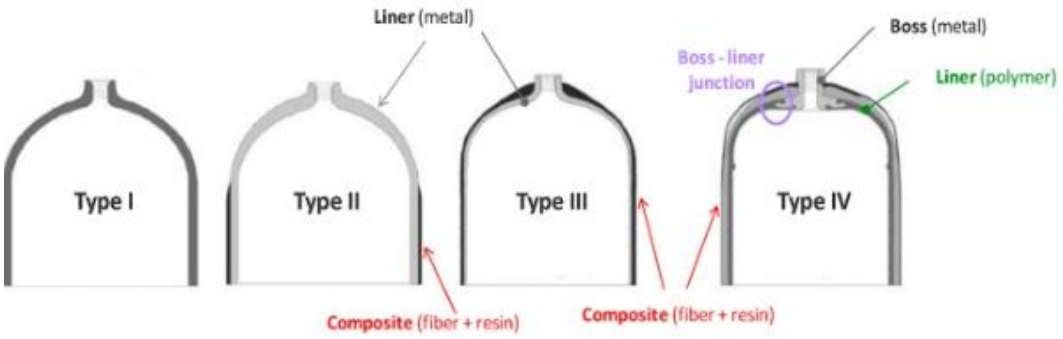

Figure 14: Hydrogen compressed tank types [131].

Type I: Representing the most economical choice, these vessels are crafted from metallic materials, capable of enduring pressures up to 30 bar. The primary construction materials include steel or aluminium alloy. However, for elevated hydrogen pressures or densities, the

metal wall thickness must be proportionately increased. This results in a heavier storage vessel, significantly reducing the net hydrogen gravimetric energy density. The vessels exhibit an exceptionally low gravimetric energy density, successfully storing about 1 wt% H_2 [130].

Type II: The cylindrical portion of the metallic walls of these vessels is covered in fibre resin composite [131], [132]. They weigh between 30 and 40 percent less than Type I, but at a 50% higher cost [133].

Type III or Type IV pressure vessels are constructed with the use of fully composite materials, consisting of either plastic or carbon fibres embedded in a polymer matrix through a filament winding process [131]. The key distinction between Type III and Type IV lies in their mechanical resistance. In Type III vessels, typically over 5% of the mechanical strength is attributed to a liner, often made of metal, classifying it as a Type III pressure vessel. In contrast, Type IV pressure vessels predominantly feature a liner made of polymer, with infrequent use of an exceptionally thin metal liner [131].

Compressed hydrogen-powered fuel cell vehicles have entered the commercial market, with an increasing number of units being sold and actively used on the roads. Notable examples include the Toyota Mirai (2021) and the Hyundai Nexo, an advanced model from the earlier Hyundai Tucson. These vehicles use compressed H_2 stored at 700 bar in three Type IV cylinders, enabling them to cover distances exceeding 600 km on a single charge [134], [135]. In addition, Hyundai has further introduced a commercial truck that operates on hydrogen at 350 bar and capable of traveling approximately 400 km on a full fill [130].

ii. Liquid / Cryogenic H_2 Storage

An alternative method to enhance the density of pure hydrogen involves its liquefaction. Liquefying hydrogen enables it to achieve a density of approximately 70 kg/m³ at atmospheric pressure [136]. Notably, liquid hydrogen (LH_2) has garnered significant attention for various compelling reasons, including its status as the cleanest fuel, the highest energy-to-weight ratio among alternative fuels, favourable chemical and physical properties, and an energy storage capacity around 2.8 times that of gasoline [137].

Nevertheless, the significant energy requirements of the liquefaction process and loss of LH_2 through boil-off during storage present a notable obstacle to storing hydrogen in liquid form. With the exceptionally low boiling point of hydrogen around -253 °C at 1 bar, and considering that hydrogen gas does not cool down during throttling at temperatures surpassing 73 °C, pre-cooling becomes essential in the liquefaction process.

This necessitates the utilization of evaporating liquid nitrogen, thereby adding to the increased energy needs of the entire procedure [117]. In this context, based on helium-cooled hydrogen liquefaction cycles, Yuksel et al. [138] devised a unique technique for hydrogen liquefaction, which they reported to have energy and exergy efficiencies of 70.12% and 57.13%, respectively.

Moreover, in order to reduce the rate of heat transfer by convection and conduction, liquid hydrogen is typically stored in tanks with double walls and a high vacuum between them. Materials such as alumina-coated polyester sheets, layers of glass fibre and aluminium foil that alternate, or perlite particles, silica, or aluminium are also used to act as a shield against radiation-induced heat transfer [129], [139].

Furthermore, this storage approach is commonly employed for fulfilling storage and transportation needs on a medium to large scale, such as in truck delivery and the shipping of hydrogen across continents, as depicted in Figure 15. A cryogenic tanker has the capability to convey 5000 kg of hydrogen, approximately five times the capacity of trailers carrying compressed hydrogen gas tubes [133].

Figure 15: Left: Cryogenic trailer, Right: Conceptual design for carriers of liquid hydrogen [133].

These H_2 storage methods are limited by the energy density per volume, pressure vessel cost and H_2 production rate. Because hydrogen has a low density, it must be stored in a huge pressure vessel. Pressurised and cryogenic tanks are more costly because they require composite materials such as carbon fibre, which account for 75% of the vessel's cost. In addition, the energy required to compress and liquefy hydrogen results in high manufacturing

costs [131]. Concerns have also been raised about the vessel's safety when it is utilised in crowded environments [132].

2.3.4.2 Chemical Storage

i. Metal Hydrides

Storing hydrogen in solid materials presents several benefits in comparison to storing it under pressure or in a liquid state, particularly in terms of volumetric density. Solid compounds have the ability to reversibly absorb hydrogen under specific temperature and pressure conditions [131]. Metal hydrides, which are metallic alloys, exhibit the ability to absorb hydrogen, making them efficient storage systems capable of both absorbing and releasing hydrogen [28].

The formation of hydroxides is initiated through the process of dissociative chemisorption. Initially, the hydrogen molecule dissociates on the solid surface, and its individual atoms then infiltrate the metallic host [131]. The bonding mechanism between hydrogen and the host material plays a crucial role in determining the formation of various hydride groups. These compounds fall into distinct categories, namely interstitial metal hydrides characterized by metallic bonding, covalent hydrides, and ionic hydrides formed through ionic bonding. The umbrella term "complex metal hydrides" encompasses both ionic and covalent hydrides as a general classification [131].

The hydrogen release from these hydrides is directly affected by their temperature. It is recognized that metal hydrides can retain hydrogen at levels ranging from 1% to 2% of their weight. Nevertheless, employing active heating to help in the removal of hydrogen can elevate this capacity from 5% to 7% of the hydride weight [28]. Typically, a considerable number of metal hydrides necessitate a moderate amount of energy, usually ranging from 20 to 55 kilojoules per mole of hydrogen [130]. A compilation of some metal hydrides, including their respective hydrogen storage capacities, is presented in Table 3.

MgH_2 has attracted significant interest and extensive research within the realm of metal hydrides. Researchers have extensively explored its capacity for hydrogen storage, revealing its high gravimetric energy density, affordability and abundance. In addition, the volumetric energy density of MgH_2 has been found to be almost double that of liquid hydrogen [11], [140], [141]. Due to the promising characteristics of MgH_2, considerable efforts have been devoted to enhancing its properties, with a focus on lowering the temperature and improving the rates of hydrogenation and dehydrogenation [130]. In this context, Johnson et al. [142] observed improved kinetics when they utilised a combination of MgH_2 and $LiBH_4$ (complex hydride).

MgH_2's weight percent H_2 capacity rose to 11.4 wt%, and the reaction's associated enthalpy change decreased to 45 kJ/mol H2. The hydrogen loading temperature drops to 200 °C, according to Li et al.'s [143] observations using graphite and MgH_2. MgH_2–$NaAlH_4$, MgH_2–$Mg(AlH_4)_2$, and MgH_2–AlH_3 are further instances of hydride composites.

Table 3: Characteristics of metal hydrides for hydrogen storage [130].

Metal hydride	**Desorption temperature (°C)**	**Desorption enthalpy (kJ/mol H2)**	**H_2 capacity (wt%)**
MgH_2–$LiBH_4$	>350	45	11.4
Mg_2NiH_4	>280	65	3.59
MgH_2	>300	75	7.6
MgH_2–$NaAlH_4$ (1:1 M)	>175	-	7.6
Mg_2FeH_6	>300	77.6	5.5
MgH_2–$LiAlH_4$ (1:1 M)	>250	45	9.4
$LaNi_5H_6$	>100	31	1.4

Desorption of hydrogen from metal hydrides necessitates a temperature range of 120–200 °C due to the pronounced interaction between the metal hydride and hydrogen. Furthermore, the properties or attributes defining metal hydrides as storage vessels are outlined as [132]:

- Significant hydrogen mass density
- Greater storage capacity for hydrogen (in comparison to compressed and liquid forms)
- High safety measures
- Enhanced purity of hydrogen
- Favourable reversible cycle performance
- Minimal operating and maintenance expenses, along with reduced purchased energy requirements

ii. Carbon Nanotubes (CNs)

Carbon nanotubes have garnered attention for their potential as hydrogen storage materials due to their elevated surface areas and thermal stability [28]. These tubular carbon structures, measuring around 2 nanometres in size, have the theoretical capability to store hydrogen within their tube structures. While carbon nanotubes and metal hybrids share similarities in their storage methods, the quantity of hydrogen stored in nanotubes can surpass that of metal

hybrids. As a result, the advancement of nanotube technology is regarded as a promising approach in the field of hydrogen storage [28].

The carbon nanotubes (CNs) are renowned for their exceptional gas adsorption characteristics because they have superior properties. These properties include the capacity to create a finely powdered substance with a highly porous structure and the presence of specific interactions between carbon atoms and the corresponding gas molecules [144]. Nanotubes are distinguished by their structural composition, which includes single-walled nanotubes (SWNT) and multi-walled nanotubes (MWNT) [144]. Figure 16 illustrates the delivered amount of H_2 adsorption in carbon nanotubes during the gas desorption [132].

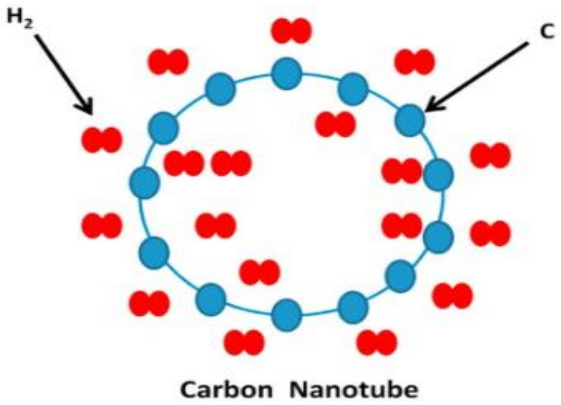

Figure 16: Hydrogen absorption in carbon nanotubes [145].

2.3.5 Plant Process Design for Hydrogen Production

While there has been extensive research on the technical aspects of hydrogen production in conventional and non-conventional ways, including the efficiency and scalability of different methods, the design of hydrogen production plants is a critical aspect. However, there is a limited number of openly available reports addressing the optimal technical analysis of plant process design which, for hydrogen production involves several key steps, including the process flow diagram, heat and material balances, equipment selection and sizing, process simulation, cost estimation, and safety considerations. The process flow diagram illustrates the sequence of operations and the flow of materials within the plant.

Heat and material balances analyse the energy and material requirements of each unit operation. Equipment selection and sizing determine the appropriate equipment for each process step based on capacity, efficiency and other criteria. Process simulation uses software tools to model and optimize the plant performance. Cost estimation involves evaluating the

capital and operating costs of the plant. Safety considerations ensure that the plant operates safely and mitigates potential hazards. By following these steps, a comprehensive and efficient hydrogen production plant can be designed.

Researchers such as Ekpotu et al. [146] explored the use of solar energy for the production of green hydrogen in Lagos state, Nigeria, leveraging the abundant solar resources in the region. The researchers employed ASPEN Hysys to simulate and design the green hydrogen production process. In addition, Microsoft Visio was used to create an instrumentation diagram, as depicted in Figure 17. The study also delved into the application of Fuzzy-PID control in the PEM electrolysis system. Both systems were deemed applicable and significant in controlling the PEM electrolysis process. The solar systems achieved a 100% renewable fraction, effectively preventing any further increase in greenhouse gas (GHG) emissions.

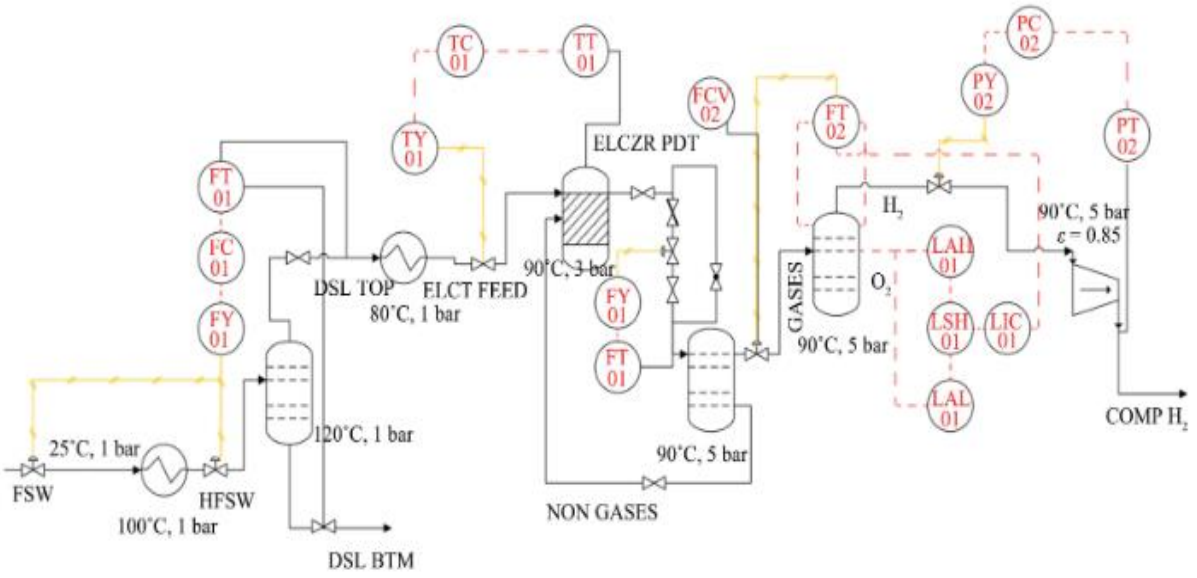

Figure 17: Process and instrumentation diagram (P&ID) for the production of green hydrogen from water using the ASPEN system with a focus on solar energy [146].

Devkota et al. [147] conducted a study focusing on the process design and optimization of on-site hydrogen production from ammonia. The investigation covered reactor design, energy conservation, and NO_X control. The process flow diagram illustrating hydrogen production from ammonia decomposition is depicted in Figure 18. The theoretical modelling and simulation were executed through the use of Aspen Plus V.12. The foundational calculations of Devkota et al. were based on a feed of 4000 kg/hr of pure ammonia, maintained at a temperature of 298 K and a pressure of 10 bar. The developed process demonstrated the

capability to produce approximately 514 kg/hr of 99.99% pure hydrogen from the 4000 kg/hr ammonia feed. To facilitate the decomposition of the remaining ammonia, 9% of the fresh feed, including undecomposed ammonia and waste hydrogen, was used as fuel.

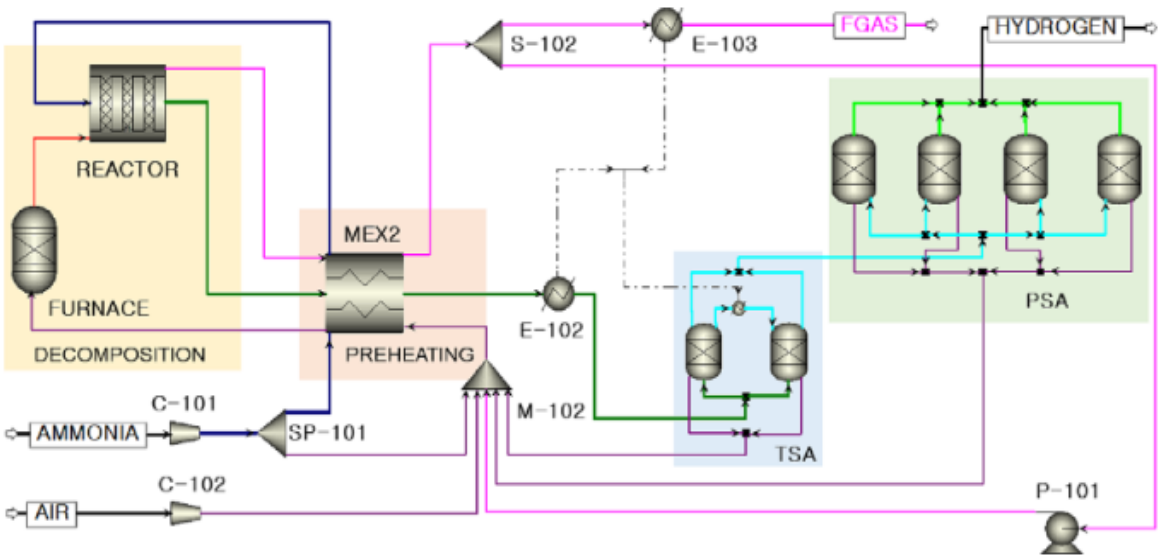

Figure 18: Process flow diagram depicting the units for ammonia decomposition, combustion, and hydrogen purification [147].

The study identified the optimal operating temperature of the fired furnace to be 1500 K, resulting in a maximum thermal efficiency of 59%. A key aspect of energy optimization involved preheating a pressurized air–fuel mixture, incorporating unreacted ammonia and waste hydrogen and using waste heat from the product and flue gas streams. This optimization technique contributed to a fuel saving of approximately 22%. Furthermore, the researchers observed that an increase in the proportion of hydrogen in the fuel mixture led to elevated NO_X emissions. To mitigate this, they implemented the recirculation of flue gas technique, effectively minimizing NO_X emissions in the process.

3 THEORETICAL APPROACH / MODELLING DEVELOPMENT

3.1 Model of Green Hydrogen Production

To build a green hydrogen plant, extensive chemical process modelling is essential. It involves multiple phases and a variety of equations to accurately represent complex physical and chemical dynamics. These equations are crucial for simulating material balance and fluid behaviour, which is the key factor to designing reactors, separators and other equipment for optimal performance. This process integrates diverse fields of engineering and science to ensure that the plant design is optimized and operational.

This section focuses on creating a comprehensive model of a green hydrogen production facility. The model encompasses interconnected components that are crucial to the plant functionality, including Electrolysers, heaters, coolers, separators, splitters, mixers, pumps, and a purge system as shown in Figure 19. These components interact through material and energy streams, establishing a cohesive operational framework. Such integration ensures that the outputs of each component serve as inputs for subsequent processes, thereby enhancing the efficiency and functionality of the hydrogen production system. This model acts as a chemical process basis for subsequent design steps such as Energy Balances, Process and Instrumentation Diagrams (P & IDs) and Process Control. It is deliberately developed in terms of Mathematical Equations (Mathematical Modelling) to permit versatility. That is, it should be able to accommodate changes in plant capacities as necessary. The design should be understood as part of the large effort to consider the potential for the generation of green hydrogen in Lesotho. The approach used is that of Material Balance and all the assumptions are based on the understanding that mass is neither created nor destroyed. It is the basis for Material Balance designs.

Each unit in the following Process Flow Steps is treated independently at a time. However, it is linked to upstream and downstream units through streams. Each stream has Variables (in the form of letters) representing total molar flows in and out of units and component flows making up the total and represented by variables. The components in this case are Water, Hydrogen, NaOH and Oxygen. Minor impurities are ignored but they are taken care of by the Purge Unit. Unknown variables are represented by question marks while the rest are assumed to be known. The assumption that some variables are known depends on the fact that they could either come

from solved upstream processes or they can be found from chemical laws or reference handbooks.

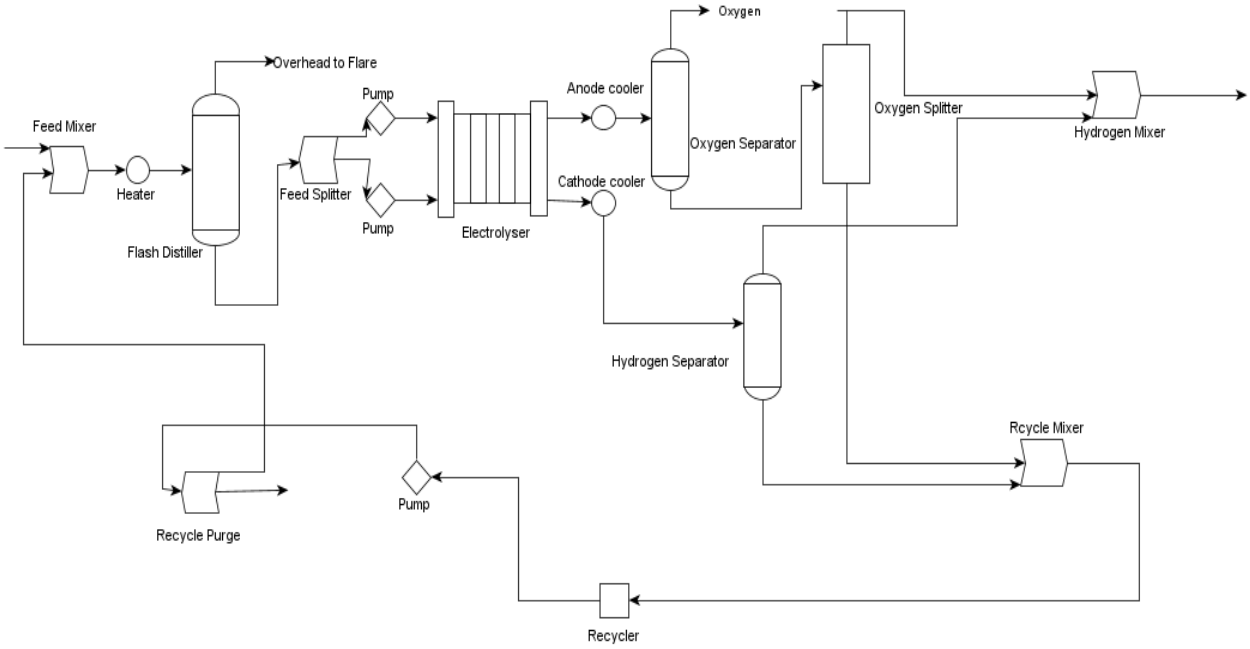

Figure 19: Process Flow Chart

3.2 Plant Components

3.2.1 Feed Mixer

In a green hydrogen alkaline electrolysis plant, the feed mixer shown in Figure 20 assumes a pivotal role in preparing the electrolyte solution that is vital for efficient hydrogen production. It ensures thorough homogenization of the electrolyte solution, typically composed of water and potassium hydroxide or sodium hydroxide, to maintain consistent conductivity and optimize electrolysis performance. The mixer facilitates the dissolution of solid electrolyte materials, preventing the presence of undissolved particles that could hinder efficiency or damage equipment.

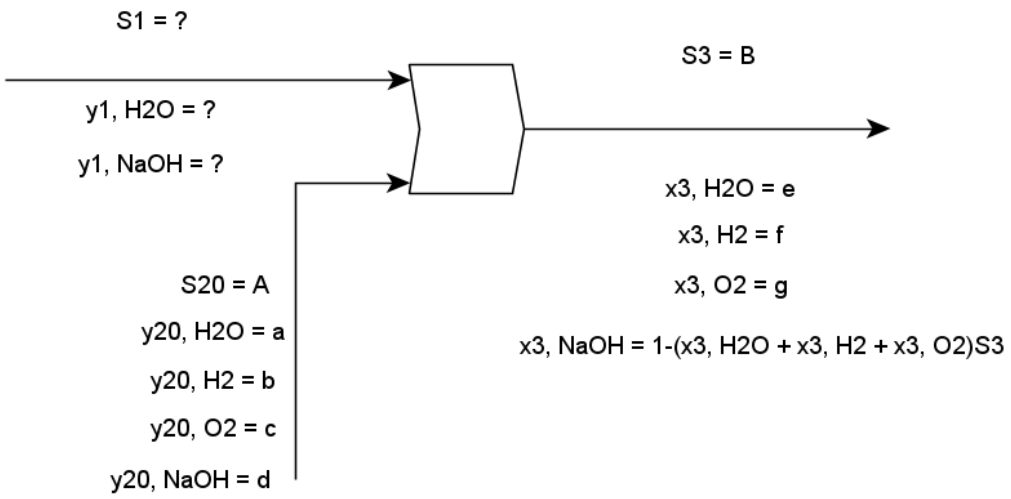

Figure 20: Feed Mixer

In addition, the feed mixer promotes a uniform distribution of heat throughout the solution, preventing localized overheating and thus stabilizing the electrolysis process. By keeping the electrolyte solution in constant motion, the mixer prevents solids from settling. They could otherwise cause inconsistencies and potential equipment issues. Moreover, when additional chemicals or additives are necessary to enhance process efficiency or preserve hydrogen purity, the feed mixer ensures their even dispersion within the solution.

3.2.1.1 MASS BALANCE

I. Total Balance

According to Equation 26, the total inflow molar flow rate equals the total outflow molar flow rate.

$$S_1 + A = B \quad (26)$$

II. Component Balances

(a) Water Balance

According to Equation 27, the total inflow molar flow rate of water equals the total outflow molar flow rate.

$$y_{1,H_2O}S_1 + aA = eB \quad (27)$$

(b) Hydrogen Balance

According to Equation 28, the total inflow molar flow rate of hydrogen equals the total outflow molar flow rate.

$$bA = fB \quad (28)$$

(c) Oxygen Balance

According to Equation 29, the total inflow molar flow rate of oxygen equals the total outflow molar flow rate.

$$cA = gB \quad (29)$$

(d) Sodium Hydroxide Balance

According to Equation 30, the total inflow molar flow rate of Sodium Hydroxide equals 1 minus the total outflow molar flow rate.

$$y_{1,NaOH}S_1 + dA = hB \quad (30)$$

3.2.1.2 First degree of freedom analysis

Number of unknowns = 3**:** S_1, y_{1,H_2O}, $y_{1,NaOH}$

Number of independent equations = 3: Equations 28 and 29 do not have variables and therefore are not independent equations.

Number of degrees of freedom = 3 – 3 = 0

This problem can be solved by **Substitutions**

I. Total Balance

Solve for S_1 by rearranging Equation 26

$$\boldsymbol{S_1 = B - A} \quad (31)$$

II. Component Balances

(a) Water Balance

Rearrange Equation 27 to solve for y_{1,H_2O}

$$y_{1,H_2O} = \frac{eB - aA}{S_1} \quad (32)$$

Substitute Equation 31 into Equation 32

$$\boldsymbol{y_{1,H_2O} = \frac{eB - aA}{B - A}} \quad 33$$

(b) Sodium Hydroxide Balance

Rearrange equation 30 to solve for $y_{1,NaOH}$

$$y_{1,NaOH} = \frac{hB - dA}{S_1} \quad 34$$

Substitute Equation 31 into Equation 34

$$\boldsymbol{y_{1,NaOH} = \frac{hB - dA}{B - A}} \quad 35$$

3.2.2 Feed Heater

The feed heater is essential for optimizing the electrolysis process. By preheating the feed material, such as water or an electrolyte solution, to the optimal temperature before it enters the electrolysis cell, the feed heater increases reaction rates and enhances overall energy efficiency. This is due to the fact that elevated temperatures speed up the electrochemical reactions within the cell, thereby reducing the electrical energy needed to sustain operational conditions. Additionally, maintaining a consistent feed temperature ensures stable process conditions, which helps avoid fluctuations that could adversely affect reaction rates and the stability of the electrolyte solutions. It is important to note that the feed heater only raises the temperature of the stream without changing its mass or composition, which means it does not affect material balance calculations.

3.2.3 Inlet Separator

There are three separators. However, the first, depicted in Figure 21, is a flash distiller. This unit functions primarily as a pressure relief device known as a flare. Its main purpose is to swiftly lower system pressure by enabling a portion of the process stream to vaporize. Although it does separate some components based on their volatility, this is a secondary outcome to its

primary function of pressure reduction. The other two separators are designed to achieve high product purity but employ a similar operational principle.

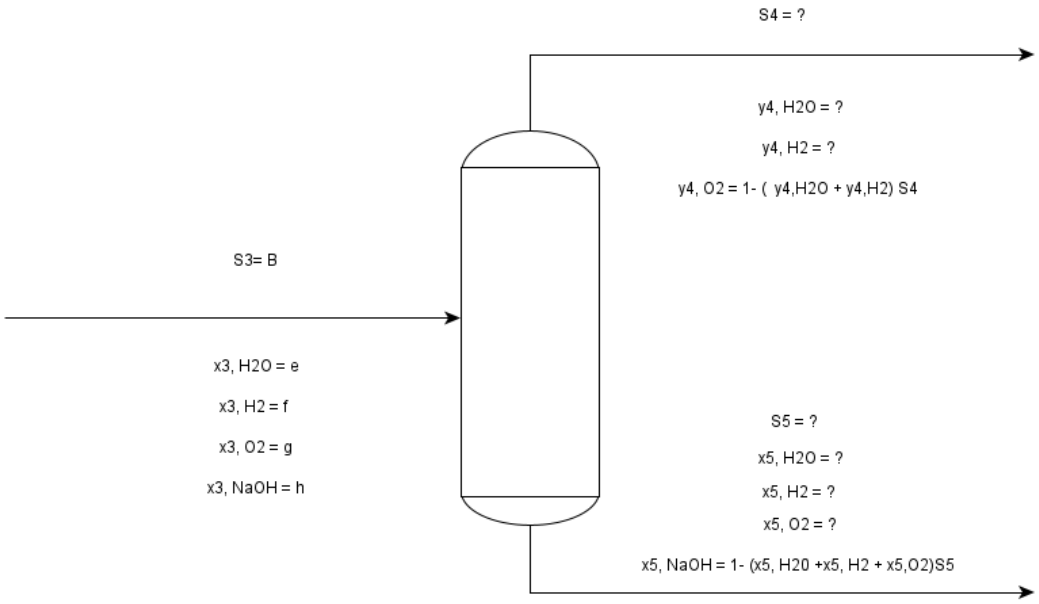

Figure 21: Separator

3.2.3.1 MASS BALANCE

I. Total Balance

$$B = S_4 + S_5 \quad (36)$$

II. Component Balances

(a) Water Balance

$$\mathrm{eB} = \mathrm{y}_{4,\mathrm{H_2O}}\mathrm{S}_4 + \mathrm{x}_{5,\mathrm{H_2O}}\mathrm{S}_5 \quad (37)$$

(b) Hydrogen Balance

$$\mathrm{fB} = \mathrm{y}_{4,\mathrm{H_2}}\mathrm{S}_4 + \mathrm{x}_{5,\mathrm{H_2}}\mathrm{S}_5 \quad (38)$$

(c) Oxygen Balance

$$gB = (1 - y_{4,H_2} - y_{4,H_2O}))S_4 + x_{5,O_2}S_5 \quad (39)$$

(d) Sodium Hydroxide Balance

$$hB = (1 - (x_{5,H_2O} + x_{5,H_2} + x_{5,O_2}))S_5 \quad 40$$

3.2.3.2 Degree of freedom analysis

In this case, there is no need for a degree of freedom analysis because, based on the Rachford-Rice Equations (Equations 41 and 42) [148], which is applied to a case where we have multicomponent feed that has to be flashed into its vapour fractions and liquid residual, all this would be unknowns in the material balance equations 37, 38 and 39.

$$\sum_{\mathbf{i=1}}^{\mathbf{n}} \mathbf{i} = \frac{\mathbf{z_i(K_i - 1)}}{\mathbf{1 + \frac{V}{F}(K_i - 1)}} = \mathbf{0} \quad 41$$

$z_i -$ molar fraction of component i in the feed liquid

$\frac{V}{F} -$ molar fraction of feed that is vaporised;

$V -$ moles of feed that is vaporised

To estimate V in Equation 41, an iteration method such as Newton-Raphson method is applied [149]. Once the V is determined, equation 42 can be used to find the moles fractions of components in both in the liquid x_i and in the vapour y_i.

$$\mathbf{x_i} = \frac{\mathbf{z_i}}{\mathbf{1 + \frac{V}{F}(K_i - 1)}} \quad 42$$

$$y_i = K_i x_i \quad 43$$

where:

$F -$ moles of incoming feed vaporised

$K_i -$ equilibrium constant of component i

First, we assume that the presence of NaOH dissolved in water does not affect the solutions behaviour. This allows the view of NaOH as acting independently of the whole water-hydrogen-oxygen solution. That means the total of the fluids is viewed as made of eB, fB and gB. In this case, V represents moles of feed that is vaporised and (1-V) is moles of feed that is not vaporised but excludes NaOH.

$$x_{5,H_2O,frac} = \frac{\frac{e}{(e+f+g)}}{1+\frac{V}{B(e+f+g)}\left(K_{H_2O}-1\right)} \quad 44$$

$$x_{5,H_2,frac} = \frac{\frac{f}{(e+f+g)}}{1+\frac{V}{B(e+f+g)}\left(K_{H_2}-1\right)} \quad 45$$

$$x_{5,O_2,frac} = \frac{\frac{g}{(e+f+g)}}{1+\frac{V}{B(e+f+g)}\left(K_{O_2}-1\right)} \quad 46$$

Let

$$S_5 = \delta + \tau \quad 47$$

where

$\delta -$ the total amount of volatiles (water, hydrogen and oxygen) leaving the separator in the bottoms and $\tau -$ the total amount of NaOH leaving the separator at the bottoms.

δ can be viewed as representing moles of feed (excluding NaOH) that are not vaporised as in Equation 48.

$$\delta = (1-V) \quad 48$$

Since

$$x_{5,H_2O,frac} + x_{5,H_2,frac} + x_{5,O_2,frac} = 1 \quad 49$$

Then

$$x_{5,H_2O=} \frac{x_{5,H_2O,frac}\delta}{S_5} \quad 50$$

$$x_{5,H_2O=} \frac{\left(\frac{\frac{e}{(e+f+g)}}{1+\frac{V}{B(e+f+g)}\left(K_{H_2O}-1\right)}\right)(1-V)}{S_5} \quad 51$$

The same thing can be done to find x_{5,H_2} and x_{5,O_2}. For Sodium Hydroxide:

$$x_{5,NaOH} = \frac{\tau}{S_5} \quad 52$$

The tops for water and oxygen molar fractions are as follows:

$$y_{4,H_2O} = K_{H_2O}\left(\frac{\frac{e}{(e+f+g)}}{1+\frac{V}{B(e+f+g)}\left(K_{H_2O}-1\right)}\right) \quad 53$$

$$y_{4,H_2} = K_{H_2}\left(\frac{\frac{f}{(e+f+g)}}{1+\frac{V}{B(e+f+g)}\left(K_{H_2}-1\right)}\right) \quad 54$$

$$y_{4,O_2} = K_{O_2}\left(\frac{\frac{g}{(e+f+g)}}{1+\frac{V}{B(e+f+g)}\left(K_{H_2O}-1\right)}\right) \quad 55$$

Also,

$$F = B\,(e+f+g) \quad 56$$

$$F_{Tot} = B\,(e+f+g) + hB = B \quad 57$$

$$S_4 = V \quad 58$$

$$S_5 = F_{Tot} - V = B - V \quad 59$$

3.2.4 Feed Splitter

A feed splitter shown in Figure 22 is a unit that splits a process stream into two or more streams without altering the original feed's characteristics or composition. This unit operation ensures that the total mass and energy of the input stream equals the total mass and energy of the output streams by adhering to the rules of mass and energy conservation. Furthermore, by distributing the components among the resultant streams in a proportionate manner according to predetermined split ratios, the feed splitter preserves the feed component distribution. Moreover, a feed splitter is an important tool for improving process efficiency and control. The division of the feed stream into multiple streams enables more flexible and efficient process operations. For example, various streams can be routed to distinct units for processing, enabling parallel or sequential processes. Furthermore, the feed splitter can be utilised to manage the flow rates of various streams, ensuring that the operation runs efficiently and consistently. This control is critical for ensuring product quality and preventing system constraints.

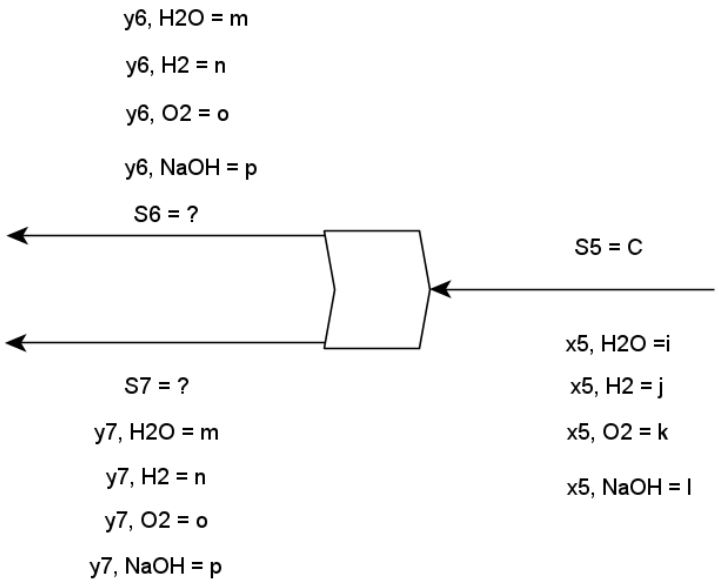

Figure 22: Feed Splitter

3.2.4.1 MASS BALANCE

I. Total Balance

According to Equation 60, the inflow molar flow rate equals the total outflow molar flow rate.

$$C = S_6 + S_7 \qquad 60$$

AUXILLIARY EQUATION

There is one Equation and two unknowns

$$S_6 = S_7 \quad (61)$$

3.2.4.2 First Degree of freedom analysis

Number of unknowns = 2**:** S_6, S_7

Number of independent equations = 2:

Number of Degrees of freedom = 2 – 2 = 2

Substitute Equation 61 into Equation 60

$$C = S_7 + S_7 \ = 2S_7 \quad (62)$$

Therefore,

$$\boldsymbol{S_7 = \frac{C}{2}} \quad (63)$$

Solving forS_6, substitute Equation 63 into Equation 61

$$\boldsymbol{S_6 = \frac{C}{2}} \quad (64)$$

3.2.5 Alkaline Electrolyser

In a green hydrogen electrolysis plant, an alkaline electrolyser is crucial for generating hydrogen through the electrolysis of water. This process involves using an electric current to split water (H_2O) into hydrogen (H_2) and oxygen (O_2) gases. Typically, the electrolyte in an alkaline electrolyser is a concentrated aqueous solution of potassium hydroxide (KOH) or sodium hydroxide (NaOH), which enhances conductivity and efficiency. The electrolyser comprises two electrodes: the cathode (negative electrode) and the anode (positive electrode), illustrated in Figure 23.

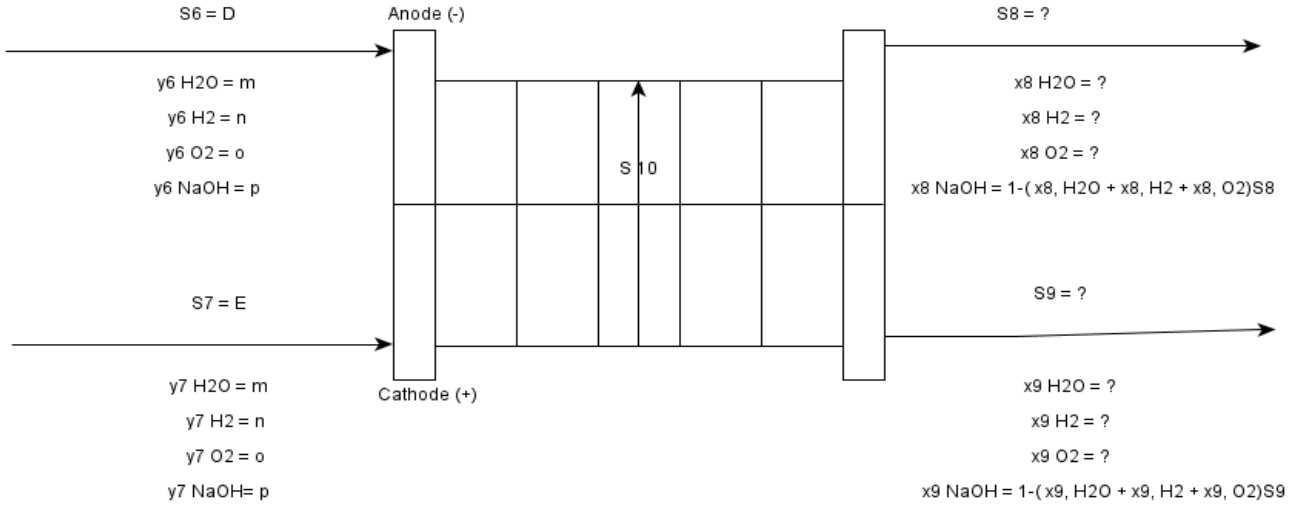

Figure 23: Alkaline Electrolyser

To ensure that the hydrogen and oxygen gases remain separate, the electrolyser employs a diaphragm or membrane that permits ion passage while preventing gas mixing. During operation, the cathode facilitates reduction, where water molecules gain electrons to form hydrogen gas and hydroxide ions (OH^-). Simultaneously, at the anode, oxidation occurs as hydroxide ions lose electrons to produce oxygen gas and water. The hydrogen and oxygen gases produced at their respective electrodes are collected individually and can be stored or used in diverse applications.

3.2.5.1 Material balance on the cathode side

Considering all species that enter, exit, and interact with the system is necessary to maintain material balance on the cathode side of an electrochemical cell, such as an electrolyser. The following Chemical Equations should be used in developing material balances, especially in the degree of freedom analysis and creation of auxiliary equations.

$$2H_2O + 2e^- \rightarrow H_2 + 2OH^- \quad (65)$$

$$2OH^- \rightarrow \frac{1}{2}O_2 + 2H_2O + 2e^- \quad (66)$$

I. Total Balance

According to Equation 67, the total molar outflow rate is equal to the total molar inflow rate minus the molar flow of hydrogen produced, the molar flow of hydroxide ions produced, and the molar flow of water consumed. The quantity of hydrogen gas generated during the

electrolysis process per unit of time is shown by the molar flow of hydrogen produced, with hydrogen gas normally emerging at the cathode. Simultaneously, the molar flow of hydroxide ions generated indicates the amount of hydroxide ions generated per unit time, typically at the anode in an alkaline electrolysis setup. The rate at which water molecules are used in these electrolysis reactions to produce hydrogen gas and hydroxide ions is also measured by the molar flow of water consumed.

$$S_9 + S_{10} = E + \dot{n}_{H_2\ produced} + \dot{n}_{OH^-_{produced}} - \dot{n}_{H_2O\ consumed} \quad 67$$

II. Component Balances

(a) Water Balance

The amount of output water on the cathode side is equal to the inflow water minus the water consumed, according to Equation 68.

$$x_{9,H_2O} S_9 = mE - \dot{n}_{H_2O\ consumed} \quad 68$$

(b) Hydrogen Balance

Equation 69 illustrates that the quantity of outlet hydrogen on the cathode side is equal to the sum of the hydrogen generated and the inlet hydrogen.

$$x_{9_{H_2}} S_9 = nE + \dot{n}_{H_2\ produced} \quad 69$$

(c) Oxygen Balance

Equation 70 illustrates that the oxygen outlet flow rate is equal to its inlet flow rate.

$$x_{9O_2} S_9 = oE \quad 70$$

(d) Hydroxide Ions

The quantity of hydroxide ions that leave the cathode side equals the amount that is produced, as demonstrated by Equation 71.

$$(x_{10OH^-})\, S_{10} = \dot{n}_{OH^-_{produced}} \quad 71$$

(e) Sodium Hydroxide balance over the entire hydrolyser

The rate of sodium hydroxide outflow is determined by subtracting the rate of water, hydrogen, and oxygen outflow from 1, then multiplying the result by the outflow of the stream S_4 as shown in Equation 72.

$$pE = (1 - (x_{9,H_2O} + x_{9,H_2} + x_{9,O_2}))S_9 \quad 72$$

3.2.5.2 First Degree of Freedom Analysis

The term "degrees of freedom" (DOF) describes the quantity of independent variables or parameters that can be changed without going against any limitations imposed by the equations governing the system.

$$Number\ of\ Unknowns = 9$$

$$= x_{9,H_2O}, S_9, x_{9,H_2}, x_{9,O_2}, \dot{n}_{H_2\ produced}, \dot{n}_{H_2O\ reacted}, x_{10OH^-}, S_{10}, \dot{n}_{OH^-_{produced}}$$

$$Number\ of\ Independent\ Equations = 5$$

$$Degree\ of\ Freedom\ Analysis = 9 - 5 = 4$$

This problem cannot be solved, there are two more equations needed

AUXILIARY FOR THE CATHODE SIDE

The cathode and anode reaction balances using the Extend of Reaction Method [ref?]

I. Total balance

Species i's total output molar flow is equal to its stoichiometric coefficient multiplied by the extent of reaction, plus its inlet molar flow as shown in Equation 73.

$$\dot{n}_i = \dot{n}_i{}^0 + v\xi \quad 73$$

II. Component Balances

(a) Cathode Water balance

The molar flow of water produced is equal to the molar flow at the inlet minus two times the extent of reaction. Since water is being consumed in line with Equation 74, the stoichiometric coefficient has a negative sign.

$$\dot{n}_{H_2O_{prduced}} = \dot{n}_{H_2O_{in}}{}^0 - 2\xi \quad 74$$

(b) Cathode Electron Balance

Equation 75 states that because electrons are being used, the molar flow of electrons produced is equal to the flow of electrons entering minus two times the extent of reaction.

$$\dot{n}_{e^-produced} = \dot{n}_{e^-}{}^{0}{}_{in} - 2\xi \quad 75$$

(c) Cathode Hydrogen Balance

The extent of reaction plus the molar flow at the inlet equals the molar flow of hydrogen produced. Equation 76 dictates the production of hydrogen, so the stoichiometric coefficient is positive.

$$\dot{n}_{H_2\,produced} = \dot{n}_{H_2}{}^{0}{}_{in} + \xi \quad 76$$

(d) Cathode Hydroxide Balance

The amount of hydroxide ions generated in terms of molar flow equals the inlet molar flow plus twice the extent of the reaction. As hydroxide ions are generated according to Equation 77, the stoichiometric coefficient is positively indicated.

$$\dot{n}_{OH^-produced} = \dot{n}_{OH^-_{in}}{}^{0} + 2\xi \quad 77$$

Substitution for water

Conversion is based on cathode water, as in Equation 78 where conversion factor λ and $\dot{n}_{OH^-}{}^{0}$ are known.

$$\lambda = \frac{\dot{n}_{H_20}{}^{0}{}_{in} - \dot{n}_{H_20 produced}}{\dot{n}_{H_20}{}^{0}{}_{in}} \quad 78$$

Rearranging to find molar flow of water produced

$$\dot{n}_{H_20 produced} = \dot{n}_{H_20}{}^{0}{}_{in} - \lambda\dot{n}_{H_20}{}^{0}{}_{in} \quad 79$$

Since

$$\dot{n}_{H_2O\,consumed} = \lambda\dot{n}_{H_20}{}^{0}{}_{in} \quad 80$$

$$mE = \dot{n}_{H_2O}{}_{in}{}^{0} \quad 81$$

Therefore, by substituting Equation 81 into Equation 80,

$$\boldsymbol{\dot{n}_{H_2O\,consumed} = \lambda mE} \quad 82$$

Equation 82 is the first independent equation in the auxiliary analyses.

Substitution to find extend of reaction, ξ

$$\xi = \frac{\dot{n}_{H_2O}{}^{0}{}_{in} - \left(\dot{n}_{H_20}{}^{0}{}_{in} - \lambda\dot{n}_{H_20}{}^{0}{}_{in}\right)}{2} \quad (83)$$

Substitution for Hydrogen

$$\dot{n}_{H_2}{}^{0} = 0 \quad (84)$$

Because no inlet hydrogen takes part in the reaction,

Substituting Equation 83 into equation 84,

$$\dot{n}_{H_2} = \frac{\dot{n}_{H_2O}{}^{0}{}_{cat} - \left(\dot{n}_{H_20}{}^{0}{}_{cat} - \lambda\dot{n}_{H_20}{}^{0}{}_{cat}\right)}{2} \quad (85)$$

Substitute Equations 81 and 82 into 85

$$\dot{n}_{H_2} = \frac{mE - (mE - \lambda mE)}{2} \quad (86)$$

$$\dot{n}_{H_2\,produced} = \dot{n}_{H_2} = \frac{\lambda mE}{2} \quad (87)$$

Equation 87 is the second independent equation in the auxiliary analyses

Substitution for Cathode Hydroxide Ion

$$\dot{n}_{OH^-}{}^{0}{}_{in} = 0 \quad (88)$$

Because there is no inlet hydroxyl taking part in the reaction

By substituting equation 83 into Equation 88

$$\dot{n}_{OH^-in} = \dot{n}_{H_2O}{}^{0}{}_{in} - \left(\dot{n}_{H_20}{}^{0}{}_{in} - \lambda\dot{n}_{H_20}{}^{0}{}_{in}\right) \quad (89)$$

Since,

$$mE = \dot{n}_{H_2O}{}^{0}{}_{in} \quad (90)$$

$$\dot{n}_{OH^-produced} = mE - (mE - \lambda mE) \quad (91)$$

$$\boldsymbol{\dot{n}_{OH^-produced} = \lambda mE} \quad (92)$$

Equation 92 is the third independent equation in the auxiliary analyses

The fourth and the last Auxiliary Equation is that

$$\boldsymbol{f_{10,OH^-} = 1} \quad 93$$

3.2.5.3 Second Degree of Freedom Analysis

$$Number\ of\ Unknowns = 9$$

$$= x_{9,H_2O}, S_9, x_{9,H_2}, x_{9,O_2}, \dot{n}_{H_2\ produced}, \dot{n}_{H_2O\ reacted}, x_{10OH^-}, S_{10}, \dot{n}_{OH^-_{produced}}$$

$$Number\ of\ Independent\ Equations = 9$$

$$Degree\ of\ Freedom\ Analysis = 9 - 9 = 0$$

The problem can be solved by **Final substitution**

I. Total Balance

$$S_9 + S_{10} = E + \dot{n}_{H_2\ produced} + \dot{n}_{OH^-_{produced}} - \dot{n}_{H_2O\ consumed} \quad 94$$

$$S_9 = \left(E + \dot{n}_{H_2\ produced} + \dot{n}_{OH^-_{produced}} - \dot{n}_{H2O\ consumed}\right) - S_{10} \quad 95$$

By substituting Equations 82 and 87 into 95

$$S_9 = E + \frac{\lambda m E}{2} - \lambda m E \quad 96$$

Therefore,

$$\boldsymbol{S_9 = \frac{E(2 - \lambda m)}{2}} \quad 97$$

II. Component Balances

(a) Water Balance

$$x_{9,H_2O} S_9 = mE - \dot{n}_{H_2O\ consumed} \quad 98$$

By substituting Equations 82 and 97

$$x_{9,H_2O} = \frac{mE - \lambda m E}{\frac{E(2 - \lambda m)}{2}} \quad 99$$

Therefore,

$$\boldsymbol{x_{9,H_2O} = \frac{2m(1 - \lambda)}{2 - \lambda m}} \quad 100$$

(b) Hydrogen Balance

$$x_{9_{H_2}} S_9 = nE + \dot{n}_{H_2\ produced} \quad 101$$

Substituting equations 87 and 97 into 101

$$x_{9_{H_2}} = \frac{nE + \frac{\lambda m E}{2}}{\frac{E(2-\lambda m)}{2}} \quad 102$$

Therefore,

$$\boldsymbol{x_{9_{H_2}} = \frac{2n + \lambda m}{2 - \lambda m}} \quad 103$$

(c) Oxygen Balance

$$x_{9O_2} S_9 = oE \quad 104$$

Substituting Equation 97 into 104 Equation 105

$$x_{9O_2} = \frac{oE}{\frac{E(2-\lambda m)}{2}} \quad 105$$

Therefore,

$$\boldsymbol{x_{9O_2} = \frac{2o}{2 - \lambda m}} \quad 106$$

(d) Hydroxide Ion Balance

$$(x_{10OH^-})\, S_{10} = \dot{n}_{OH^-_{produced}} \quad 107$$

By substituting Equation 92 into Equation 107

$$S_{10} = \lambda m E \quad 108$$

(e) Sodium Hydroxide Balance Over the Entire Hydrolyser

Sodium Hydroxide Balance is a dependent Equation

$$pE = (1 - (x_{9,H_2O} + x_{9,H_2} + x_{9,O_2}))S_9 \quad 109$$

Since

$$x_{9,\ NaOH} = (1 - (x_{9,H_2O} + x_{9,H_2} + x_{9,O_2}))S_9 \quad 110$$

$$pE = x_{9,\ NaOH}\, S_9 \quad 111$$

$$x_{9,\ NaOH} = \frac{pE}{S_9} \quad 112$$

Substitute Equation 97 into Equation 112

$$x_{9,\ NaOH} = \frac{pE}{\frac{E(2-\lambda m)}{2}} \quad 113$$

Therefore,

$$\boldsymbol{x_{9,\ NaOH} = \frac{2p}{2-\lambda m}} \quad 114$$

3.2.5.4 Material balance on the anode side

An electrolyser's anode side material balance is a methodical way to monitor the movement of materials (molecules or ions) into and out of the anode compartment.

I. Total Balance

According to Equation 115, the inflow flow rate plus the amount of water produced on the anode equals the total outflow rate.

$$S_8 = D + \dot{n}_{O_2\ produced} + \dot{n}_{H_2O\ produced} \quad 115$$

II. Component Balances

(a) Water Balance

According to Equation 116, the water's output flow rate is equal to its inlet flow rate plus the amount of water produced.

$$x_{8_{H_2O}} S_8 = mD + \dot{n}_{H_2O\ produced} \quad 116$$

(b) Hydrogen Balance

Hydrogen flows out at the same rate that it enters on the anode side as shown by Equation 117.

$$x_{8_{H_2}} S_8 = nD \quad 117$$

(c) Oxygen Balance

Equation 118 shows that the oxygen flow rate at the output is equal to the oxygen flow rate at the input plus the oxygen that is produced.

$$x_{8_{O_2}} S_8 = oD + \dot{n}_{O_2\ produced} \quad 118$$

(d) Sodium Hydroxide Balance Over the Entire Hydrolyser

The rate of sodium hydroxide outflow is determined by subtracting the rate of water, hydrogen, and oxygen outflow from 1, then multiplying the result by the outflow of the stream S_3 as shown in Equation 119.

$$pD = (1 - (x_{8_{H_2O}} + x_{8_{H_2}} + x_{8_{O_2}}))S_8 \quad 119$$

3.2.5.5 First Degree of Freedom Analysis

$Number\ of\ Unknowns = 6 = x_{8_{H_2O}}, S_8, x_{8_{H_2}}, x_{8_{O_2}}, \dot{n}_{H_2O\ produced}, \dot{n}_{O_2\ produced}$

$Number\ of\ Independent\ Equations = 4$

$Degree\ of\ Freedom\ Analysis = 6 - 4 = 2$

This problem cannot be solved

AUXILIARY FOR THE ANODE SIDE

I. Total balance

Equation 120 indicates that the total output molar flow of Species i is equal to its inlet molar flow plus its stoichiometric coefficient multiplied by the extent of reaction.

$$\dot{n}_i = \dot{n}_i{}^0 + v\xi \quad 120$$

II. Component Balances

(a) Anode Hydroxide balance

The molar hydroxide ion flow generated at the anode is equal to the molar hydroxide ion flow from the cathode side at the input, minus two times the reaction's extent. Due to the consumption of hydroxide ions, the stoichiometric coefficient is negative as shown in Equation 121.

$$\dot{n}_{OH^-\,an,produced} = \dot{n}_{OH^-}{}^0{}_{cat,in} - 2\xi \quad 121$$

(b) Oxygen Balance

Equation 122 states that the molar flow of oxygen produced is equal to the molar flow of oxygen entering the system plus half of the reaction's extent. The fact that oxygen is being produced accounts for the positive stoichiometric coefficient.

$$\dot{n}_{O_2\,an,produced} = \dot{n}_{O_2\,an.in}{}^0 + \frac{1}{2}\xi \quad 122$$

(c) Anode Water Balance

The molar flow of water generated is equal to the molar inflow plus twice the reaction's extent, as stated in Equation 123. Since water is being generated, the stoichiometric coefficient is positive.

$$\dot{n}_{H_2O\,an,,produced} = \dot{n}_{H_2O}{}^{0}{}_{an,in} + 2\xi \quad (123)$$

(d) Anode Electron Balance

According to Equation 124, the molar flow of electrons produced is equal to the flow of electrons entering plus two times the extent of the reaction and since electrons are being produced, the stoichiometric coefficient is positive.

$$\dot{n}_{e^-\,an,produced} = \dot{n}_{e^-}{}^{0}{}_{an,in} + 2\xi \quad (124)$$

Conversion is based on anode hydroxide ions, as in Equation 125 where conversion factor λ and $\dot{n}_{OH^-}{}^{0}$ are known.

$$\lambda = \frac{\dot{n}_{OH^-}{}^{0}{}_{cat,in} - \dot{n}_{OH^-\,an,produced}}{\dot{n}_{OH^-}{}^{0}{}_{cat,in}} \quad (125)$$

Assume λ as 1 because all entering hydroxide ions are used up

$$\lambda = 1 \quad (126)$$

Substitute Equation 126 into Equation 125

$$1 = \frac{\dot{n}_{OH^-}{}^{0}{}_{cat,in} - \dot{n}_{OH^-\,an,produced}}{\dot{n}_{OH^-}{}^{0}{}_{cat,in}} \quad (127)$$

Rearranging to make $\dot{n}_{OH^-\,an,produced}$

$$\dot{n}_{OH^-\,an,produced} = \dot{n}_{OH^-}{}^{0}{}_{cat,in} - \lambda\left(\dot{n}_{OH^-}{}^{0}{}_{cat,in}\right) \quad (128)$$

$$\dot{n}_{OH^-\,an,produced} = \dot{n}_{OH^-}{}^{0}{}_{cat,in} - 1\left(\dot{n}_{OH^-}{}^{0}{}_{cat,in}\right) \quad (129)$$

Since there are no hydroxide ions produced at the anode, the molar flow is of production is equal to 0.

$$\dot{n}_{OH^-\,an,produced} = 0 \quad (130)$$

Therefore, the molar flow of hydroxide ions generated is equal to the molar flow of hydroxide ions from the cathode at input minus twice the reaction extent.

$$\dot{n}_{OH^-an,produced} = \dot{n}_{OH^-}{}^{0}{}_{cat,in} - 2\xi \quad (131)$$

Solving for ξ

$$\xi = \frac{\dot{n}_{OH^-}{}^{0}{}_{cat,in}}{2} \quad (132)$$

Substitution for oxygen

$$\dot{n}_{O_2}{}^{0} = 0 \quad (133)$$

Because there is no inlet oxygen taking part in the reaction

$$\dot{n}_{O_2\,an,produced} = \dot{n}_{O_2\,an.in}{}^{0} + \frac{1}{2}\xi \quad (134)$$

Substitute Equation 132 into Equation 134

$$\dot{n}_{O_2 an,produced} = \frac{1}{2}\left(\frac{\dot{n}_{OH^-}{}^{0}{}_{cat,in}}{2}\right) \quad (135)$$

According to Equation 144

$$\dot{n}_{OH^-cat,in} = \lambda_{an} mE = \dot{n}_{OH^-cat,produced} \quad (136)$$

$$\dot{n}_{O_2 an,produced} = \frac{\dot{n}_{OH^-}{}^{0}{}_{cat,in}}{4} \quad (137)$$

Therefore,

$$\dot{n}_{O_2 an,produced} = \frac{\lambda_{an} mE}{4} \quad (138)$$

Substitution for water

$$\dot{n}_{H_2O}{}^{0} = 0 \quad (139)$$

Because there is no inlet water taking part in the reaction

$$\dot{n}_{H_2O\,an,produced} = \dot{n}_{H_2O\,an,in}{}^{0} + 2\xi \quad (140)$$

Substituting Equation 132 into Equation 140

$$\dot{n}_{H_2O\ an,produced} = 2\left(\frac{\dot{n}_{OH^-}{}^{0}{}_{cat,in}}{2}\right) \quad (141)$$

Since,

$$\dot{n}_{H_2O\ an,produced} = \dot{n}_{OH^-}{}^{0}{}_{cat,in} \quad (142)$$

Substituting Equation 144 into Equation 142

$$\dot{n}_{H_2O\ an,produced} = \lambda_{an} mE \quad (143)$$

3.2.5.6 Second Degree of Freedom Analysis

$Number\ of\ Unknowns = 6 = x_{8_{H_2O}}, S_8, x_{8_{H_2}}, x_{8_{O_2}}, \dot{n}_{H_2O\ produced}, \dot{n}_{O_2\ produced}$

$Number\ of\ Independent\ Equations = 6$

$Degree\ of\ Freedom\ Analysis = 6 - 6 = 0$

This problem can be solved.

Substitution 2

$$\dot{n}_{OH^-cat} = \lambda_{an} mE = \dot{n}_{OH^-cat,produced} \quad (144)$$

I. Total Balance

$$S_8 = D + \dot{n}_{O_2\ produced} + \dot{n}_{H_2O\ produced} \quad (145)$$

Substitute Equations 138 into Equation 143

$$S_8 = D + \frac{\lambda_{an} mE}{4} + \lambda_{an} mE \quad (146)$$

Therefore,

$$\boldsymbol{S_8 = \frac{4D + 5\lambda_{an} mE}{4}} \quad (147)$$

II. Component Balances

(a) Water Balance

$$x_{8_{H_2O}} S_8 = mD + \dot{n}_{H_2O\ produced} \quad (148)$$

Rearrange Equation 148 to solve for $x_{8_{H_2O}}$

$$x_{8_{H_2O}} = \frac{mD + \dot{n}_{H_2O\ produced}}{S_8} \quad (149)$$

Substitute Equations 143 and 147 to give Equation 150

$$x_{8_{H_2O}} = \frac{mD + \lambda_{an} mE}{\frac{4D + 5\lambda_{an} mE}{4}} \quad (150)$$

Therefore,

$$\boldsymbol{x_{8_{H_2O}} = \frac{4(mD + \lambda_{an} mE)}{4D + 5\lambda_{an} mE}} \quad (151)$$

(b) Hydrogen Balance

$$x_{8_{H_2}} S_8 = nD \quad (152)$$

Rearrange Equation 152 to solve for $x_{8_{H_2}}$

$$x_{8_{H_2}} = \frac{nD}{S_8} \quad (153)$$

Substitute Equation 147 into Equation 153

$$x_{8_{H_2}} = \frac{nD}{\frac{4D + 5\lambda_{an} mE}{4}} \quad (154)$$

Therefore,

$$\boldsymbol{x_{8_{H_2}} = \frac{4nD}{4D + 5\lambda_{an} mE}} \quad (155)$$

(c) Oxygen Balance

$$x_{8_{O_2}} S_8 = oD + \dot{n}_{O_2\ produced} \quad (156)$$

Rearrange Equation 156 to solve for $x_{8_{O_2}}$

$$x_{8_{O_2}} = \frac{oD + \dot{n}_{O_2\ produced}}{S_8} \quad (157)$$

By substituting Equations 138 and 147 into Equation 157, forming Equation 158

$$x_{8_{O_2}} = \frac{oD + \frac{\lambda_{an} mE}{4}}{\frac{4D + 5\lambda_{an} mE}{4}} \quad (158)$$

Therefore,

$$\boldsymbol{x_{8_{O_2}} = \frac{4oD + \lambda_{an} mE}{4D + 5\lambda_{an} mE}} \quad (159)$$

(d) Sodium Hydroxide Balance over the Entire Hydrolyser

$$pD = (1 - (x_{8_{H_2O}} + x_{8_{H_2}} + x_{8_{O_2}}))S_8 \quad 160$$

Since

$$x_{8,NaOH} = 1 - \left(x_{8_{H_2O}} + x_{8_{H_2}} + x_{8_{O_2}}\right) S_8 \quad 161$$

$$pD = x_{8,NaOH}\, S_8 \quad 162$$

Rearrange Equation 162 to solve for $x_{8,NaOH}$

$$x_{8,NaOH} = \frac{pD}{S_8} \quad 163$$

Substituting equation 147 into Equation 163

$$x_{8,NaOH} = \frac{pD}{\frac{4D+5\lambda_{an}mE}{4}} \quad 164$$

Therefore,

$$\boldsymbol{x_{8,NaOH} = \frac{4pD}{4D + 5\lambda_{an}mE}} \quad 165$$

3.2.6 Anode and Cathode Coolers

The coolers for both the anode and cathode play a crucial role in maintaining optimal temperatures for the electrolyte and electrodes. Operating outside this temperature range can significantly decrease electrolysis efficiency, hasten electrode degradation and trigger unwanted side reactions. These coolers remove excess heat, thereby preventing overheating that could otherwise cause thermal stress, damage electrolyser components, and pose safety risks.

In addition, anode and cathode coolers contribute to system stability by ensuring even temperature distribution throughout the cell. This prevents localized hotspots may compromise material integrity or reduce operational efficiency. Effective cooling also supports efficient electrolyte circulation, which is vital for maintaining consistent reaction conditions and maximizing ionic conductivity. As the coolers have no impact on the mass or composition of the stream, but simply lower its temperature, they are disregarded in the material balance.

3.2.7 Oxygen and Hydrogen Separators

Figure 24 and Figure 25 depict oxygen and hydrogen separators respectively. The oxygen separator isolates oxygen gas produced at the anode to prevent hazardous recombination with hydrogen and other impurities. Similarly, the hydrogen separator plays a critical role by

isolating hydrogen gas generated at the cathode that ensuring it remains free from impurities, especially oxygen.

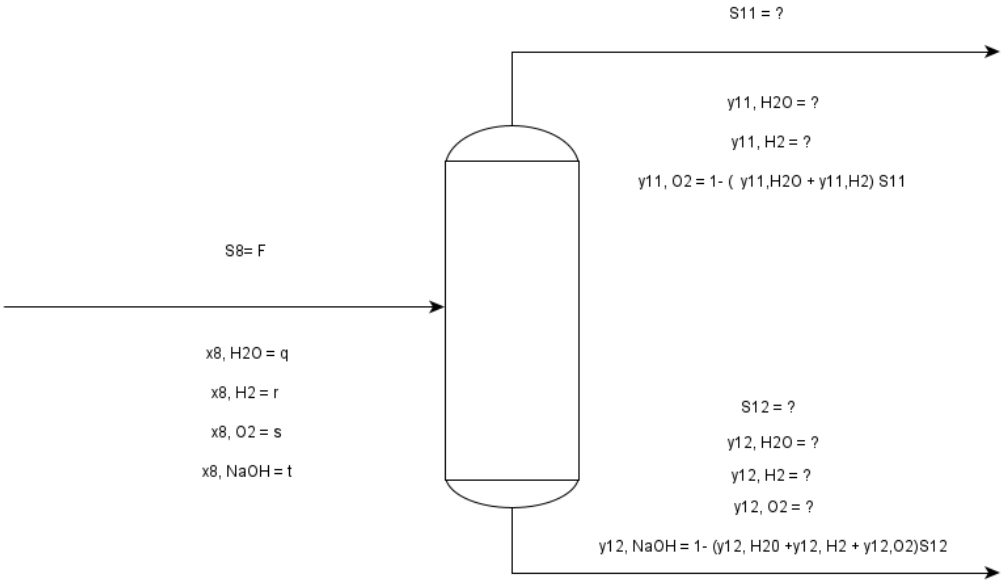

Figure 24: Oxygen Separator

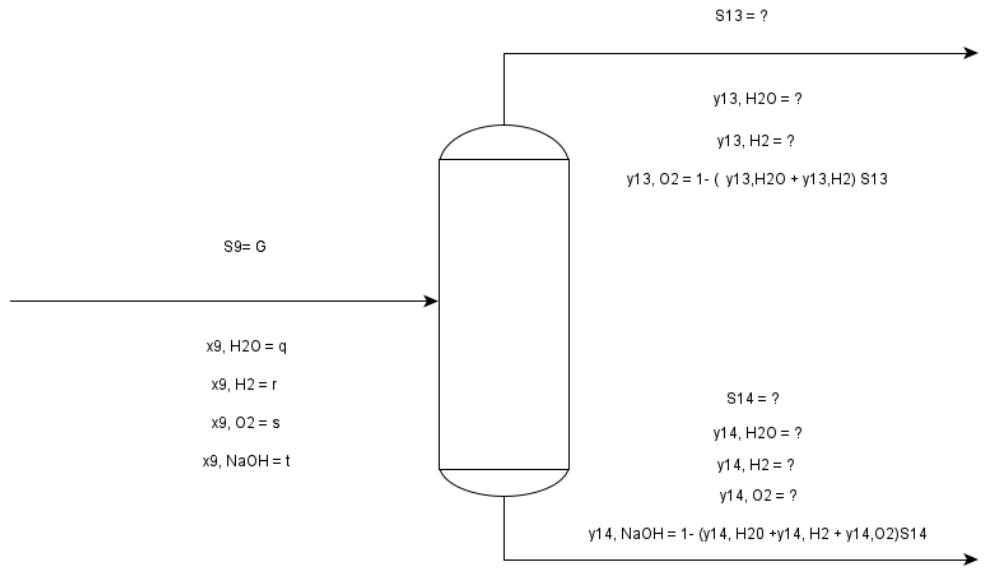

Figure 25: Hydrogen Separator

This separation is crucial as oxygen, if mixed with hydrogen, poses an explosion hazard. The hydrogen is purified to meet various application standards. Effective separation of these gases

is vital for maintaining electrolysis process efficiency and producing high-purity hydrogen. These separators function similarly to the inlet separator, and therefore, the same equations apply in simulating these units.

3.2.8 Oxygen Splitter

In electrolysis, hydrogen and oxygen are produced separately but can occasionally mix due to the process. This cross-contamination, although minimal, presents challenges. Figure 26 illustrates an oxygen splitter designed to effectively eliminate residual oxygen from the hydrogen stream. The oxygen splitter's main purpose is to increase the generated hydrogen's purity. The quality and safety of hydrogen can be negatively impacted by relatively small quantities of oxygen present in the stream, especially in situations where high purity is essential, like in fuel cells. Oxygen and other impurities can harm fuel cells, shortening their lifespan and efficiency.

By eliminating any remaining oxygen, the oxygen splitter ensures that the hydrogen satisfies strict purity standards, enhancing its suitability for such delicate uses. Furthermore, there is significant risk associated with the amount of oxygen present in the hydrogen stream from a safety perspective. Because hydrogen is very flammable, combining it with oxygen may render the mixture highly explosive. Thus, by effectively separating oxygen from the hydrogen and reducing the possibility of explosive reactions, the oxygen splitter lowers this risk. This safety improvement is essential for averting potentially hazardous situations and ensuring the safe functioning of hydrogen generating systems.

.

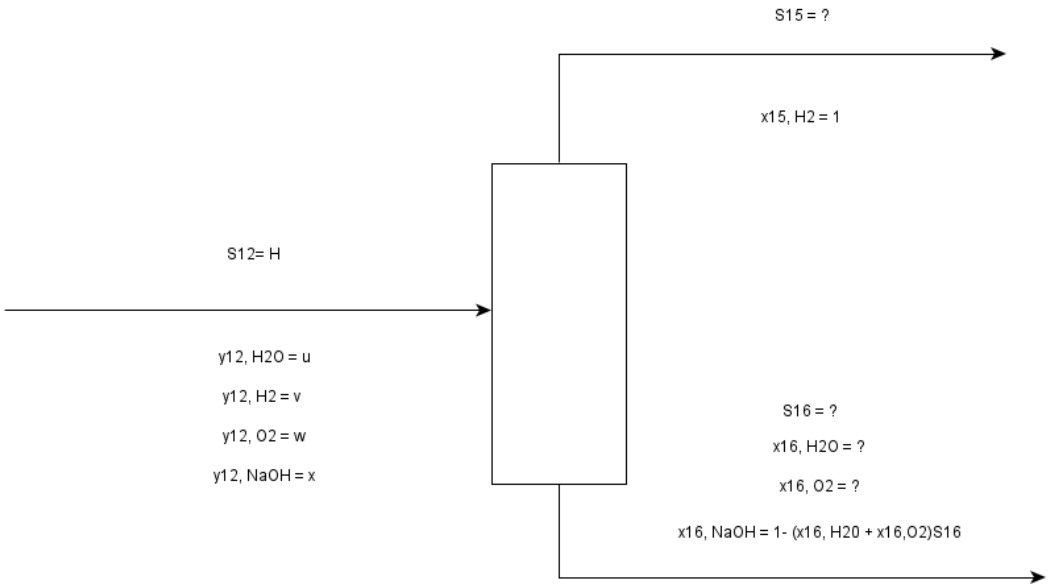

Figure 26: Oxygen Splitter

3.2.8.1 MASS BALANCE

I. Total Balance

The inlet molar flow rate (H) equals the total molar flow rates on the outlet side

$$H = S_{15} + S_{16} \quad 166$$

II. Component Balances

(a) Water Balance

The molar fraction of water times the inlet molar flow rate is equal to the unknown molar fraction of outlet water times the molar flow rate.

$$uH = x_{16,H_2O} S_{16} \quad 167$$

(b) Hydrogen Balance

The molar fraction of hydrogen times the inlet molar flow rate is equal to the unknown outlet molar flow rate.

$$vH = S_{15} \quad 168$$

(c) Oxygen Balance

The molar fraction of oxygen times the inlet molar flow rate is equal to the unknown molar fraction of outlet oxygen times the molar flow rate.

$$wH = x_{16,O_2} S_{16} \quad (169)$$

(d) Sodium Hydroxide Balance

The molar fraction of Sodium Hydroxide times the inlet molar flow rate is equal one minus unknown molar fractions of outlet water, hydrogen and oxygen times the molar flow rate.

$$xH = (1 - (x_{16,H_2O} + x_{16,H_2} + x_{16,O_2}))S_{16} \quad (170)$$

3.2.8.2 First Degree of freedom analysis

Number of unknowns = 4**:** S_{15}, S_{16}, x_{16,H_2O}, x_{16,O_2}

Number of independent equations = 4:

Number of Degrees of freedom = 4-4= 0

This problem can be solved by **Substitution.**

I. Total Balance

$$H = S_{15} + S_{16} \quad (171)$$

Substitute Equation 168 into Equation 171

$$H = vH + S_{16} \quad (172)$$

Solve for S_{16}

$$\boldsymbol{S_{16} = H - vH} \quad (173)$$

II. **Component Balances**

(a) Water Balance

Rearrange Equation 167 to solve for x_{16,H_2O}

$$x_{16,H_2O} = \frac{uH}{S_{16}} \quad (174)$$

Substitute Equation 173 into Equation 174

$$x_{16,H_2O} = \frac{uH}{H - vH} \quad (175)$$

$$\boldsymbol{x_{16,H_2O} = -\frac{u}{v-1}} \quad (176)$$

(b) Hydrogen Balance

$$\boldsymbol{vH = S_{15}} \quad (177)$$

(c) **Oxygen Balance**

Rearrange Equation 169 to solve for x_{16,O_2}

$$x_{16,O_2} = \frac{wH}{S_{16}} \quad 178$$

Substitute equation 173 into Equation 178

$$x_{16,O_2} = \frac{wH}{H - vH} \quad 179$$

$$\boldsymbol{x_{16,O_2} = -\frac{w}{v-1}} \quad 180$$

(d) Sodium Hydroxide Balance

$$xH = (1 - (x_{16,H_2O} + x_{16,H_2} + x_{16,O_2}))S_{16} \quad 181$$

Since

$$x_{16,NaOH} = (1 - (x_{16,H_2O} + x_{16,H_2} + x_{16,O_2}))S_{16} \quad 182$$

$$xH = x_{16,NaOH}S_{16} \quad 183$$

Solve for $x_{8,NaOH}$

$$x_{16,NaOH} = \frac{xH}{S_{16}} \quad 184$$

Substitute equation 173 into Equation 184

$$\boldsymbol{x_{16,NaOH} = -\frac{x}{v-1}} \quad 185$$

3.2.9 Hydrogen Mixer

The hydrogen mixer shown in Figure 27 is pivotal in maintaining high purity of produced hydrogen. It blends hydrogen streams to achieve desired concentrations, removes impurities and gases introduced during production or storage, and regulates hydrogen flow rates. This ensures consistent production levels, preventing fluctuations that could affect downstream processes. Safety is prioritized as the mixer controls the mixing process to prevent potential explosions or leaks by monitoring pressure and temperature. Efficiency is optimized by producing and delivering hydrogen at appropriate rates and conditions, thereby reducing energy consumption and operational costs. The mixer also ensures that hydrogen meets

industry and regulatory standards for purity and quality through continuous monitoring and adjustment, thereby supporting consistent product quality.

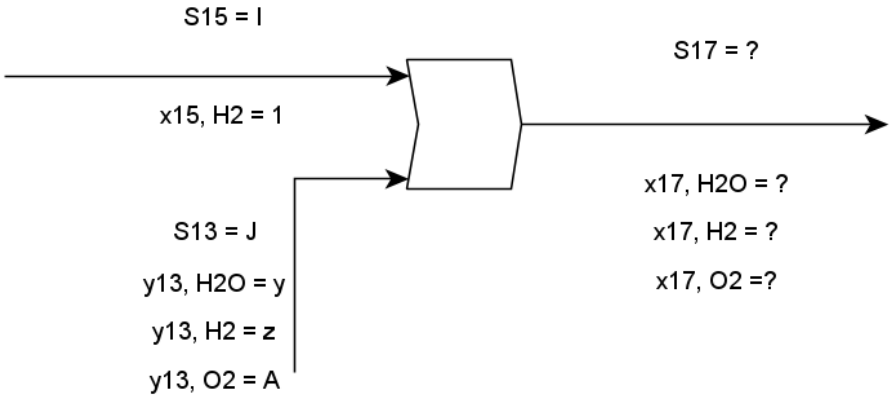

Figure 27: Hydrogen Mixer

3.2.9.1 MASS BALANCE

I. Total Balance

According to Equation 186, the total inflow molar flow rate equals the total outflow molar flow rate

$$l + J = S_{17} \tag{186}$$

II. Component Balances

(a) Water Balance

According to Equation 187, the inflow molar flow rate of water equals the outflow molar flow rate.

$$yJ = x_{17,H_2O} S_{17} \tag{187}$$

(b) Hydrogen Balance

According to Equation 188, the total inflow molar flow rate of Hydrogen equals the total outflow molar flow rate

$$I + zJ = x_{17,H_2} S_{17} \tag{188}$$

(c) Oxygen Balance

According to Equation 189, the inflow molar flow rate of Oxygen equals the total outflow molar flow rate.

$$AJ = x_{17,O_2} S_{17} \quad (189)$$

(d) Sodium Hydroxide Balance

The inflow molar flow rate of Sodium Hydroxide equals 0 and the total outflow molar flow rate is also equal to 0 as pure hydrogen is being produced.

3.2.9.2 First Degree of freedom analysis

Number of unknowns = 4**:** S_{17}, $x_{17,H_2O}, x_{17,O_2}, x_{17,H_2}$

Number of independent equations = 4:

Number of Degrees of freedom = 4-4= 0

This problem can be solved by **Substitution.**

I. Total Balance

$$S_{17} = I + J \quad (190)$$

II. Component Balances

(a) Water Balance

Rearrange Equation 187 to solve for x_{17,H_2O}

$$x_{17,H_2O} = \frac{yJ}{S_{17}} \quad (191)$$

Substitute Equation 190 into Equation 191

$$\boldsymbol{x_{17,H_2O} = \frac{yJ}{I + J}} \quad (192)$$

(b) Hydrogen Balance

Rearrange Equation 188 to solve for x_{17,H_2}

$$x_{17,H_2} = \frac{I + zJ}{S_{17}} \quad (193)$$

Substitute Equation 190 into Equation 193

$$\boldsymbol{x_{17,H_2} = \frac{I + zJ}{I + J}} \quad (194)$$

(c) Oxygen Balance

Rearrange equation 189 to solve for x_{17,O_2}

$$x_{17,O_2} = \frac{AJ}{S_{17}} \quad 195$$

Substitute Equation 190 into Equation 195

$$\boldsymbol{x_{17,O_2} = \frac{AJ}{I + J}} \quad 196$$

3.2.10 Recycle Mixer

The recycle mixer depicted in Figure 28 plays a critical role in maintaining operational efficiency and maximizing hydrogen production. It ensures the electrolyte solution, typically potassium hydroxide or sodium hydroxide, remains uniformly mixed during electrolysis. This uniformity is essential for consistent electrochemical reactions. By homogenizing the electrolyte, the recycle mixer helps maintain an even temperature distribution, preventing hotspots that could compromise efficiency and the lifespan of the electrolysis cell.

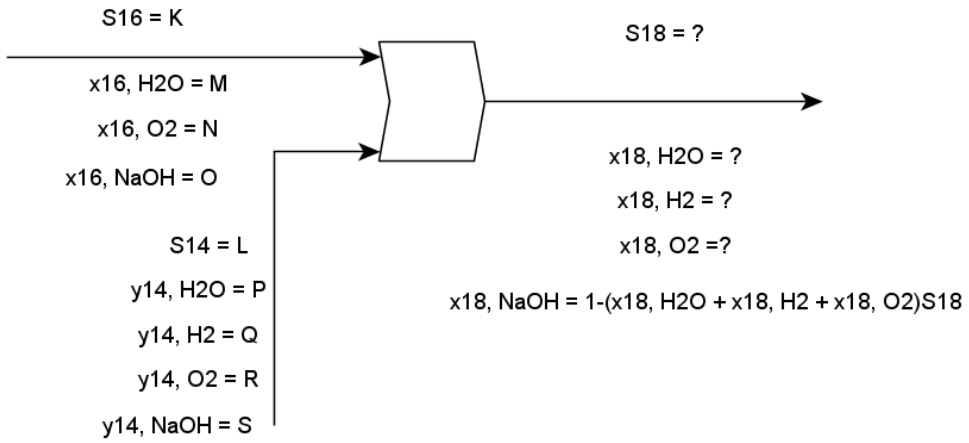

Figure 28: Recycle Mixer

During the electrolysis process, which generates hydrogen and oxygen gases, the recycle mixer helps in the separation these gases from the liquid electrolyte. Effective gas-liquid separation is crucial in preventing gas bubbles from interfering with electrochemical reactions. Proper mixing and separation improve the purity of the hydrogen and oxygen gases produced. This is critical for downstream applications.

The recycle mixer typically functions within a recirculation loop that returns electrolyte from the electrolysis cell to the tank. This continuous circulation helps to maintain optimal electrolyte concentration and temperature which are essential for consistent hydrogen production. Continuous mixing prevents sedimentation of impurities or by-products in the electrolyte solution, thereby sustaining electrolysis efficiency.

By enhancing mass transfer of reactants to electrode surfaces, the recycle mixer can improve overall electrolysis efficiency. Better mass transfer rates lead to higher hydrogen production rates, potentially reducing the over potential required for the electrolysis reaction and lowering energy consumption.

By ensuring that the electrolyte is uniformly distributed, the recycle mixer helps prevent localized electrode corrosion, thus extending the life span of the electrolysis cell. Proper mixing also mitigates the risk of gas accumulation in specific areas, reducing potential safety hazards such as explosions or leaks.

3.2.10.1 MASS BALANCE

I. Total Balance

According to Equation 197, the total inflow molar flow rate equals the total outflow molar flow rate.

$$K + L = S_{18} \quad 197$$

II. Component Balances

(a) Water Balance

According to Equation 198, the total inflow molar flow rate of water equals the total outflow molar flow rate.

$$MK + PL = x_{18,H_2O} S_{18} \quad 198$$

(b) Hydrogen Balance

According to Equation 199, the total inflow molar flow rate of hydrogen equals the total outflow molar flow rate

$$QL = x_{18,H_2} S_{18} \quad 199$$

(c) Oxygen Balance

According to Equation 200, the total inflow molar flow rate of Oxygen equals the total outflow molar flow rate

$$NK + RL = x_{18,O_2} S_{18} \quad (200)$$

(d) Sodium Hydroxide Balance

According to Equation 201, the total inflow molar flow rate of Sodium Hydroxide equals 1 minus the total outflow molar flow rates.

$$OK + SL = (1 - (x_{18,H_2O} + x_{18,H_2} + x_{18,O_2}))S_{18} \quad (201)$$

3.2.10.2 First Degree of freedom analysis

Number of unknowns = 4**:** S_{18}, $x_{18,H_2O}, x_{18,H_2}, x_{18,O_2}$

Number of independent equations = 4:

Number of Degrees of freedom = 4-4= 0

This problem can be solved by Substitution.

I. Total Balance

$$K + L = S_{18} \quad (202)$$

II. Component Balances

(a) Water Balance

Rearrange equation 198 to solve for x_{18,H_2O}

$$x_{18,H_2O} = \frac{MK + PL}{S_{18}} \quad (203)$$

Substitute Equation 202 into Equation 203

$$\boldsymbol{x_{18,H_2O} = \frac{MK + PL}{K + L}} \quad (204)$$

(b) Hydrogen Balance

Rearrange Equation 199 to solve for x_{18,H_2}

$$x_{18,H_2} = \frac{QL}{S_{18}} \quad (205)$$

Substitute Equation 202 into Equation 205

$$\boldsymbol{x_{18,H_2} = \frac{QL}{K+L}} \quad 206$$

(c) Oxygen Balance

Rearrange Equation 200 to solve for x_{18,O_2}

$$x_{18,O_2} = \frac{NK + RL}{S_{18}} \quad 207$$

Substitute Equation 202 into Equation 207

$$\boldsymbol{x_{18,O_2} = \frac{NK + RL}{K+L}} \quad 208$$

(d) Sodium Hydroxide Balance

$$OK + SL = (1 - (x_{18,H_2O} + x_{18,H_2} + x_{18,O_2}))S_{18} \quad 209$$

$$x_{18,\ NaOH}\, S_{18} = (1 - (x_{18,H_2O} + x_{18,H_2} + x_{18,O_2}))S_{18} \quad 210$$

Since

$$x_{18,\ NaOH}\, S_{18} = OK + SL \quad 211$$

Rearrange Equation 211 to solve for $x_{18,\ NaOH}$

$$x_{18,\ NaOH} = \frac{OK + SL}{S_{18}} \quad 212$$

Substitute Equation 202 into Equation 212

$$\boldsymbol{x_{18,\ NaOH} = \frac{OK + SL}{K+L}} \quad 213$$

3.2.11 Recycle Purge

The recycle purge depicted in Figure 29 is integral to maintaining the system's performance and reliability. It ensures the electrolyte quality and conductivity by eliminating impurities such as dissolved gases and metal ions. This process also regulates the concentration of the alkaline solution, typically potassium hydroxide (KOH) or sodium hydroxide (NaOH), which is crucial for efficient electrolysis.

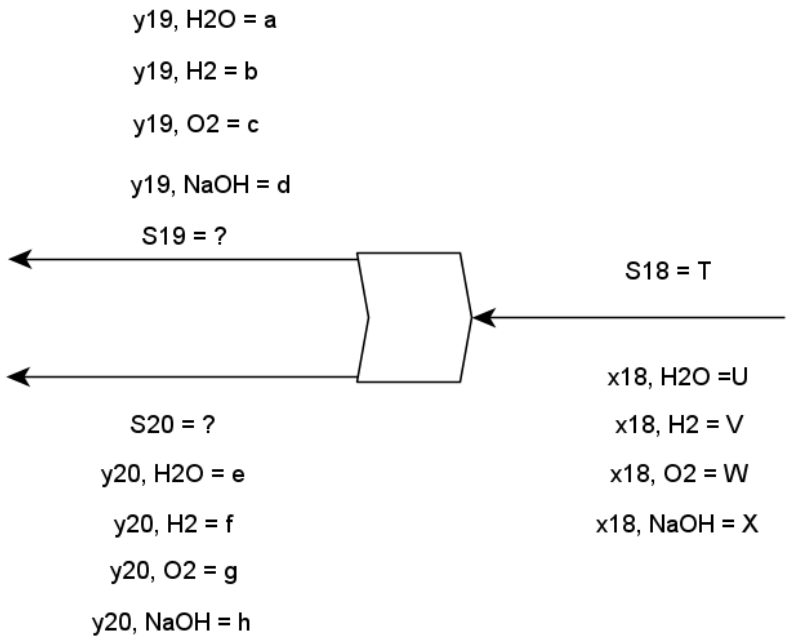

Figure 29: Recycle Purge

The purge process plays a critical role in preserving gas purity and safety. It separates residual hydrogen and oxygen gases dissolved in the electrolyte, preventing contamination and ensuring the purity of the produced hydrogen. By controlling the pressure within the electrolysis cells, it mitigates the risk of gas accumulation, thereby enhancing safety and averting potential hazards such as explosions.

Moreover, the recycle purge optimizes system efficiency by managing electrolysis-generated heat. By extracting and recycling cooled electrolyte, the system maintains optimal operating temperatures for the electrolytic reactions. This approach also reduces the occurrence of undesirable side reactions caused by impurities or excessively concentrated electrolytes, ultimately improving overall efficiency.

3.2.11.1 MASS BALANCE

I. Total Balance

According to Equation 214, the inflow molar flow rate equals the total outflow molar flow rate.

$$T = S_{19} + S_{20} \quad 214$$

AUXILLIARY EQUATION

There is one Equation and two unknowns

$$S_{20} = \varphi S_{19} \quad (215)$$

3.2.11.2 First Degree of freedom analysis

Number of unknowns = 2**:** S_{19}, S_{20}

Number of independent equations = 2:

Number of Degrees of freedom = 2 – 2 = 2

Solving for S_{19}

Substitute Equation 215 into Equation 214

$$T = S_{19} + \varphi S_{19} \quad (216)$$

$$T = S_{19}(1 + \varphi) \quad (217)$$

$$\boldsymbol{S_{19} = \frac{T}{(1+\varphi)}} \quad (218)$$

Solving for S_{20}

Substitute Equation 218 into Equation 215

$$\boldsymbol{S_{20} = \varphi \frac{T}{(1 + \varphi)}} \quad (219)$$

4 RESULTS AND DISCUSSION

In this section, we present and discuss the results from the modelling of a chemical process design for green hydrogen production, focusing on the validation of equations to ensure accurate determination of molar fractions and the evaluation of system efficiency. The modelling process involved a detailed analysis of the consumption and production rates of key substances in the system, including hydrogen, sodium hydroxide, water, and oxygen. One of the primary objectives was to validate the equations used in the model to ensure that the sum of the molar fractions for each component equals 1, reflecting the conservation of mass within the system. This validation process is crucial for confirming the accuracy of the model's calculations and ensuring reliable results. Furthermore, the variation in molar and mass fractions of hydrogen, sodium hydroxide, water, and oxygen with respect to electrolyser efficiency is illustrated through detailed graphs for each component, demonstrating the specific roles and interactions of these substances within the system. Overall, these results provide a thorough understanding of the model's performance, accuracy, and efficiency.

4.1 Feed Mixer

In order to validate Equations 33 and 35, several assumptions outlined in Table 4 were made, using UNISIM software as an ideal reference point. It is a powerful tool from Honeywell that simulates and models industrial processes [150]. These assumptions allowed for the testing of the validity of the equations. To ensure the correctness and accuracy of the equations, it is essential to use them to calculate the molar fractions of water and Sodium Hydroxide which have to sum up to 1. The results of these tests are presented in Table 5. This criterion is satisfied, thereby confirming the precision of the equations.

Table 4: Assumptions used to test Equations 33 and 35.

Substances	Symbols	Values
S_3	B	100
S_{20}	A	98.96
Water (S_{20})	a	0.867357
Sodium Hydroxide (S_{20})	d	0.132612
Water (S_3)	e	0.867479
Sodium Hydroxide (S_3)	h	0.132491

Table 5: $y_{1,H2O}$ and $y_{1,NaOH}$ Molar fractions in a feed mixer.

Symbols	Values

$y_{1,H2O}$	0.879087769
$y_{1,NaOH}$	0.120977385
Total	**1**

Simulating the mixer unit fully could not be achieved due to the reality of the recycling system. Unlike other units, the performance of this unit could only be validated based on the exact values from the first separator (and through the two other separators) and how it influences other values up to the feed mixer. Time could not allow the extensive iteration processes needed to solve the model for the three separators.

4.2 Electrolyser

4.2.1 Analysing the Cathode side of the electrolyser

For the cathode side of the electrolyser, the UNISIM design software was used to establish reference molar fractions for water, hydrogen, oxygen, and sodium hydroxide, as detailed in Table 6. Furthermore, it is crucial to validate the accuracy of Equations 100, 103, 106 and 114 by ensuring that their application in calculating the molar fractions of water, hydrogen, oxygen, and sodium hydroxide results in a total sum of 1, as demonstrated in Table 7. This criterion verifies the precision of the equations.

Table 6 : Assumptions used to test Equations 100, 103, 106 and 114

Substance	**Symbols**	**Values**
Water	$y_{7,H2O} = m$	0.867488000
Hydrogen	$y_{7,H2} = n$	0.000010000
Oxygen	$y_{7,O2} = o$	0.000007000
Sodium hydroxide	$y_{7,NaOH} = p$	0.132495000
Total		**1**

Table 7: Molar fractions in electrolyser cathode side

Substance	Symbols	Values
Water	$x_{9,H2O}$	0.816138728
Hydrogen	$x_{9,H2}$	0.045351494
Oxygen	$x_{9,O2}$	1.35592E-05
Sodium Hydroxide	$x_{9,NaOH}$	0.138502461
Total		**1**

Figure 30 and Figure 31 depict simulation graphical results created in Excel and illustrate the molar and mass fractions of water, hydrogen, oxygen, and sodium hydroxide plotted against

Electrolyser efficiency between 0 and 1. The efficiency, in this case, measures the ratio of the fraction of water that was converted to hydrogen. These graphs assess how the molar and the mass fractions change with each of them as electrolyser efficiency increases. In Figure 30, the molar fractions of water approach zero as efficiency approaches 1, while that of hydrogen increases. all of which these are expected. This happens because water is consumed at the cathode to produce hydrogen. In contrast, the molar fraction values of oxygen remain constant and negligible because no oxygen is produced on the cathode side and the little that exists comes from recycling. The molar fractions of sodium hydroxide increase gradually since it does not participate directly in the reaction but it has to take the lost water space.

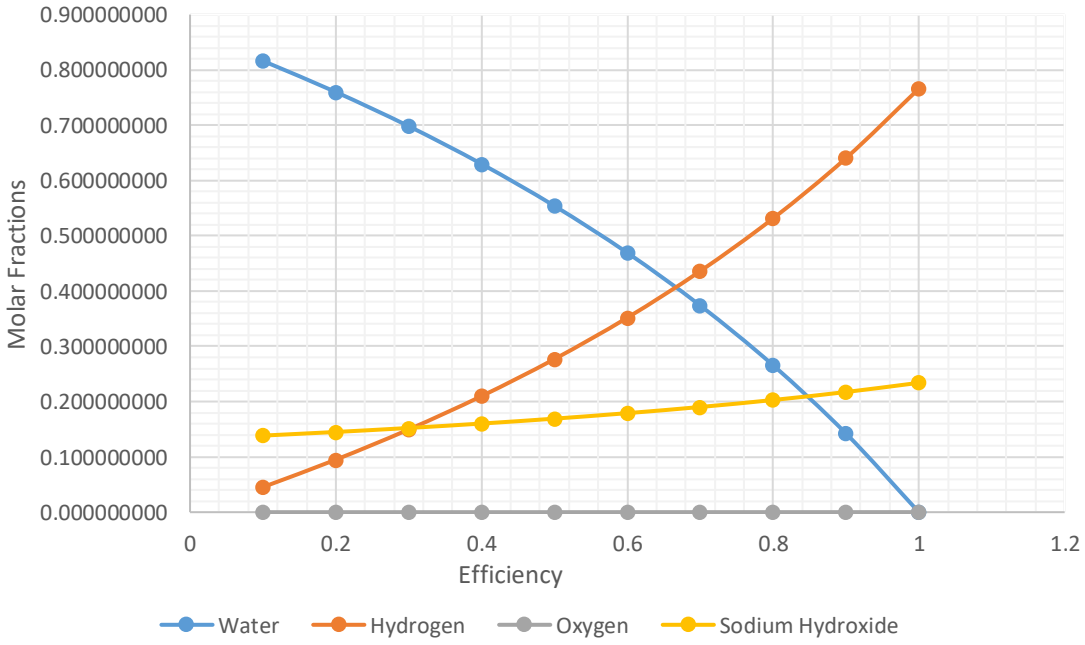

Figure 30 Molar fraction variation with electrolyser efficiency on the cathode side of an electrolyser

Furthermore, because molar fraction pertains to substance moles whereas mass fraction pertains to masses, plotting the mass fractions of water, hydrogen, oxygen, and sodium hydroxide, as depicted in Figure 31, yields distinct trends. Due to the higher molar mass of sodium hydroxide, its graph displays a greater mass fraction. Given that hydrogen is the lightest, its contribution in terms of mass is no longer as pronounced as its molar fraction, while oxygen is still negligible. Here lies the hydrogen conundrum. It has the highest energy density per kg of other alternative fuels. However, it is extremely light. This means that its storage

becomes complex as it needs to be compressed to squeeze in as much mass as possible into containers since it exists as gas at room temperature.

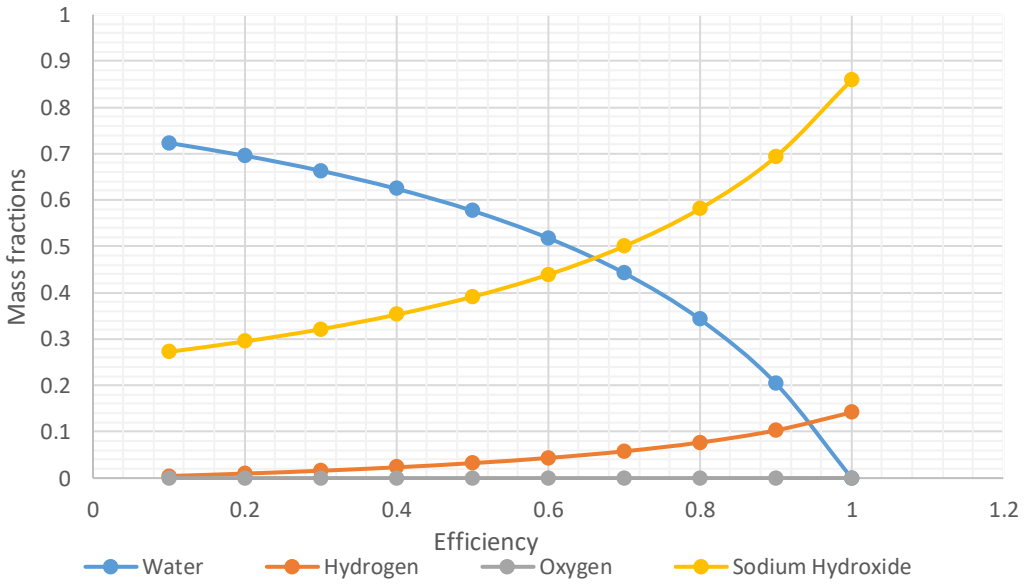

Figure 31: Mass fraction variation with electrolyser efficiency on the cathode side of an electrolyser

4.2.2 Analysing the Anode side of the Electrolyser

Referential molar fractions for water, hydrogen, oxygen, and sodium hydroxide are established on the anode side of the electrolyser using the UNISIM design software, as shown in Table 8. As shown in Table 7, it is imperative to confirm that the molar fractions calculated by Equations 151, 155, 159 and 165 yield a total sum of 1. Failure to do so invalidates the equations.

Table 8: Assumptions used in testing Equations 151, 155, 159 and 165.

Substances	**Symbols**	**Values**
Water	$y_{6,H2O} = m$	0.867488
Hydrogen	$y_{6,H2} = n$	0.000010
Oxygen	$y_{6,O2} = o$	0.000007
Sodium hydroxide	$y_{6,NaOH} = p$	0.132495
Total		**1**

Table 9: Molar fractions in electrolyser Anode side

Substances	**Symbols**	**Values**
Water	$x_{8,H2O}$	0.867488

Hydrogen	$x_{8,H2}$	0.000010
Oxygen	$x_{8,O2}$	0.000007
Sodium hydroxide	$x_{8,NaOH}$	0.132495
Total		**1**

Figure 32 and Figure 33 display graphical results from Excel simulations, showing variations in molar and mass fractions of water, hydrogen, oxygen, and sodium hydroxide with electrolyser efficiency. In Figure 32, the molar fraction of water decreases towards 1, while hydrogen is negligible. Oxygen's molar fraction also rises as it is produced in this side, whereas sodium hydroxide's molar fraction gradually decreases as other substances take more space.

Figure 33 presents mass fraction plots of the same substances, revealing more patterns. Sodium hydroxide, with its higher molar mass, exhibits decreasing mass fractions. Oxygen increase is now more pronounced. In contrast, the mass fraction of water decreases slightly although water is being produced on this side. Due to the low molecular weight of hydrogen, its mass fraction is in the realm of negligible levels.

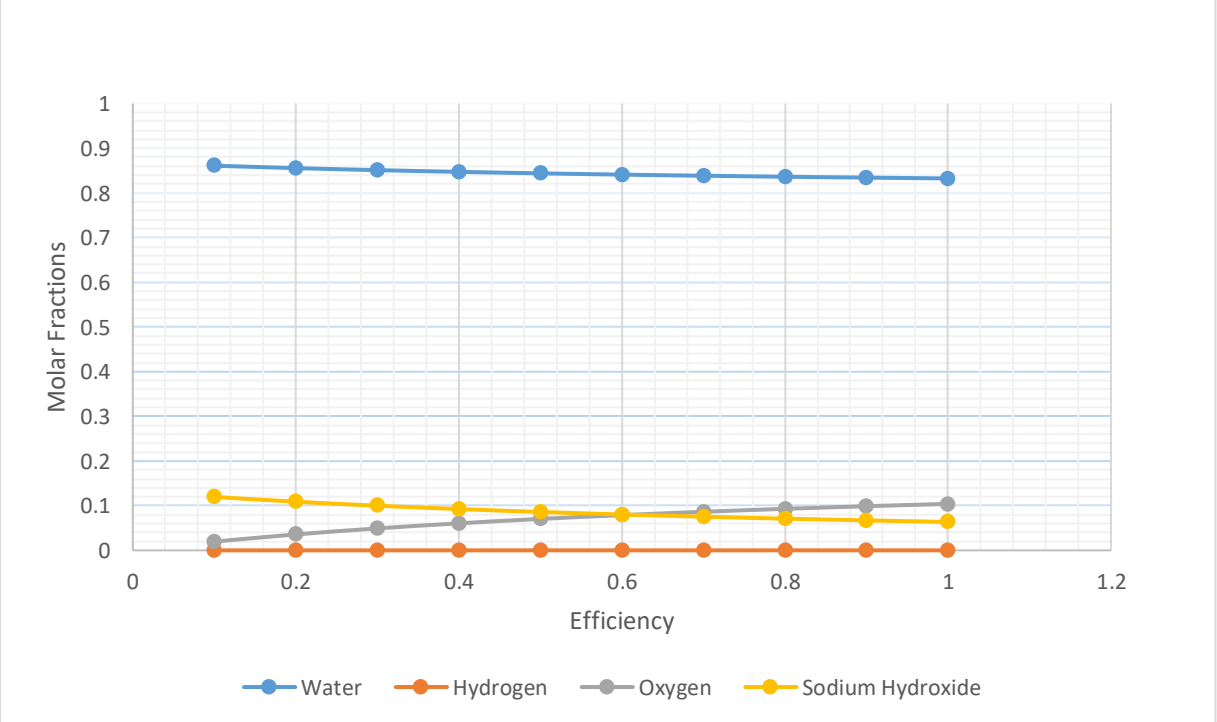

Figure 32: Molar fraction variation with electrolyser efficiency on the anode side of an electrolyser

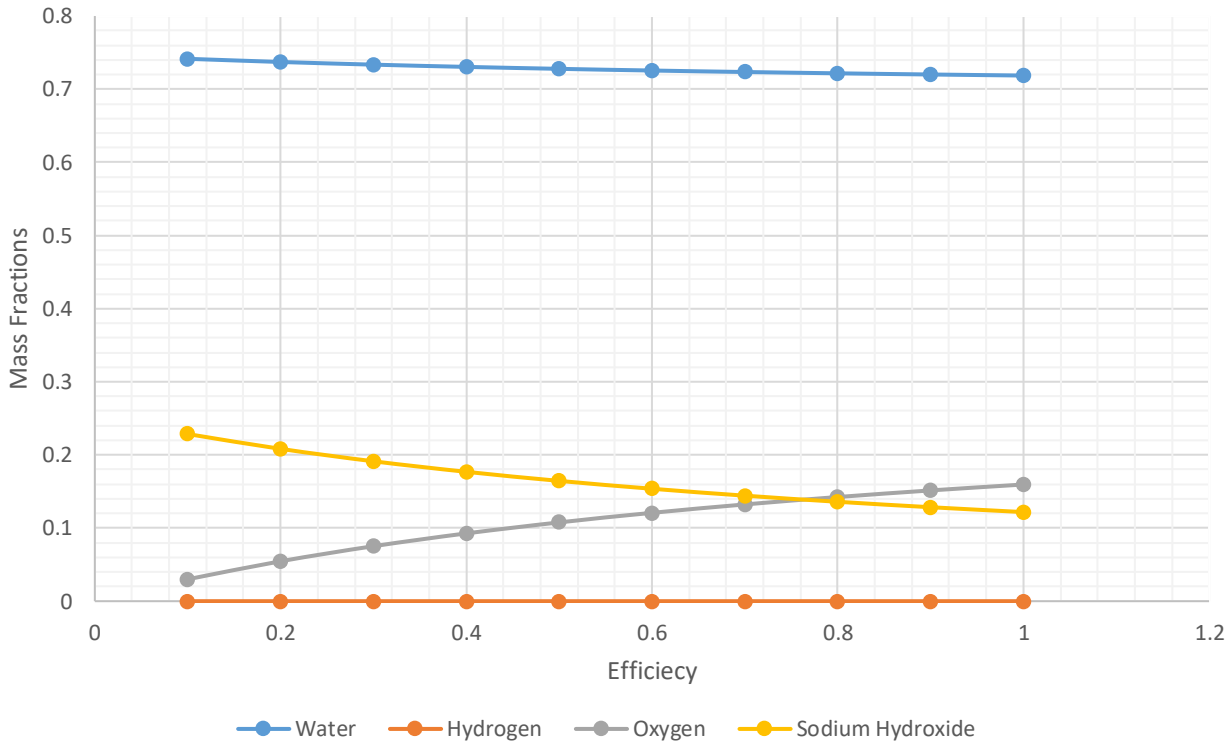

Figure 33: Mass fraction variation with electrolyser efficiency on the cathode side of an electrolyser

4.3 Analysis of an Oxygen Splitter

In this analysis, the molar fractions specifically derived from the cathode and anode sides of the electrolyser and not that of the separator because the separator was not fully developed were considered. The idea was to gauge the behaviour of the model irrespective of the source of data. Using the UNISIM design software, Table 10 establishes reference molar fractions for water, hydrogen, oxygen, and sodium hydroxide streaming from the anode side of the electrolyser. To ensure accuracy, it is crucial to verify that the molar fractions computed using Equations 176, 177, 180 and 185 add up to 1. Table 11 presents evidence demonstrating their accuracy.

Table 10: Assumptions used to test Equations 176, 177, 180 and 185

Substance	**Variable**	**Values**
S_{12}	H =	50.04
Water	u =	0.867584
Hydrogen	v =	0.000001
Oxygen	w =	0.000024
Sodium Hydroxide	x =	0.132391

Total		**1**

Table 11: Molar fractions in Oxygen splitter

Substances	Symbols	Values
Water	$x_{16,H2O}$	0.867584868
Oxygen	$x_{16,O2}$	2.4E-05
Sodium hydroxide	$x_{16,NaOH}$	0.132391132
Total		**1**

4.3.1 Using Molar fractions from the Anode Side of the electrolyser

By using the molar fractions from the anode side of the electrolyser, the researcher obtained the graphical representations shown in Figure 34 and Figure 35. Figure 34 illustrates that water has the highest molar fractions, which decrease slightly as the efficiency approaches 1. Similarly, the molar fractions of sodium hydroxide decrease as the efficiency approaches 1, while the molar fractions of oxygen increase.

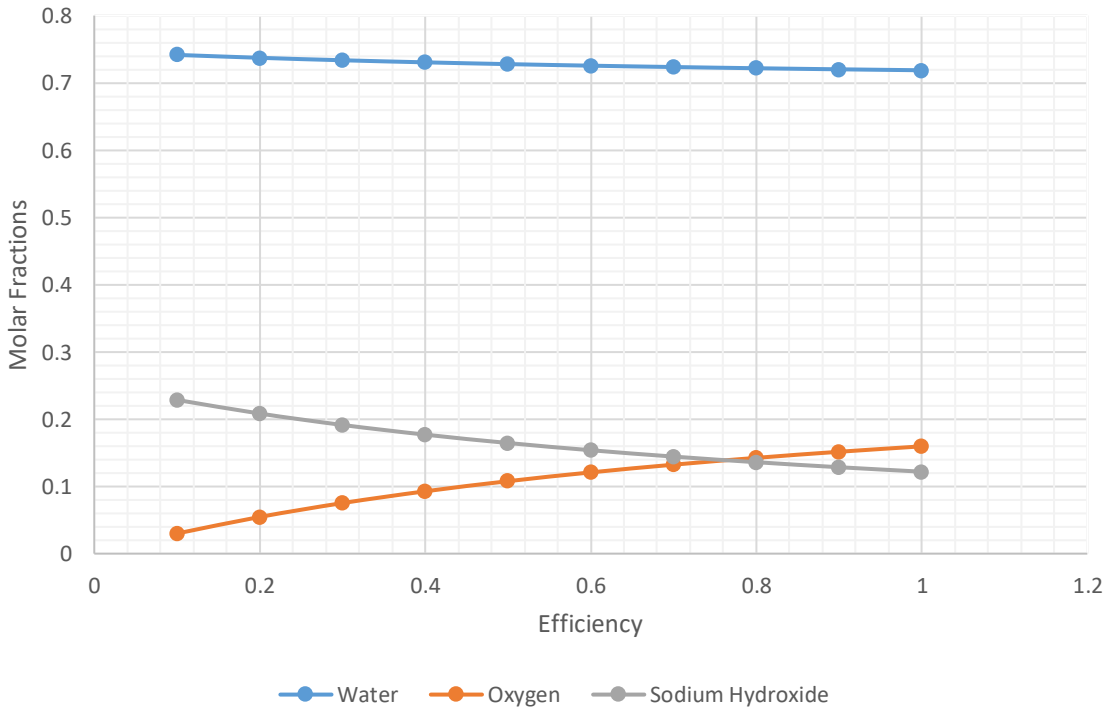

Figure 34: Molar fraction variation with electrolyser efficiency in an Oxygen Splitter

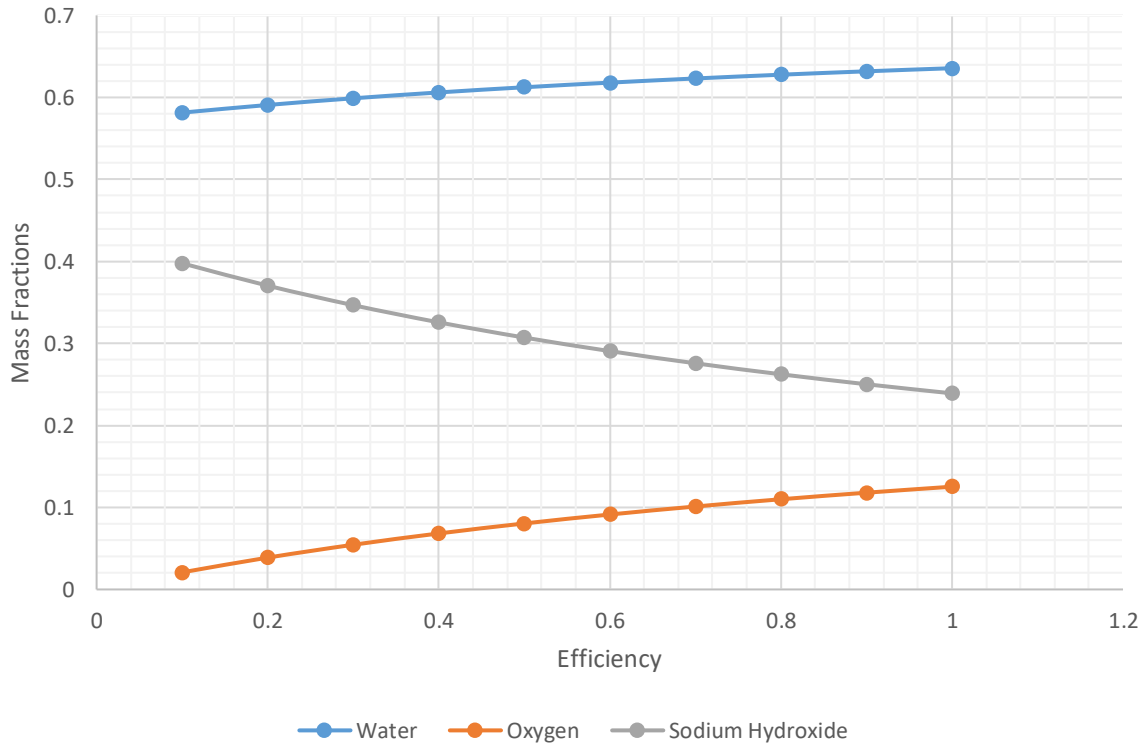

Figure 35: Mass fraction variation with electrolyser efficiency in an Oxygen Splitter

In contrast, Figure 35 presents a different perspective by showing the mass fractions. The graph for sodium hydroxide indicates a higher mass fraction due to its greater molar mass which decreases with electrolyser efficiency. Conversely, the mass fraction of water increases, as opposed to its molar fraction which went down. In addition, the mass fraction of oxygen still shows a notable increase.

4.4 Analysis of a Hydrogen Mixer

For this component, the present researcher based calculations on the molar flow rates and molar fractions derived from both the oxygen separator and the cathode side of the electrolyser. Using UNISIM design software, Table 12 was created to establish reference values for molar fractions of water, hydrogen, oxygen, and sodium hydroxide, alongside their corresponding molar flow rates. These values were then used to validate the equations. It is crucial to ensure accuracy by verifying that the sum of molar fractions computed using Equations 192, 194 and 196 equals 1. Table 13 provides evidence confirming their accuracy.

Table 12: Assumptions used to test Equations 192, 194 and 196

Substances	**Symbols**	**Values**

S_{15}	I =	4.61E-05
Hydrogen		1
S_{13}	J =	3.99E-02
Water	y =	0.019306
Hydrogen	z =	0.972585
Oxygen	A =	0.008109

Table 13: Molar fractions in Hydrogen mixer.

Substances	**Symbols**	**Values**
Water	$x_{17,H2O}$	1.93E-02
Hydrogen	$x_{17,H2}$	9.73E-01
Oxygen	$x_{17,O2}$	0.008099643
Total		**1**

Figure 36 and Figure 37 depict graphical outcomes derived from Excel simulations and illustrate the changes in molar and mass fractions of water, hydrogen, oxygen, and sodium hydroxide across an efficiency spectrum from 0 to 1. These graphs analyse the progression of the fractions with incremental adjustments. In Figure 36, the molar fractions of water decrease as the efficiency approached 1 while the molar fractions of hydrogen increase as the efficiency approached 1. Oxygen's molar fractions remain consistently negligible due to no production of oxygen.

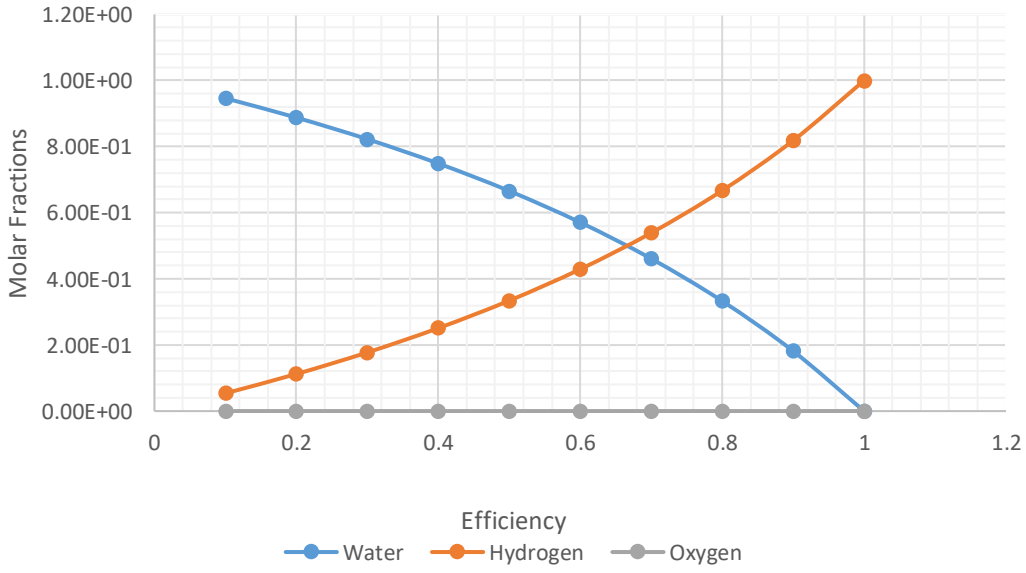

Figure 36: Molar fraction variation with electrolyser efficiency in a Hydrogen Mixer

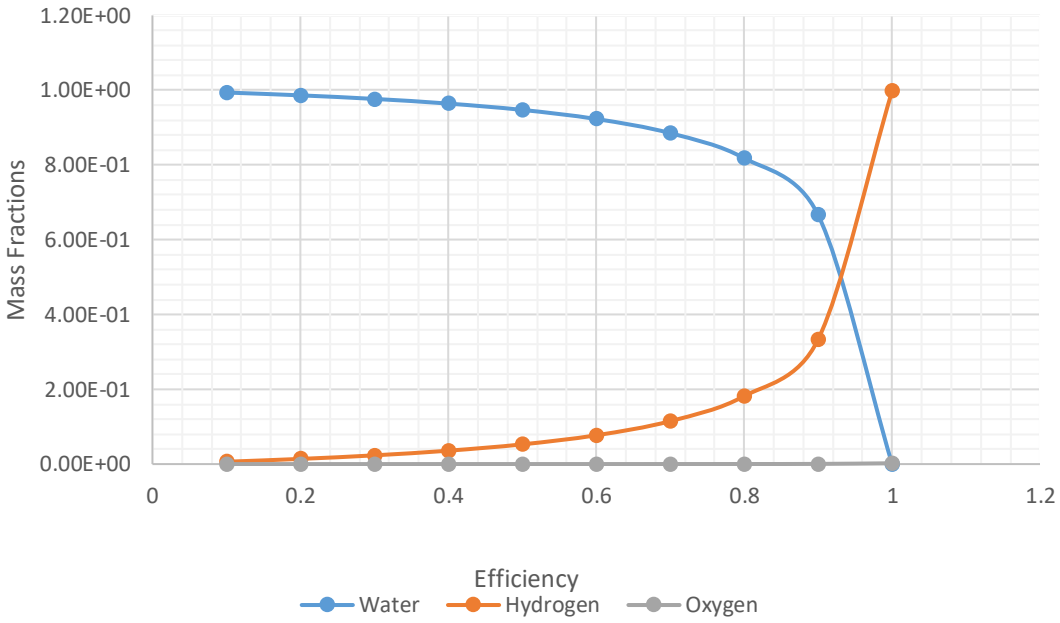

Figure 37: Mass fraction variation with electrolyser efficiency in a Hydrogen Mixer.

Mass fraction diagrams of the same compounds are shown in Figure 37, where variations are noticeable. In comparison to its molar fraction, the mass fraction of water drops significantly as efficiency approaches 1. Although hydrogen has a smaller molecular weight its mass fraction increases significantly as efficiency approaches 1. The mass fraction of Oxygen does not show any increase.

4.5 Analysis of a Recycle Mixer

For this part, the calculations relied on the molar flow rates and proportions obtained from both the oxygen separator and the cathode side of the electrolyser. We used UNISIM design software to generate Table 14, which details the molar fractions of water, hydrogen, oxygen, and sodium hydroxide, along with their respective flow rates. These data points were crucial for validating our equations. To ensure precision and validity, the total molar fractions are computed using Equations 204, 206, 208 and 213 add up to 1. Table 15 serves as verification of their accuracy.

Table 14: Assumptions used in testing Equations 204, 206, 208 and 213.

Substances	**Symbols**	**Values**
S_{16}	K =	50.04
Water	M =	0.867585

Oxygen	N =	0.000024
Sodium Hydroxide	O =	0.132391
S_{14}	L =	49.92
Water	P =	0.867255
Hydrogen	Q =	0.000037
Oxygen	R =	0.000001
Sodium Hydroxide	S =	0.132708

Table 15: Molar fractions in a Recycle mixer.

Substances	**Symbols**	**Values**
Water	$x_{18,H2O}$	0.867420198
Hydrogen	$x_{18,H2}$	1.84778E-05
Oxygen	$x_{18,O2}$	1.25138E-05
Sodium hydroxide	$x_{18,NaOH}$	0.13254931
Total		**1**

Figure 38 and Figure 39 display graphical results generated from Excel simulations. They depict the changes in molar and mass fractions of water, hydrogen, oxygen, and sodium hydroxide with electrolyser efficiency. The two figures show how these fractions evolve with incremental adjustments. In Figure 38, the molar fraction of water decreases as it approaches an efficiency of 1 while those of hydrogen increase significantly. Oxygen molar fractions also increase, nearing an efficiency of 1 while those of sodium hydroxide decrease slightly as efficiency approaches 1.

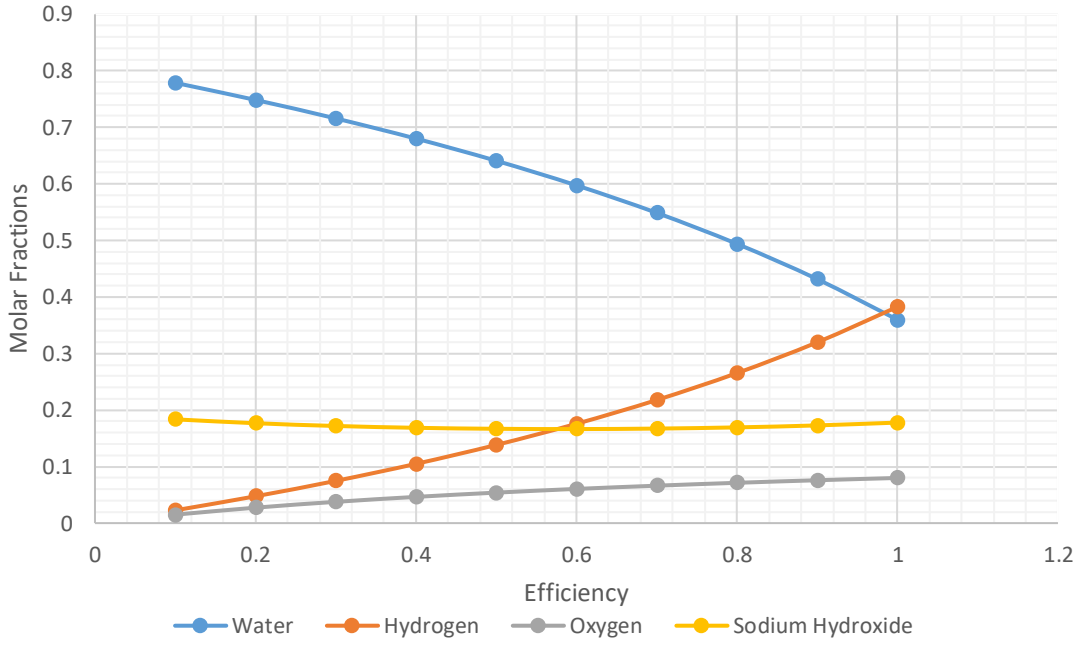

Figure 38: Molar fraction variation with electrolyser efficiency in a Recycle Mixer

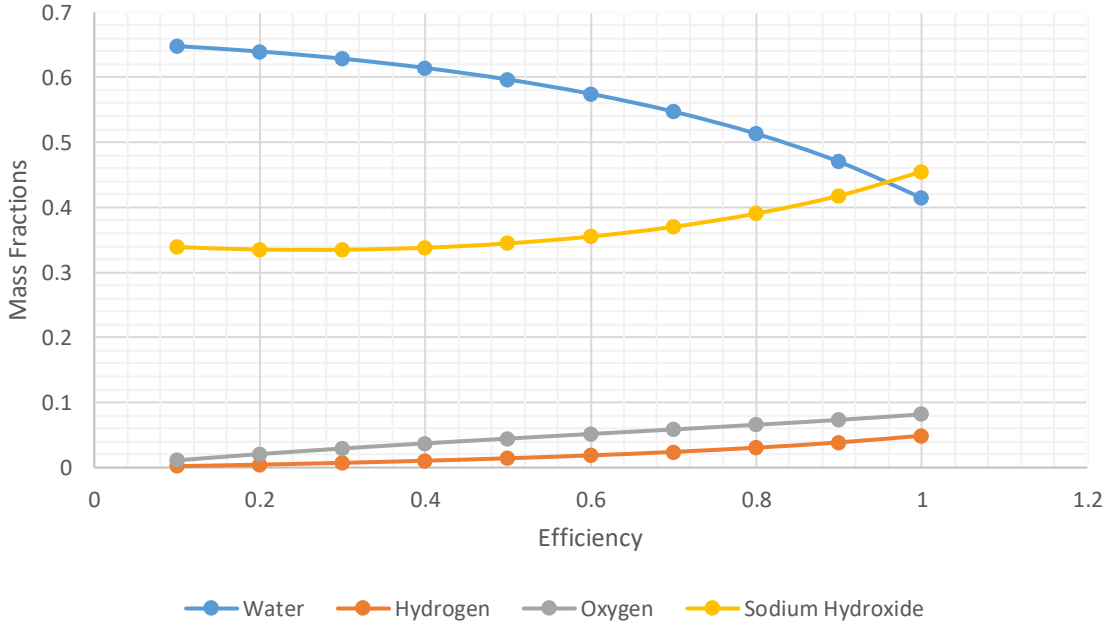

Figure 39: Mass fraction variation with electrolyser efficiency in a Recycle Mixer

Figure 39 presents mass fraction diagrams of the same compounds, highlighting noticeable variations. Sodium hydroxide exhibits an upward trend in mass fractions as efficiency approaches 1 due to its high molar mass. In contrast, despite its molar fraction, the mass fraction

of water decreases nearing an efficiency of 1. The mass fractions of hydrogen and oxygen increase gradually as they approach an efficiency of 1.

4.6 Analysis of Recycle Purge Unit

To simulate this component, the value of the inlet molar flow rate, T, is constant at 99.96 and varied φ from 0 to 1. Table 16 displays the corresponding calculated molar flow rates of S_{19} and S_{20} as φ shifts within this range. According to Equations 218 and 219, the molar flow rates of both streams must total T for each variation. Therefore, the results in Table 16 confirm the accuracy of the equations.

Table 16: Molar flow rates of S_{19} and S_{20}

	Values									
Efficiency	0.1	0.2	0.3	0.4	0.5	0.6	0.7	0.8	0.9	1
S19	90.97	83.3	76.89	71.4	66.64	62.47	58.8	55.53	52.61	49.98
S20	9.08	16.66	23.07	28.56	33.32	37.49	41.16	44.43	47.35	49.98
Total	99.96	99.96	99.96	99.96	99.96	99.96	99.96	99.96	99.96	99.96

Figure 40 presents a plot of molar flow rates as a function of φ. It illustrates that S_{19} starts with a higher molar flow rate compared to S_{20}. However, as φ approaches 1, the molar flow rate of S_{19} gradually decreases. On the other hand, S_{20} begins with a lower molar flow rate but experiences an increase as φ nears 1. Notably, the molar flow rates of both S_{19} and S_{20} converge and become equal when φ equals 1.

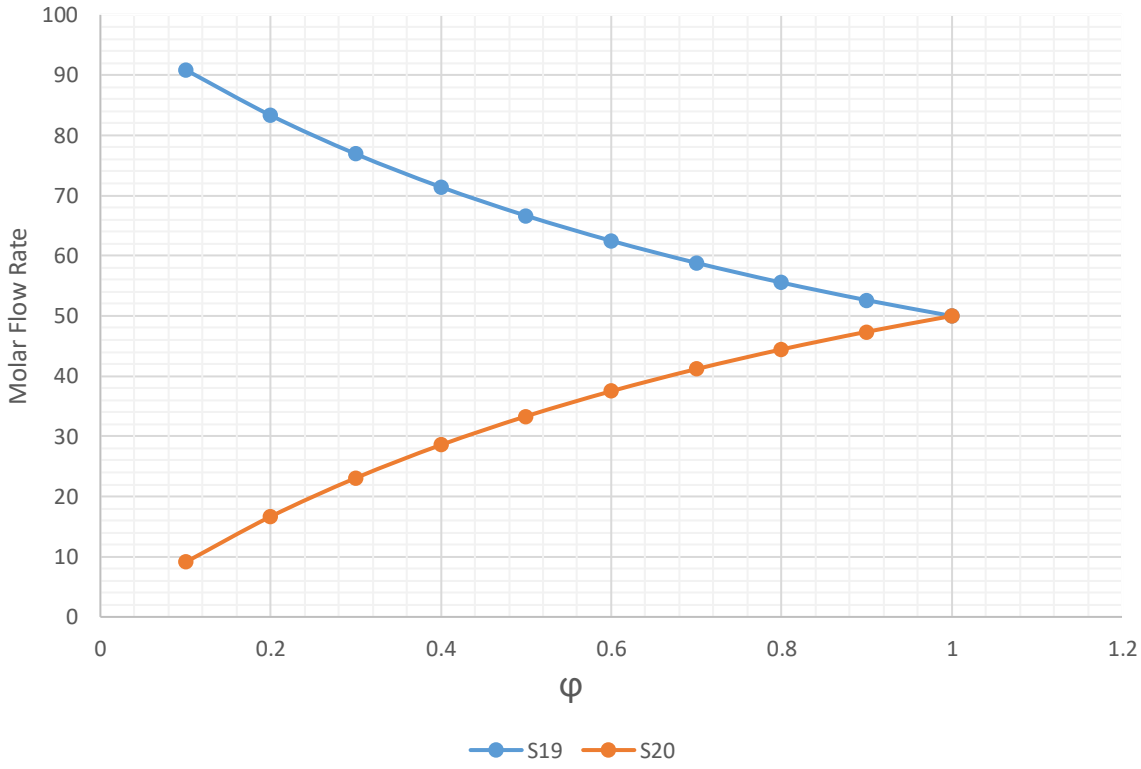

Figure 40: Molar Flow rates of S19 and S20 at φ between 0 and 1.

5 CONCLUSION AND RECOMMENDATIONS

5.1 Concluding Remarks

In conclusion, simulating a feed mixer within a plant and thus achieving accurate system simulation proves challenging due to the intricate dynamics of the separator. Specifically, the complexity lies in iteratively calculating inlet molar flow rates and fractions to capture the system's behaviour effectively. Until the behaviour of the separator is resolved through these iterative calculations, any simulation of the feed mixer may be deemed inaccurate.

To validate the equations crucial for this simulation, the assumptions presented in Table 4 are made and tested against UNISIM software as a baseline. It was essential to ensure that equations accurately calculated molar fractions of water and Sodium Hydroxide, summing up to 1, as verified in Table 5. Similarly, equations determining molar fractions on the cathode and anode sides of the electrolyser were validated (Table 6 and Table 7), confirming their precision through rigorous testing against software-generated references.

Graphical results from Excel simulations (Figures Figure *30*Figure 31, Figure *32*Figure 33) depicted trends in molar and mass fractions across incremental variations. They illustrated how molar fractions of water and hydrogen changed due to consumption and production in electrolytic reactions, while mass fractions reflected differences in molecular weights. Notably, sodium hydroxide consistently exhibited higher mass fractions due to its greater molar mass, contrasting with the decreasing mass fraction of water.

Further validation focused on molar fractions derived from the anode side of the electrolyser (TablesTable *10* and Table *11*), which is essential for accuracy in subsequent calculations of an Oxygen Splitter. Figures Figure *34*Figure 35 elaborated on these fractions, showing how they varied with increasing increments, which is crucial for understanding their impact within the system. Moreover, calculations involving molar flow rates and fractions from both the oxygen separator and the electrolyser sides detailed in Tables Table *12* and Table *13*, corroborate equation accuracy.

Graphical outcomes from Excel (Figures Figure *36*Figure 37, Figure *38*Figure 39) continued to demonstrate evolving molar and mass fractions across varying conditions. These visualizations highlighted the changing dynamics of water, hydrogen, oxygen, and sodium hydroxide fractions that are essential for comprehensive system analysis. Lastly, the

consistency in molar flow rates of streams S_{19} and S_{20} under different φ conditions (Table 16, Figure 40) provided a conclusive validation of the equations governing the flow rate calculations.

Overall, the study demonstrates that the equations accurately model the system, as evidenced by the consistent verification against the reference values and the graphical analysis of molar and mass fractions. These observations emphasize the critical role of accurate simulation in understanding system behaviour and ensuring reliable predictions crucial for optimizing plant operations and efficiency.

5.2 Limitations

Modelling the green hydrogen plant presented several significant challenges; foremost among them is the constraint of time. These limitations have influenced the depth and thoroughness of the modelling process in multiple ways. Firstly, there was insufficient time to perform iterative refinements essential for optimizing plant design and operational efficiency in the three separators that form part of the entire process. Each iteration cycle (which normally involves adjusting the parameters, validating the assumptions and recalculating the outputs, required extensive time investments that were not feasible under the tight project deadlines. Moreover, accurate energy balanced calculations, critical for assessing energy inputs and outputs in hydrogen production, were not done due to time constraints.

Integrating renewable energy resources, the cornerstone of green hydrogen production, also suffers under time limitations. Effective integration of variable renewable sources such as solar and wind requires sophisticated modelling to predict energy availability, optimize usage and manage fluctuations. Insufficient time for detailed modelling has resulted in missed opportunities to maximize renewable energy utilization or to optimize energy supply and demand balance within the plant operations. Furthermore, the complexity of green hydrogen plant systems, encompassing electrolysis, compression, purification, and storage processes, demands comprehensive data and interdisciplinary expertise. Time constraints have limited the scope of modelling to primary processes, potentially overlooking secondary factors such as equipment degradation, operational variability or environmental impacts.

5.3 Recommendations

In order to effectively address the complexities involved in modelling a green hydrogen plant several key strategies can significantly improve the process. Firstly, adequate time allocation is crucial. This includes allowing thorough iterations to refine designs, accurately calculate energy balances and integrate renewable energy sources effectively. Establishing realistic project timelines that prioritise these aspects can alleviate the pressures of tight deadlines, ensuring comprehensive and optimized plant designs.

Enhancing data collection efforts is equally vital. Thorough data gathering on equipment specifications, renewable energy potentials, local climate conditions and operational parameters can enhance the quality and availability of input data for simulations. This minimizes uncertainties in model outputs and boosts prediction reliability. Using advanced modelling tools and simulation software capable of handling the intricacies of green hydrogen plant systems is another critical recommendation. These tools facilitate precise energy balance calculations, dynamic simulation of renewable energy integration and optimization of operational strategies in order to support informed decision-making.

Interdisciplinary collaboration is essential for successful modelling. Involving experts from chemical engineering, renewable energy systems and data analytics ensures a holistic approach. This collaboration fosters a comprehensive understanding of plant dynamics and enables modelling that considers technical, economic and environmental factors simultaneously. Furthermore, a rigorous validation of assumptions and model outputs using real-world data and operational feedback is essential. Pilot studies or small-scale demonstrations can validate the accuracy and reliability of model predictions, guiding further refinements.

To maintain long-term operational efficiency and environmental responsibility, continuous optimization of plant design and operations is the key factor. This includes adapting control strategies to respond to variable renewable energy inputs, minimizing operational costs and reducing environmental impacts. Staying abreast of technological advancements in hydrogen production and renewable energy integration ensures that modelling frameworks incorporate the latest innovations and best practices. By implementing these strategies, stakeholders can effectively address the challenges of modelling green hydrogen plants as well as promote sustainable and efficient hydrogen production from renewable sources.

REFERENCES

[1] S. K. Dash, S. Chakraborty, and D. Elangovan, 'A Brief Review of Hydrogen Production Methods and Their Challenges', *Energies*, vol. 16, no. 3, Art. no. 3, Jan. 2023, doi: 10.3390/en16031141.

[2] S. Shiva Kumar and V. Himabindu, 'Hydrogen production by PEM water electrolysis – A review', *Mater. Sci. Energy Technol.*, vol. 2, no. 3, pp. 442–454, Dec. 2019, doi: 10.1016/j.mset.2019.03.002.

[3] B. M. Taele, L. Mokhutšoane, I. Hapazari, S. B. Tlali, and M. Senatla, 'Grid electrification challenges, photovoltaic electrification progress and energy sustainability in Lesotho', *Renew. Sustain. Energy Rev.*, vol. 16, no. 1, pp. 973–980, Jan. 2012, doi: 10.1016/j.rser.2011.09.019.

[4] T. Ramachaea, '70MW Solar Power Project', Lesotho Electricity Generation Company. Accessed: Jul. 31, 2024. [Online]. Available: https://www.legco.co.ls/projects/70mw-solar-power-project/

[5] L. Z. Thamae, R. I. Thamae, and T. M. Thamae, 'Assessing a decade of regulatory performance for the Lesotho electricity industry', *Util. Policy*, vol. 35, pp. 91–101, Aug. 2015, doi: 10.1016/j.jup.2015.07.006.

[6] LEWA, 'LEWA-Annual-Report-2021-22', 2022. Accessed: Jul. 31, 2024. [Online]. Available: https://www.lewa.org.ls/download/lewa-annual-report-2021-22/

[7] The World Bank, 'Lesotho-Renewable-Energy-and-Energy-Access-Project.pdf'. The World Bank, Jan. 08, 2020. Accessed: Jan. 23, 2023. [Online]. Available: https://documents1.worldbank.org/curated/en/808341580698850813/pdf/Lesotho-Renewable-Energy-and-Energy-Access-Project.pdf

[8] DWA, 'DWA – Ministry of Natural Resources'. Accessed: Jan. 26, 2024. [Online]. Available: https://www.water.org.ls/dwa/, https://www.water.org.ls/dwa/

[9] H. Ishaq, I. Dincer, and C. Crawford, 'A review on hydrogen production and utilization: Challenges and opportunities', *Int. J. Hydrog. Energy*, vol. 47, no. 62, pp. 26238–26264, Jul. 2022, doi: 10.1016/j.ijhydene.2021.11.149.

[10] S. Ali, A. Gamal, and M. M. Khader, 'Development of highly active and coke-resilient Ni-based catalysts for low-temperature steam reformation of methane', *Catal. Commun.*, vol. 175, p. 106605, Feb. 2023, doi: 10.1016/j.catcom.2023.106605.

[11] F. Zhang, P. Zhao, M. Niu, and J. Maddy, 'The survey of key technologies in hydrogen energy storage', *Int. J. Hydrog. Energy*, vol. 41, no. 33, pp. 14535–14552, Sep. 2016, doi: 10.1016/j.ijhydene.2016.05.293.

[12] O. Machhammer, A. Bode, and W. Hormuth, 'Financial and Ecological Evaluation of Hydrogen Production Processes on Large Scale', *Chem. Eng. Technol.*, vol. 39, no. 6, pp. 1185–1193, 2016, doi: 10.1002/ceat.201600023.

[13] D. Scheiblehner, H. Antrekowitsch, D. Neuschitzer, S. Wibner, and A. Sprung, 'Hydrogen Production by Methane Pyrolysis in Molten Cu-Ni-Sn Alloys', *Metals*, vol. 13, no. 7, p. 1310, Jul. 2023, doi: 10.3390/met13071310.

[14] N. Sazali, 'Emerging technologies by hydrogen: A review', *Int. J. Hydrog. Energy*, vol. 45, no. 38, pp. 18753–18771, Jul. 2020, doi: 10.1016/j.ijhydene.2020.05.021.

[15] S. S. Garud, F. Tsang, I. A. Karimi, and S. Farooq, 'Green hydrogen from solar power for decarbonization: What will it cost?', *Energy Convers. Manag.*, vol. 286, p. 117059, Jun. 2023, doi: 10.1016/j.enconman.2023.117059.

[16] O. Schmidt, A. Gambhir, I. Staffell, A. Hawkes, J. Nelson, and S. Few, 'Future cost and performance of water electrolysis: An expert elicitation study', *Int. J. Hydrog. Energy*, vol. 42, no. 52, pp. 30470–30492, Dec. 2017, doi: 10.1016/j.ijhydene.2017.10.045.

[17] M. Fallah Vostakola, B. Salamatinia, and B. Amini Horri, 'A Review on Recent Progress in the Integrated Green Hydrogen Production Processes', *Energies*, vol. 15, no. 3, Art. no. 3, Jan. 2022, doi: 10.3390/en15031209.
[18] I. Marouani *et al.*, 'Integration of Renewable-Energy-Based Green Hydrogen into the Energy Future', *Processes*, vol. 11, no. 9, Art. no. 9, Sep. 2023, doi: 10.3390/pr11092685.
[19] I. A. Gondal, S. A. Masood, and R. Khan, 'Green hydrogen production potential for developing a hydrogen economy in Pakistan', *Int. J. Hydrog. Energy*, vol. 43, no. 12, pp. 6011–6039, Mar. 2018, doi: 10.1016/j.ijhydene.2018.01.113.
[20] D. Gielen, F. Boshell, D. Saygin, M. D. Bazilian, N. Wagner, and R. Gorini, 'The role of renewable energy in the global energy transformation', *Energy Strategy Rev.*, vol. 24, pp. 38–50, Apr. 2019, doi: 10.1016/j.esr.2019.01.006.
[21] E. Kötter, L. Schneider, F. Sehnke, K. Ohnmeiss, and R. Schröer, 'The future electric power system: Impact of Power-to-Gas by interacting with other renewable energy components', *J. Energy Storage*, vol. 5, pp. 113–119, Feb. 2016, doi: 10.1016/j.est.2015.11.012.
[22] M. Momirlan and T. N. Veziroglu, 'The properties of hydrogen as fuel tomorrow in sustainable energy system for a cleaner planet', *Int. J. Hydrog. Energy*, vol. 30, no. 7, pp. 795–802, Jul. 2005, doi: 10.1016/j.ijhydene.2004.10.011.
[23] C. Rivkin, R. Burgess, and W. Buttner, 'Hydrogen Technologies Safety Guide', National Renewable Energy Lab. (NREL), Golden, CO (United States), NREL/TP-5400-60948, Jan. 2015. doi: 10.2172/1169773.
[24] F. Dawood, M. Anda, and G. M. Shafiullah, 'Hydrogen production for energy: An overview', *Int. J. Hydrog. Energy*, vol. 45, no. 7, pp. 3847–3869, Feb. 2020, doi: 10.1016/j.ijhydene.2019.12.059.
[25] R. D. McCarty, J. Hord, and H. M. Roder, *Selected Properties of Hydrogen (engineering Design Data)*. U.S. Department of Commerce, National Bureau of Standards, 1981.
[26] A. Staykov, S. M. Lyth, and M. Watanabe, 'Photocatalytic Water Splitting', in *Hydrogen Energy Engineering: A Japanese Perspective*, K. Sasaki, H.-W. Li, A. Hayashi, J. Yamabe, T. Ogura, and S. M. Lyth, Eds., in Green Energy and Technology. , Tokyo: Springer Japan, 2016, pp. 159–174. doi: 10.1007/978-4-431-56042-5_12.
[27] J. Töpler and J. Lehmann, Eds., *Hydrogen and Fuel Cell: Technologies and Market Perspectives*. Berlin, Heidelberg: Springer Berlin Heidelberg, 2016. doi: 10.1007/978-3-662-44972-1.
[28] H. T. Arat and M. G. Sürer, 'State of art of hydrogen usage as a fuel on aviation', *Eur. Mech. Sci.*, vol. 2, no. 1, pp. 20–30, Dec. 2017, doi: 10.26701/ems.364286.
[29] IRENA, 'Green hydrogen: A guide to policy making', *Int. Renew. Energy Agency*, 2020, Accessed: Sep. 18, 2023. [Online]. Available: https://www.irena.org/-/media/Files/IRENA/Agency/Publication/2020/Nov/IRENA_Green_hydrogen_policy_2020.pdf
[30] C. J. Boreham *et al.*, 'Hydrogen in Australian natural gas: occurrences, sources and resources', *APPEA J.*, vol. 61, no. 1, p. 163, 2021, doi: 10.1071/AJ20044.
[31] A. Majumdar, J. M. Deutch, R. S. Prasher, and T. P. Griffin, 'A framework for a hydrogen economy', *Joule*, vol. 5, no. 8, pp. 1905–1908, Aug. 2021, doi: 10.1016/j.joule.2021.07.007.
[32] L. Mosca *et al.*, 'Process design for green hydrogen production', *Int. J. Hydrog. Energy*, vol. 45, no. 12, pp. 7266–7277, Mar. 2020, doi: 10.1016/j.ijhydene.2019.08.206.
[33] IEA, 'The Future of Hydrogen', 2019, Accessed: Oct. 26, 2023. [Online]. Available: https://www.hydrogenexpo.com/media/9370/the_future_of_hydrogen_iea.pdf

[34] M. A. S. M. A. S, S. M. H. R. S. M. H. R, A. P. A. P, and K. C. K. C, 'Generation of Bio-Hydrogen by Chemical Looping Water Splitting and Pyrolysis: Role of Catalyst and Recent Advancements', *Ethiop. J. Appl. Sci. Technol.*, pp. 25–32, Jun. 2023.
[35] C. M. Kalamaras and A. M. Efstathiou, 'Hydrogen Production Technologies: Current State and Future Developments', *Conf. Pap. Energy*, vol. 2013, pp. 1–9, Jun. 2013, doi: 10.1155/2013/690627.
[36] P. J. Megía, A. J. Vizcaíno, J. A. Calles, and A. Carrero, 'Hydrogen Production Technologies: From Fossil Fuels toward Renewable Sources. A Mini Review', *Energy Fuels*, vol. 35, no. 20, pp. 16403–16415, Oct. 2021, doi: 10.1021/acs.energyfuels.1c02501.
[37] T. E. Lipman, 'Hydrogen Production Science and Technology', in *Fuel Cells and Hydrogen Production: A Volume in the Encyclopedia of Sustainability Science and Technology, Second Edition*, T. E. Lipman and A. Z. Weber, Eds., in Encyclopedia of Sustainability Science and Technology Series. , New York, NY: Springer, 2019, pp. 783–798. doi: 10.1007/978-1-4939-7789-5_755.
[38] L. Barelli, G. Bidini, F. Gallorini, and S. Servili, 'Hydrogen production through sorption-enhanced steam methane reforming and membrane technology: A review', *Energy*, vol. 33, no. 4, pp. 554–570, Apr. 2008, doi: 10.1016/j.energy.2007.10.018.
[39] P. Nikolaidis and A. Poullikkas, 'A comparative overview of hydrogen production processes', *Renew. Sustain. Energy Rev.*, vol. 67, pp. 597–611, Jan. 2017, doi: 10.1016/j.rser.2016.09.044.
[40] D. Hariharan *et al.*, 'Catalytic partial oxidation reformation of diesel, gasoline, and natural gas for use in low temperature combustion engines', *Fuel*, vol. 246, pp. 295–307, Jun. 2019, doi: 10.1016/j.fuel.2019.02.003.
[41] R. Ma, B. Xu, and X. Zhang, 'Catalytic partial oxidation (CPOX) of natural gas and renewable hydrocarbons/oxygenated hydrocarbons—A review', *Catal. Today*, vol. 338, pp. 18–30, Nov. 2019, doi: 10.1016/j.cattod.2019.06.025.
[42] P. Arku, B. Regmi, and A. Dutta, 'A review of catalytic partial oxidation of fossil fuels and biofuels: Recent advances in catalyst development and kinetic modelling', *Chem. Eng. Res. Des.*, vol. 136, pp. 385–402, Aug. 2018, doi: 10.1016/j.cherd.2018.05.044.
[43] M. Luneau *et al.*, 'Deactivation mechanism of Ni supported on Mg-Al spinel during autothermal reforming of model biogas', *Appl. Catal. B Environ.*, vol. 203, pp. 289–299, Apr. 2017, doi: 10.1016/j.apcatb.2016.10.023.
[44] R. Baruah, M. Dixit, P. Basarkar, D. Parikh, and A. Bhargav, 'Advances in ethanol autothermal reforming', *Renew. Sustain. Energy Rev.*, vol. 51, pp. 1345–1353, Nov. 2015, doi: 10.1016/j.rser.2015.07.060.
[45] R. Tariq, F. Maqbool, and S. Z. Abbas, 'Small-scale production of hydrogen via auto-thermal reforming in an adiabatic packed bed reactor: Parametric study and reactor's optimization through response surface methodology', *Comput. Chem. Eng.*, vol. 145, p. 107192, Feb. 2021, doi: 10.1016/j.compchemeng.2020.107192.
[46] M. Yue, H. Lambert, E. Pahon, R. Roche, S. Jemei, and D. Hissel, 'Hydrogen energy systems: A critical review of technologies, applications, trends and challenges', *Renew. Sustain. Energy Rev.*, vol. 146, p. 111180, Aug. 2021, doi: 10.1016/j.rser.2021.111180.
[47] N. A. Burton, R. V. Padilla, A. Rose, and H. Habibullah, 'Increasing the efficiency of hydrogen production from solar powered water electrolysis', *Renew. Sustain. Energy Rev.*, vol. 135, p. 110255, Jan. 2021, doi: 10.1016/j.rser.2020.110255.
[48] IEA, 'Global Hydrogen REVIEW 2021', 2021, Accessed: Nov. 05, 2023. [Online]. Available: https://www.iea.org/reports/global-hydrogen-review-2021
[49] M. Pérez-Vigueras, R. Sotelo-Boyás, R. D. G. González-Huerta, and F. Bañuelos-Ruedas, 'Feasibility analysis of green hydrogen production from oceanic energy', *Heliyon*, vol. 9, no. 9, p. e20046, Sep. 2023, doi: 10.1016/j.heliyon.2023.e20046.

[50] D. Mazzeo, M. S. Herdem, N. Matera, and J. Z. Wen, 'Green hydrogen production: Analysis for different single or combined large-scale photovoltaic and wind renewable systems', *Renew. Energy*, vol. 200, pp. 360–378, Nov. 2022, doi: 10.1016/j.renene.2022.09.057.
[51] A. Al-Sharafi, A. Z. Sahin, T. Ayar, and B. S. Yilbas, 'Techno-economic analysis and optimization of solar and wind energy systems for power generation and hydrogen production in Saudi Arabia', *Renew. Sustain. Energy Rev.*, vol. 69, pp. 33–49, Mar. 2017, doi: 10.1016/j.rser.2016.11.157.
[52] H. Ishaq and I. Dincer, 'Comparative assessment of renewable energy-based hydrogen production methods', *Renew. Sustain. Energy Rev.*, vol. 135, p. 110192, Jan. 2021, doi: 10.1016/j.rser.2020.110192.
[53] R. Bhandari and R. R. Shah, 'Hydrogen as energy carrier: Techno-economic assessment of decentralized hydrogen production in Germany', *Renew. Energy*, vol. 177, pp. 915–931, Nov. 2021, doi: 10.1016/j.renene.2021.05.149.
[54] F. J. Vivas, A. De las Heras, F. Segura, and J. M. Andújar, 'A review of energy management strategies for renewable hybrid energy systems with hydrogen backup', *Renew. Sustain. Energy Rev.*, vol. 82, pp. 126–155, Feb. 2018, doi: 10.1016/j.rser.2017.09.014.
[55] E. L. V. Eriksson and E. MacA. Gray, 'Optimization and integration of hybrid renewable energy hydrogen fuel cell energy systems – A critical review', *Appl. Energy*, vol. 202, pp. 348–364, Sep. 2017, doi: 10.1016/j.apenergy.2017.03.132.
[56] V. Khare, S. Nema, and P. Baredar, 'Solar–wind hybrid renewable energy system: A review', *Renew. Sustain. Energy Rev.*, vol. 58, pp. 23–33, May 2016, doi: 10.1016/j.rser.2015.12.223.
[57] Z. Li, P. Guo, R. Han, and H. Sun, 'Current status and development trend of wind power generation-based hydrogen production technology', *Energy Explor. Exploit.*, vol. 37, no. 1, pp. 5–25, Jan. 2019, doi: 10.1177/0144598718787294.
[58] Y. Kalinci, A. Hepbasli, and I. Dincer, 'Biomass-based hydrogen production: A review and analysis', *Int. J. Hydrog. Energy*, vol. 34, no. 21, pp. 8799–8817, Nov. 2009, doi: 10.1016/j.ijhydene.2009.08.078.
[59] T. R. Ayodele, M. A. Alao, A. S. O. Ogunjuyigbe, and J. L. Munda, 'Electricity generation prospective of hydrogen derived from biogas using food waste in south-western Nigeria', *Biomass Bioenergy*, vol. 127, p. 105291, Aug. 2019, doi: 10.1016/j.biombioe.2019.105291.
[60] M. D. Mukelabai, U. K. G. Wijayantha, and R. E. Blanchard, 'Renewable hydrogen economy outlook in Africa', *Renew. Sustain. Energy Rev.*, vol. 167, p. 112705, Oct. 2022, doi: 10.1016/j.rser.2022.112705.
[61] S. Rahmouni, B. Negrou, N. Settou, J. Dominguez, and A. Gouareh, 'Prospects of hydrogen production potential from renewable resources in Algeria', *Int. J. Hydrog. Energy*, vol. 42, no. 2, pp. 1383–1395, Jan. 2017, doi: 10.1016/j.ijhydene.2016.07.214.
[62] T. R. Ayodele and J. L. Munda, 'Potential and economic viability of green hydrogen production by water electrolysis using wind energy resources in South Africa', *Int. J. Hydrog. Energy*, vol. 44, no. 33, pp. 17669–17687, Jul. 2019, doi: 10.1016/j.ijhydene.2019.05.077.
[63] M. D'Isidoro *et al.*, 'Estimation of solar and wind energy resources over Lesotho and their complementarity by means of WRF yearly simulation at high resolution', *Renew. Energy*, vol. 158, pp. 114–129, Oct. 2020, doi: 10.1016/j.renene.2020.05.106.
[64] B. M. Taele, L. Mokhutšoane, and I. Hapazari, 'An overview of small hydropower development in Lesotho: Challenges and prospects', *Renew. Energy*, vol. 44, pp. 448–452, Aug. 2012, doi: 10.1016/j.renene.2012.01.086.

[65] S. E. Hosseini and M. A. Wahid, ‘Hydrogen production from renewable and sustainable energy resources: Promising green energy carrier for clean development’, *Renew. Sustain. Energy Rev.*, vol. 57, pp. 850–866, May 2016, doi: 10.1016/j.rser.2015.12.112.
[66] F. Safari and I. Dincer, ‘A review and comparative evaluation of thermochemical water splitting cycles for hydrogen production’, *Energy Convers. Manag.*, vol. 205, p. 112182, Feb. 2020, doi: 10.1016/j.enconman.2019.112182.
[67] M. El-Shafie, S. Kambara, and Y. Hayakawa, ‘Hydrogen Production Technologies Overview’, *J. Power Energy Eng.*, vol. 07, no. 01, pp. 107–154, 2019, doi: 10.4236/jpee.2019.71007.
[68] M. A. Khan *et al.*, ‘Recent Progresses in Electrocatalysts for Water Electrolysis’, *Electrochem. Energy Rev.*, vol. 1, no. 4, pp. 483–530, Dec. 2018, doi: 10.1007/s41918-018-0014-z.
[69] S. Shiva Kumar and H. Lim, ‘An overview of water electrolysis technologies for green hydrogen production’, *Energy Rep.*, vol. 8, pp. 13793–13813, Nov. 2022, doi: 10.1016/j.egyr.2022.10.127.
[70] D. Lim *et al.*, ‘Impact of voltage degradation in water electrolyzers on sustainability of synthetic natural gas production: Energy, economic, and environmental analysis’, *Energy Convers. Manag.*, vol. 245, p. 114516, Oct. 2021, doi: 10.1016/j.enconman.2021.114516.
[71] B. Lee, D. Lim, H. Lee, and H. Lim, ‘Which water electrolysis technology is appropriate?: Critical insights of potential water electrolysis for green ammonia production’, *Renew. Sustain. Energy Rev.*, vol. 143, p. 110963, Jun. 2021, doi: 10.1016/j.rser.2021.110963.
[72] S. Shiva Kumar and V. Himabindu, ‘Boron-Doped Carbon nanoparticles supported palladium as an efficient hydrogen evolution electrode in PEM water electrolysis’, *Renew. Energy*, vol. 146, pp. 2281–2290, Feb. 2020, doi: 10.1016/j.renene.2019.08.068.
[73] W. Hall, T. Spencer, G. Renjith, and S. Dayal, ‘A PATHWAY FOR SCALING UP LOW CARBON HYDROGEN ACROSS THE ECONOMY’, 2020.
[74] F. Yu, L. Yu, I. K. Mishra, Y. Yu, Z. F. Ren, and H. Q. Zhou, ‘Recent developments in earth-abundant and non-noble electrocatalysts for water electrolysis’, *Mater. Today Phys.*, vol. 7, pp. 121–138, Dec. 2018, doi: 10.1016/j.mtphys.2018.11.007.
[75] B. Yodwong, D. Guilbert, M. Phattanasak, W. Kaewmanee, M. Hinaje, and G. Vitale, ‘AC-DC Converters for Electrolyzer Applications: State of the Art and Future Challenges’, *Electronics*, vol. 9, no. 6, p. 912, May 2020, doi: 10.3390/electronics9060912.
[76] F. Superchi, F. Papi, A. Mannelli, F. Balduzzi, F. M. Ferro, and A. Bianchini, ‘Development of a reliable simulation framework for techno-economic analyses on green hydrogen production from wind farms using alkaline electrolyzers’, *Renew. Energy*, vol. 207, pp. 731–742, May 2023, doi: 10.1016/j.renene.2023.03.077.
[77] A. Ajanovic, M. Sayer, and R. Haas, ‘The economics and the environmental benignity of different colors of hydrogen’, *Int. J. Hydrog. Energy*, vol. 47, no. 57, pp. 24136–24154, Jul. 2022, doi: 10.1016/j.ijhydene.2022.02.094.
[78] S. A. Grigoriev, V. N. Fateev, D. G. Bessarabov, and P. Millet, ‘Current status, research trends, and challenges in water electrolysis science and technology’, *Int. J. Hydrog. Energy*, vol. 45, no. 49, pp. 26036–26058, Oct. 2020, doi: 10.1016/j.ijhydene.2020.03.109.
[79] M. David, C. Ocampo-Martínez, and R. Sánchez-Peña, ‘Advances in alkaline water electrolyzers: A review’, *J. Energy Storage*, vol. 23, pp. 392–403, Jun. 2019, doi: 10.1016/j.est.2019.03.001.
[80] D. Sampangi, R. SUB, S. D, D. Bhagawan, and H. Vurimindi, ‘Synthesis of Polysulfone and Zirconium Oxide Coated Asbestos Composite Separators for Alkaline Water Electrolysis’, *Chem. Eng. Process Tech. ISSN 2333-6633*, Jun. 2017.

[81] D. Burnat *et al.*, ‘Composite membranes for alkaline electrolysis based on polysulfone and mineral fillers’, *J. Power Sources*, vol. 291, pp. 163–172, Sep. 2015, doi: 10.1016/j.jpowsour.2015.04.066.
[82] S. Liu, B. Li, S. V. Mohite, P. Devaraji, L. Mao, and R. Xing, ‘Ultrathin MoS2 nanosheets in situ grown on rich defective Ni0.96S as heterojunction bifunctional electrocatalysts for alkaline water electrolysis’, *Int. J. Hydrog. Energy*, vol. 45, no. 55, pp. 29929–29937, Nov. 2020, doi: 10.1016/j.ijhydene.2020.08.034.
[83] Z. Lv *et al.*, ‘Co-Constructing Interfaces of Multiheterostructure on MXene (Ti3C2Tx)-Modified 3D Self-Supporting Electrode for Ultraefficient Electrocatalytic HER in Alkaline Media’, *Adv. Funct. Mater.*, vol. 31, no. 29, p. 2102576, 2021, doi: 10.1002/adfm.202102576.
[84] U. Y. Qazi, R. Javaid, M. Zahid, N. Tahir, A. Afzal, and X.-M. Lin, ‘Bimetallic NiCo–NiCoO2 nano-heterostructures embedded on copper foam as a self-supported bifunctional electrode for water oxidation and hydrogen production in alkaline media’, *Int. J. Hydrog. Energy*, vol. 46, no. 36, pp. 18936–18948, May 2021, doi: 10.1016/j.ijhydene.2021.03.046.
[85] H. A. Miller *et al.*, ‘Green hydrogen from anion exchange membrane water electrolysis: a review of recent developments in critical materials and operating conditions’, *Sustain. Energy Fuels*, vol. 4, no. 5, pp. 2114–2133, May 2020, doi: 10.1039/C9SE01240K.
[86] D. Henkensmeier, M. Najibah, C. Harms, J. Žitka, J. Hnát, and K. Bouzek, ‘Overview: State-of-the Art Commercial Membranes for Anion Exchange Membrane Water Electrolysis’, *J. Electrochem. Energy Convers. Storage*, vol. 18, no. 2, p. 024001, May 2021, doi: 10.1115/1.4047963.
[87] P. Thangavel, G. Kim, and K. S. Kim, ‘Electrochemical integration of amorphous NiFe (oxy)hydroxides on surface-activated carbon fibers for high-efficiency oxygen evolution in alkaline anion exchange membrane water electrolysis’, *J. Mater. Chem. A*, vol. 9, no. 24, pp. 14043–14051, Jun. 2021, doi: 10.1039/D1TA02883A.
[88] I. Jang *et al.*, ‘Electron-deficient titanium single-atom electrocatalyst for stable and efficient hydrogen production’, *Nano Energy*, vol. 78, p. 105151, Dec. 2020, doi: 10.1016/j.nanoen.2020.105151.
[89] M. J. Jang *et al.*, ‘Superior performance and stability of anion exchange membrane water electrolysis: pH-controlled copper cobalt oxide nanoparticles for the oxygen evolution reaction’, *J. Mater. Chem. A*, vol. 8, no. 8, pp. 4290–4299, Feb. 2020, doi: 10.1039/C9TA13137J.
[90] W. Guo, J. Kim, H. Kim, and S. H. Ahn, ‘Cu–Co–P electrodeposited on carbon paper as an efficient electrocatalyst for hydrogen evolution reaction in anion exchange membrane water electrolyzers’, *Int. J. Hydrog. Energy*, vol. 46, no. 38, pp. 19789–19801, Jun. 2021, doi: 10.1016/j.ijhydene.2021.03.120.
[91] J. Wang *et al.*, ‘Non-precious-metal catalysts for alkaline water electrolysis: operando characterizations, theoretical calculations, and recent advances’, *Chem. Soc. Rev.*, vol. 49, no. 24, pp. 9154–9196, Dec. 2020, doi: 10.1039/D0CS00575D.
[92] Y. Wang, W. Li, L. Ma, W. Li, and X. Liu, ‘Degradation of solid oxide electrolysis cells: Phenomena, mechanisms, and emerging mitigation strategies—A review’, *J. Mater. Sci. Technol.*, vol. 55, pp. 35–55, Oct. 2020, doi: 10.1016/j.jmst.2019.07.026.
[93] I. V. Pushkareva, A. S. Pushkarev, S. A. Grigoriev, P. Modisha, and D. G. Bessarabov, ‘Comparative study of anion exchange membranes for low-cost water electrolysis’, *Int. J. Hydrog. Energy*, vol. 45, no. 49, pp. 26070–26079, Oct. 2020, doi: 10.1016/j.ijhydene.2019.11.011.
[94] A. María Villarreal Vives, R. Wang, S. Roy, and A. Smallbone, ‘Techno-economic analysis of large-scale green hydrogen production and storage’, *Appl. Energy*, vol. 346, p. 121333, Sep. 2023, doi: 10.1016/j.apenergy.2023.121333.

[95] IRENA, ‘Green hydrogen cost reduction: Scaling up electrolysers to meet the 1.5C climate goal’, *Int. Renew. Energy Agency Abu Dhabi*, 2020, Accessed: Sep. 18, 2023. [Online]. Available: https://www.irena.org/-/media/Files/IRENA/Agency/Publication/2020/Dec/IRENA_Green_hydrogen_cost_2020.pdf

[96] S. Shiva Kumar, S. U. B. Ramakrishna, K. Naga Mahesh, B. Rama Devi, and V. Himabindu, ‘Palladium supported on phosphorus–nitrogen dual-doped carbon nanoparticles as cathode for hydrogen evolution in PEM water electrolyser’, *Ionics*, vol. 25, no. 6, pp. 2615–2625, Jun. 2019, doi: 10.1007/s11581-018-2783-0.

[97] S. Shiva Kumar, S. U. B. Ramakrishna, D. Bhagawan, and V. Himabindu, ‘Preparation of RuxPd1-xO2 electrocatalysts for the oxygen evolution reaction (OER) in PEM water electrolysis’, *Ionics*, vol. 24, no. 8, pp. 2411–2419, Aug. 2018, doi: 10.1007/s11581-017-2359-4.

[98] S. U. B. Ramakrishna, D. Srinivasulu Reddy, S. Shiva Kumar, and V. Himabindu, ‘Nitrogen doped CNTs supported Palladium electrocatalyst for hydrogen evolution reaction in PEM water electrolyser’, *Int. J. Hydrog. Energy*, vol. 41, no. 45, pp. 20447–20454, Dec. 2016, doi: 10.1016/j.ijhydene.2016.08.195.

[99] B. Lee, H. Lee, J. Heo, C. Moon, S. Moon, and H. Lim, ‘Stochastic techno-economic analysis of H2 production from power-to-gas using a high-pressure PEM water electrolyzer for a small-scale H2 fueling station’, *Sustain. Energy Fuels*, vol. 3, no. 9, pp. 2521–2529, Aug. 2019, doi: 10.1039/C9SE00275H.

[100] S. Shiva Kumar, S. U. B. Ramakrishna, B. Rama Devi, and V. Himabindu, ‘Phosphorus-doped carbon nanoparticles supported palladium electrocatalyst for the hydrogen evolution reaction (HER) in PEM water electrolysis’, *Ionics*, vol. 24, no. 10, pp. 3113–3121, Oct. 2018, doi: 10.1007/s11581-018-2471-0.

[101] M. Upadhyay, S. Lee, S. Jung, Y. Choi, S. Moon, and H. Lim, ‘Systematic assessment of the anode flow field hydrodynamics in a new circular PEM water electrolyser’, *Int. J. Hydrog. Energy*, vol. 45, no. 41, pp. 20765–20775, Aug. 2020, doi: 10.1016/j.ijhydene.2020.05.164.

[102] M. Upadhyay *et al.*, ‘Three-dimensional CFD simulation of proton exchange membrane water electrolyser: Performance assessment under different condition’, *Appl. Energy*, vol. 306, p. 118016, Jan. 2022, doi: 10.1016/j.apenergy.2021.118016.

[103] A. Buttler and H. Spliethoff, ‘Current status of water electrolysis for energy storage, grid balancing and sector coupling via power-to-gas and power-to-liquids: A review’, *Renew. Sustain. Energy Rev.*, vol. 82, pp. 2440–2454, Feb. 2018, doi: 10.1016/j.rser.2017.09.003.

[104] M. Carmo, D. L. Fritz, J. Mergel, and D. Stolten, ‘A comprehensive review on PEM water electrolysis’, *Int. J. Hydrog. Energy*, vol. 38, no. 12, pp. 4901–4934, Apr. 2013, doi: 10.1016/j.ijhydene.2013.01.151.

[105] S. Shiva Kumar and V. Himabindu, ‘Hydrogen production by PEM water electrolysis – A review’, *Mater. Sci. Energy Technol.*, vol. 2, no. 3, pp. 442–454, Dec. 2019, doi: 10.1016/j.mset.2019.03.002.

[106] A. Nechache and S. Hody, ‘Alternative and innovative solid oxide electrolysis cell materials: A short review’, *Renew. Sustain. Energy Rev.*, vol. 149, p. 111322, Oct. 2021, doi: 10.1016/j.rser.2021.111322.

[107] C. Choe, S. Cheon, J. Gu, and H. Lim, ‘Critical aspect of renewable syngas production for power-to-fuel via solid oxide electrolysis: Integrative assessment for potential renewable energy source’, *Renew. Sustain. Energy Rev.*, vol. 161, p. 112398, Jun. 2022, doi: 10.1016/j.rser.2022.112398.

[108] F. Shen, R. Wang, and M. C. Tucker, 'Long term durability test and post mortem for metal-supported solid oxide electrolysis cells', *J. Power Sources*, vol. 474, p. 228618, Oct. 2020, doi: 10.1016/j.jpowsour.2020.228618.
[109] Q. Fang, L. Blum, N. H. Menzler, and D. Stolten, 'Solid Oxide Electrolyzer Stack with 20,000 h of Operation', *ECS Trans.*, vol. 78, no. 1, pp. 2885–2893, May 2017, doi: 10.1149/07801.2885ecst.
[110] S. Shiva Kumar and H. Lim, 'An overview of water electrolysis technologies for green hydrogen production', *Energy Rep.*, vol. 8, pp. 13793–13813, Nov. 2022, doi: 10.1016/j.egyr.2022.10.127.
[111] P. Li *et al.*, 'Performance enhanced of NiCe0.8Sm0.2O1.9 hydrogen electrode for reversible solid oxide cells with cadmium substitution', *J. Electroanal. Chem.*, vol. 882, p. 115018, Feb. 2021, doi: 10.1016/j.jelechem.2021.115018.
[112] Y.-D. Kim *et al.*, 'Cobalt-free perovskite Ba1-xNdxFeO3-δ air electrode materials for reversible solid oxide cells', *Ceram. Int.*, vol. 47, no. 6, pp. 7985–7993, Mar. 2021, doi: 10.1016/j.ceramint.2020.11.149.
[113] A. Nechache and S. Hody, 'Alternative and innovative solid oxide electrolysis cell materials: A short review', *Renew. Sustain. Energy Rev.*, vol. 149, p. 111322, Oct. 2021, doi: 10.1016/j.rser.2021.111322.
[114] A. Nechache, M. Cassir, and A. Ringuedé, 'Solid oxide electrolysis cell analysis by means of electrochemical impedance spectroscopy: A review', *J. Power Sources*, vol. 258, pp. 164–181, Jul. 2014, doi: 10.1016/j.jpowsour.2014.01.110.
[115] F. Tietz, D. Sebold, A. Brisse, and J. Schefold, 'Degradation phenomena in a solid oxide electrolysis cell after 9000 h of operation', *J. Power Sources*, vol. 223, pp. 129–135, Feb. 2013, doi: 10.1016/j.jpowsour.2012.09.061.
[116] S. He, Y. Zou, K. Chen, and S. P. Jiang, 'A critical review of key materials and issues in solid oxide cells', *Interdiscip. Mater.*, vol. 2, no. 1, pp. 111–136, 2023, doi: 10.1002/idm2.12068.
[117] A. G. Olabi *et al.*, 'Large-vscale hydrogen production and storage technologies: Current status and future directions', *Int. J. Hydrog. Energy*, vol. 46, no. 45, pp. 23498–23528, Jul. 2021, doi: 10.1016/j.ijhydene.2020.10.110.
[118] J. Jia *et al.*, 'Solar water splitting by photovoltaic-electrolysis with a solar-to-hydrogen efficiency over 30%', *Nat. Commun.*, vol. 7, no. 1, Art. no. 1, Oct. 2016, doi: 10.1038/ncomms13237.
[119] N. A. Kelly and T. L. Gibson, 'Improved photovoltaic energy output for cloudy conditions with a solar tracking system', *Sol. Energy*, vol. 83, no. 11, pp. 2092–2102, Nov. 2009, doi: 10.1016/j.solener.2009.08.009.
[120] A. Mio, E. Barbera, A. Massi Pavan, A. Bertucco, and M. Fermeglia, 'Sustainability analysis of hydrogen production processes', *Int. J. Hydrog. Energy*, vol. 54, pp. 540–553, Feb. 2024, doi: 10.1016/j.ijhydene.2023.06.122.
[121] M. Temiz and I. Dincer, 'Design and analysis of a floating photovoltaic based energy system with underground energy storage options for remote communities', *J. Energy Storage*, vol. 55, p. 105733, Nov. 2022, doi: 10.1016/j.est.2022.105733.
[122] T. S. Uyar and D. Beşikci, 'Integration of hydrogen energy systems into renewable energy systems for better design of 100% renewable energy communities', *Int. J. Hydrog. Energy*, vol. 42, no. 4, pp. 2453–2456, Jan. 2017, doi: 10.1016/j.ijhydene.2016.09.086.
[123] M. Benghanem *et al.*, 'Hydrogen Production Methods Based on Solar and Wind Energy: A Review', *Energies*, vol. 16, no. 2, Art. no. 2, Jan. 2023, doi: 10.3390/en16020757.
[124] K. Almutairi, S. S. Hosseini Dehshiri, S. J. Hosseini Dehshiri, A. Mostafaeipour, A. Issakhov, and K. Techato, 'A thorough investigation for development of hydrogen projects

from wind energy: A case study', *Int. J. Hydrog. Energy*, vol. 46, no. 36, pp. 18795–18815, May 2021, doi: 10.1016/j.ijhydene.2021.03.061.
[125] S. Kudria, I. Ivanchenko, B. Tuchynskyi, K. Petrenko, O. Karmazin, and O. Riepkin, 'Resource potential for wind-hydrogen power in Ukraine', *Int. J. Hydrog. Energy*, vol. 46, no. 1, pp. 157–168, Jan. 2021, doi: 10.1016/j.ijhydene.2020.09.211.
[126] M. Abdel-Basset, A. Gamal, R. K. Chakrabortty, and M. J. Ryan, 'Evaluation of sustainable hydrogen production options using an advanced hybrid MCDM approach: A case study', *Int. J. Hydrog. Energy*, vol. 46, no. 5, pp. 4567–4591, Jan. 2021, doi: 10.1016/j.ijhydene.2020.10.232.
[127] L. Schlapbach and A. Züttel, 'Hydrogen-storage materials for mobile applications', *Nature*, vol. 414, no. 6861, Art. no. 6861, Nov. 2001, doi: 10.1038/35104634.
[128] N. Ma, W. Zhao, W. Wang, X. Li, and H. Zhou, 'Large scale of green hydrogen storage: Opportunities and challenges', *Int. J. Hydrog. Energy*, vol. 50, pp. 379–396, Jan. 2024, doi: 10.1016/j.ijhydene.2023.09.021.
[129] V. Tietze, S. Luhr, and D. Stolten, 'Bulk Storage Vessels for Compressed and Liquid Hydrogen', in *Hydrogen Science and Engineering : Materials, Processes, Systems and Technology*, John Wiley & Sons, Ltd, 2016, pp. 659–690. doi: 10.1002/9783527674268.ch27.
[130] M. R. Usman, 'Hydrogen storage methods: Review and current status', *Renew. Sustain. Energy Rev.*, vol. 167, p. 112743, Oct. 2022, doi: 10.1016/j.rser.2022.112743.
[131] H. Barthelemy, M. Weber, and F. Barbier, 'Hydrogen storage: Recent improvements and industrial perspectives', *Int. J. Hydrog. Energy*, vol. 42, no. 11, pp. 7254–7262, Mar. 2017, doi: 10.1016/j.ijhydene.2016.03.178.
[132] A. M. Abdalla, S. Hossain, O. B. Nisfindy, A. T. Azad, M. Dawood, and A. K. Azad, 'Hydrogen production, storage, transportation and key challenges with applications: A review', *Energy Convers. Manag.*, vol. 165, pp. 602–627, Jun. 2018, doi: 10.1016/j.enconman.2018.03.088.
[133] R. Moradi and K. M. Groth, 'Hydrogen storage and delivery: Review of the state of the art technologies and risk and reliability analysis', *Int. J. Hydrog. Energy*, vol. 44, no. 23, pp. 12254–12269, May 2019, doi: 10.1016/j.ijhydene.2019.03.041.
[134] Y. Wang, H. Yuan, A. Martinez, P. Hong, H. Xu, and F. R. Bockmiller, 'Polymer electrolyte membrane fuel cell and hydrogen station networks for automobiles: Status, technology, and perspectives', *Adv. Appl. Energy*, vol. 2, p. 100011, May 2021, doi: 10.1016/j.adapen.2021.100011.
[135] B. K. Hong and S. H. Kim, '(Invited) Recent Advances in Fuel Cell Electric Vehicle Technologies of Hyundai', *ECS Trans.*, vol. 86, no. 13, p. 3, Jul. 2018, doi: 10.1149/08613.0003ecst.
[136] J. R. Fekete, J. W. Sowards, and R. L. Amaro, 'Economic impact of applying high strength steels in hydrogen gas pipelines', *Int. J. Hydrog. Energy*, vol. 40, no. 33, pp. 10547–10558, Sep. 2015, doi: 10.1016/j.ijhydene.2015.06.090.
[137] A. G. Olabi, M. Mahmoud, B. Soudan, T. Wilberforce, and M. Ramadan, 'Geothermal based hybrid energy systems, toward eco-friendly energy approaches', *Renew. Energy*, vol. 147, pp. 2003–2012, Mar. 2020, doi: 10.1016/j.renene.2019.09.140.
[138] Y. E. Yuksel, M. Ozturk, and I. Dincer, 'Analysis and assessment of a novel hydrogen liquefaction process', *Int. J. Hydrog. Energy*, vol. 42, no. 16, pp. 11429–11438, Apr. 2017, doi: 10.1016/j.ijhydene.2017.03.064.
[139] A. Le Duigou, A.-G. Bader, J.-C. Lanoix, and L. Nadau, 'Relevance and costs of large scale underground hydrogen storage in France', *Int. J. Hydrog. Energy*, vol. 42, no. 36, pp. 22987–23003, Sep. 2017, doi: 10.1016/j.ijhydene.2017.06.239.

[140] I. P. Jain, C. Lal, and A. Jain, ‘Hydrogen storage in Mg: A most promising material’, *Int. J. Hydrog. Energy*, vol. 35, no. 10, pp. 5133–5144, May 2010, doi: 10.1016/j.ijhydene.2009.08.088.
[141] K. T. Møller, T. R. Jensen, E. Akiba, and H. Li, ‘Hydrogen - A sustainable energy carrier’, *Prog. Nat. Sci. Mater. Int.*, vol. 27, no. 1, pp. 34–40, Feb. 2017, doi: 10.1016/j.pnsc.2016.12.014.
[142] S. R. Johnson *et al.*, ‘Chemical activation of MgH 2 ; a new route to superior hydrogen storage materials’, *Chem. Commun.*, vol. 0, no. 22, pp. 2823–2825, 2005, doi: 10.1039/B503085D.
[143] J. Li, P. Fan, Z. Z. Fang, and C. Zhou, ‘Kinetics of isothermal hydrogenation of magnesium with TiH2 additive’, *Int. J. Hydrog. Energy*, vol. 39, no. 14, pp. 7373–7381, May 2014, doi: 10.1016/j.ijhydene.2014.02.159.
[144] F. L. Darkrim, P. Malbrunot, and G. P. Tartaglia, ‘Review of hydrogen storage by adsorption in carbon nanotubes’, *Int. J. Hydrog. Energy*, vol. 27, no. 2, pp. 193–202, Feb. 2002, doi: 10.1016/S0360-3199(01)00103-3.
[145] S. Niaz, T. Manzoor, and A. H. Pandith, ‘Hydrogen storage: Materials, methods and perspectives’, *Renew. Sustain. Energy Rev.*, vol. 50, pp. 457–469, Oct. 2015, doi: 10.1016/j.rser.2015.05.011.
[146] W. F. Ekpotu, J. T. Akintola, M. C. Obialor, and P. C. Udom, ‘A Solar Energy System Design for Green Hydrogen Production in South-Western Nigeria, Lagos State, Using HOMER & ASPEN’, *Open J. Optim.*, vol. 12, no. 02, pp. 72–97, 2023, doi: 10.4236/ojop.2023.122006.
[147] S. Devkota *et al.*, ‘Process design and optimization of onsite hydrogen production from ammonia: Reactor design, energy saving and NOX control’, *Fuel*, vol. 342, p. 127879, Jun. 2023, doi: 10.1016/j.fuel.2023.127879.
[148] J. Mikyška, ‘Robust and efficient methods for solving the Rachford–Rice equation in flash equilibrium calculation’, *Fluid Phase Equilibria*, vol. 571, p. 113803, Aug. 2023, doi: 10.1016/j.fluid.2023.113803.
[149] V. Gaganis, D. Marinakis, and N. Varotsis, ‘A general framework of model functions for rapid and robust solution of Rachford–Rice type of equations’, *Fluid Phase Equilibria*, vol. 322–323, pp. 9–18, May 2012, doi: 10.1016/j.fluid.2012.03.001.
[150] ‘Honeywell UniSim Design Suite’, Honeywell Forge. Accessed: Aug. 01, 2024. [Online]. Available: https://www.honeywellforge.ai/us/en/products/industrial-operations/honeywell-unisim-design-suite